Biochemical dissection of Mer2 in meiotic DNA double-strand break formation

Dissertation

der Mathematisch-Naturwissenschaftlichen Fakultät

der Eberhard Karls Universität Tübingen

zur Erlangung des Grades eines

Doktors der Naturwissenschaften

(Dr. rer. Nat.)

vorgelegt von

Dorota Rousová

aus Brno, Tschechische Republik

Tübingen

2022

Gedruckt mit Genehmigung der Mathematisch-Naturwissenschaftlichen Fakultät der Eberhard Karls Universität Tübingen

Tag der mündlichen Qualifikation:	2. 6. 2022
Dekan:	Prof. Dr. Thilo Stehle
1. Berichterstatter:	Dr. John Weir
2. Berichterstatter:	Prof. Dr. Erik Schäffer

Summary

Meiotic cell division is a critical step in sexual reproduction that leads to the formation of haploid gametes from a diploid cell. During genome reduction, the homologous chromosomes are segregated into daughter cells. To avoid missegregation, the chromosomes have to be physically linked via homologous recombination. This linkage is enabled by the repair of programmed double-stranded DNA breaks (DSBs) using the homologous chromosome as a repair template rather than the sister chromatid. Introducing DSBs in the genome is precarious and has to be strictly controlled to avoid irreparable damage to the organism itself and its offspring. The break site is localized by an H3K4me3 mark on nucleosomes, which is recognized by the PHD domain-containing protein Spp1. Spp1 interacts with the protein Mer2, which connects the break site with the break machinery, localized in the proximity of the chromosomal axis, via its binding to the axial proteins Hop1 and Red1. These interactions must take place at the right position in the chromosome at the right time in the cell cycle to form breaks. Although the mechanism of DSB control has been studied for many years, its underlying molecular details remain to be deciphered.

To reveal the essential molecular elements involved in this process, I used *Saccharomyces cerevisiae* as a model organism and adopted an *in vitro* approach combining biochemical and structural methods on purified recombinant proteins. The DSB control was first explored by interaction experiments with Spp1, a nucleosome mark reader, and Mer2, a chromosomal axis

interactor. The results demonstrate that they form a constitutive complex with 2:4 stoichiometry at low nanomolar affinity. Dimerization of Spp1 by Mer2 strengthens its interaction with the nucleosome. Moreover, not only Spp1 but also Mer2 is a novel nucleosome binder, forming a stable complex with recombinant nucleosomes in solution. The interaction of Mer2 with nucleosomes provides additional stability to the assembly, where Spp1 provides the specificity of the interaction and Mer2 the strength. Once the future DNA break site is localized via its interaction with Spp1 and Mer2, it must interact with the chromosomal axis formed by Hop1-Red1 and cohesin, where the break machinery is. My data reveal that the conserved C-terminal region of Mer2 specifically interacts with an axis-bound Hop1 to ensure that breaks are made only when the chromosomal axis is properly formed. An additional level of control is provided by the conserved N-terminal region of Mer2, which is crucial for DSB formation. The N-terminal region establishes a previously undescribed connection with protein Mre11, which is responsible for resection of the DSBs, thus demonstrating that the factors both to create DNA break and repair it have to be in place before the break occurs.

Collectively, these findings reveal that Mer2 serves as an interaction platform for proteins involved in the control of DSBs, rendering it an essential component of proper DSB formation and resection. Moreover, they provide insights into the molecular details of DSB control and serve as a foundation for further studies of meiotic DSB formation. Illuminating previously unnoticed levels of DSB control significantly extends our

understanding of the process of homologous recombination and, ultimately, meiosis as a whole.

Zusammenfassung

Die meiotische Zellteilung ist ein entscheidender Schritt der sexuellen Fortpflanzung, die zur Bildung haploider Gameten aus einer diploiden Zelle führt. Während diesem Prozess werden die homologen Chromosomen in Tochterzellen aufgeteilt. Um eine Fehlsegregation zu vermeiden, müssen die Chromosomen im Lauf der durch homologe Rekombination verbunden werden. Diese Verknüpfung wird durch die Reparatur programmierter doppelsträngiger DNA-Brüche (DSBs) ermöglicht, wobei das homologe Chromosom und nicht das Schwesterchromatid als Reparaturvorlage verwendet wird. Das Einschleusen von DSBs in das Genom ist riskant für die Genomstabilität und muss streng kontrolliert werden, um irreparable Schäden am Organismus und seinen Nachkommen zu vermeiden. Die Bruchstelle wird durch eine H3K4me3-Markierung auf Nukleosomen lokalisiert, die von dem die PHD-Domäne enthaltenden Protein Spp1 erkannt wird. Spp1 interagiert dann mit dem Protein Mer2, das die Bruchstelle über seine Bindung an die chromosomalen Achsenproteine Hop1 und Red1 in die Nähe der Brüche induzierenden Proteine bringt. Diese Wechselwirkungen müssen zur richtigen Zeit im Zellzyklus und an der richtigen Stelle im Chromosom stattfinden, um Brüche zu bilden. Obwohl der (grundlegende) Mechanismus der DSB-Kontrolle seit vielen Jahren untersucht wird, müssen die zugrunde liegenden molekularen Details noch entschlüsselt werden.

Um die wesentlichen molekularen Elemente zu verstehen, die an diesem Prozess beteiligt sind, verwende ich *Saccharomyces cerevisiae* als Modellorganismus und wende einen *In vitro* Ansatz an, der biochemische und strukturbiologische Methoden an

aufgereinigten rekombinanten Proteinen kombiniert. Die räumliche Kontrolle wurde zuerst durch Interaktionsexperimente mit Spp1, das die Markierungen auf den Nukleosomen erkennt, und Mer2, welches mit den an der Achse angelagerten Proteinen interagiert, untersucht. Die Ergebnisse legen nahe, dass sie einen konstitutiven Komplex mit einer 2:4-Stöchiometrie und niedriger nanomolarer Affinität bilden. Die Dimerisierung von Spp1 durch Mer2 verstärkt seine Wechselwirkung mit dem Nukleosom. Darüber hinaus ist nicht nur Spp1, sondern auch Mer2 ein neuartiger Interaktionspartner der Nukleosomen, da er in Lösung einen stabilen Komplex mit Nukleosomen bildet. Die Wechselwirkung von Mer2 mit Nukleosomen verleiht der Anordnung zusätzliche Stabilität, wobei Spp1 für die Spezifität der Wechselwirkung und Mer2 für dessen Bindungsstärke verantwortlich ist. Sobald die zukünftige Bruchstelle durch ihre Interaktion mit Spp1 und Mer2 lokalisiert ist, muss sie in Richtung der von Hop1-Red1 gebildeten Chromosomenachse gezogen werden, wo sich die, die Brüche auslösenden Proteine befinden. Unsere Daten implizieren, dass Mer2 spezifisch mit einem achsengebundenen Hop1 interagiert, um sicherzustellen, dass Brüche nur dann induziert werden, wenn die chromosomale Achse richtig gebildet ist. Ein zusätzliches Maß an Kontrolle wird durch den konservierten N-Terminus von Mer2 bereitgestellt, der für die DSB-Bildung entscheidend ist. Der N-Terminus stellt eine Verbindung mit einem DSB-Resektionsprotein, Mre11 her, was zeigt, dass nicht nur alle DSB-Faktoren vorhanden sein müssen, bevor der Bruch auftritt, sondern auch die Mittel, um ihn zu reparieren.

Zusammengenommen zeigen diese Ergebnisse, dass Mer2 als Interaktionsplattform für Proteine dient, die an der Kontrolle von DSBs beteiligt sind, weshalb es ein zentraler Bestandteil der DSB-Bildung und -Resektion ist. Darüber hinaus liefern sie Einblicke in die molekularen Details der DSB-Kontrolle und dienen als Grundlage für weitere Studien zur meiotischen DSB-Bildung. Die Betrachtung bisher unbemerkter Ebenen der DSB-Kontrolle erweitert unser Verständnis des Prozesses der homologen Rekombination, und letztendlich der Meiose als Ganzes, erheblich.

Acknowledgement

First of all, I would like to thank Dr. John Weir for accepting me as a PhD student and for supervising me throughout the years. He was always welcoming to my ideas and gave me the freedom to plan my work, but also helped me, whenever I was stuck. I am very grateful for John as a supervisor and a mentor, he supported me not only in scientific matters but also in personal ones and made me feel welcome to knock on his door, whenever I needed.

I want to thank my TAC members Prof. Dr. Erik Schäffer, Dr. Marcus Hartmann and Prof. Dr. Andrei Lupas for their insightful comments and encouragement. Also, I would like to thank in advance Prof. Dr. Marja Timmermans for agreeing to be part of my PhD thesis defense committee.

I am thankful to Dr. Gerben Vader for his valuable input not only in yeast genetics and *in vivo* experiments, but also in science and academia in general. I thank Dr. Francesca Matirolli, who helped me immensely with setting up the production of recombinant nucleosomes in our lab and was always very open and helpful, whenever I needed assistance. I appreciate the friendliness with which she welcomed me into her lab and made my stay as comfortable and worry-free as possible.

My thanks go also to all the members of the Weir group. They were always helpful, whenever I needed anything, and greatly broaden my knowledge of pop culture and Disney songs. It was fun to work with all of you and our discussions (both scientific and non-scientific) allowed me to develop both as a scientist and person. I want to thank especially Magda Firlej for undertaking this journey with me. It was great to have a friend in the lab, who

was going through the same phases as me. She was fun to work with and had many brilliant creative ideas. More importantly, she is a great person I can count on to tell me her honest opinion and act in my best interest. From the first bonding afternoon in "Bota", I felt more at home thanks to her, even though we just started a new life in a different country. I want to thank also Veronika Altmannová for taking care of the lab and managing all of us with a very calm attitude. I cannot imagine, what would happen to the lab without her. Even though her private life remains largely secret, I truly appreciate all our discussions and support. I think I will never be able to listen to Bruce Springsteen without thinking of Verča again. My thanks go also to Saskia Funk, who greatly contributed to the good mood in the lab. Besides being always willing to help me with my imperfect German, she was a great and understanding person to talk to. Our evenings of Chinese, trashy series and talks about everything always improve my mood. I also want to thank Heidi Reichle and Suzanne Astrinidis for their technical support and help with all the cloning.

I want to thank my amazing students, Andreas Blaha, Leonie Konopka, Kristina Sturm and David Liedtke, it was an honour to supervise all of you. I am very grateful, that our work relationships turned into friendships with many unforgettable moments. I will cherish the moments of seeing Andreas on the dance floor, although I am still not sure if his joints are not turning into rubber, once he starts dancing. My avocado and lemon tree, as well as construction street barriers always make me smile and think of Leonie. Coffee breaks with Kristina were always a pleasure, she made me laugh and made working in the lab much

more enjoyable. I still cherish the aloe and a use the coffee cup only on special occasions. I enjoyed all of David's fun stories, his positive approach to life and his relaxed attitude. I am very proud of all of you and happy to know you.

I am very grateful to the electron microscopy facility, especially to Katharina Hipp. She was always willing to help me and support me in any way possible, even on her days off. Additionally, she was a great person to talk to about non-scientific topics, I appreciate her input on the best hairdressers and breakfast places.

I would like to thank people from Department I for their help with all the crystallization, SEC-MALS and MST and for making me feel welcome. Especially I want to thank Chris Heim, our coffee breaks were always very insightful, both scientifically and personally.

I would like to thank all the great colleagues from FML, especially Dingwen Su, Volker Soltys, Moritz Peters and Julia Hagauer. Without you, the PhD journey would be much more demanding. I very much enjoyed all our coffee breaks, barbecues and random discussions. They really sparked joy during my time in the FML. Without our unofficial support group, my mental health would suffer immensely.

I am also thankful to Herta Soffel and Claudia Jahn for making their administrative support and making sure they all send packages to arrive on time. They made sure, that everything runs as smoothly as possible, so we can focus on research.

I want to thank also Friedrich for all the support and care he showed me, especially during the thesis writing. He managed to always calm me down during my breakdowns and helped and

supported me in any way possible. I do not know, how could not do it without him.

None of this would be possible without the support of my family and friends. They always listened to all my complaints and supported me as much as they could.

Contribution

Publication included in this dissertation:

Rousová, D., Nivsarkar, V., Altmannova, V., Raina, V.B., Funk, S.K., Liedtke, D., Janning, P., Müller, F., Reichle, H., Vader, G., Weir, J.R., 2021. Novel mechanistic insights into the role of Mer2 as the keystone of meiotic DNA break formation. eLife 10, e72330. https://doi.org/10.7554/eLife.72330

Vaishnavi Nivsarkar and Vivek B. Rain from Gerben Vader Laboratory (MPI Dortmund and Cancer Centre Amsterdam) performed spore viability assay, western blot from meiotic yeast culture and southern blot and analyzed the results (section 2.4.1).

Veronika Altmannová from John Weir lab performed co-immunoprecipitation mass-spectrometry and yeast-two hybrid assay and the subsequent analysis (sections 2.4.2 and 2.4.3). Veronika as well cloned and purified Mre11 (section 2.4.3) and together with Saskia Funk (John Weir lab) also Red1 and Red1-Hop1 complex from insect cells (section 2.3.1).

Saskia Funk (John Weir lab) carried out the radioactive phosphorylation assay (section 2.5).

Tanja Bange (Ludwig-Maximilians Universität München) performed the mass-spectrometry analysis of the phosphorylated Mer2 constructs to detect the phospho-sites (section 2.5).

Petra Janning and Franziska Müller (Max Planck Institute of Molecular Physiology, Dortmund) analyzed the crosslinked samples on mass-spectrometry (sections 2.1.2, 2.2.1, 2.3.2 and 2.4.3).

John Weir created the Hop1 homology model and the AlphaFold model of Hop1-Red1-Mer2 (section 2.3.2). He purified the DDK from yeast, performed ITC with Spp1 and Mer2 (section 2.1.2), fitted the binding curve derived from EMSA experiments (section 2.2.2) and analyzed the SAXS data (section 2.1.2).

David Liedtke (John Weir lab) helped with the cloning and purification of Mer2 constructs.

Heidi Reichle (John Weir lab) helped with cloning.

Outline

List of Figures

List of Tables

Abbreviations

aa	amino acid
AEBSF	4-(2-aminoethyl)benzenesulfonyl fluoride hydrochloride
ATP	adenosine triphosphate
BME	β-mercaptoethanol
bp	base pair
BSA	bovine serum albumin
CC	coiled-coil
CM	closure motif
CO	cross-over
COMPASS	complex of proteins associated with Set1
CV	column volume
dHJ	double Holliday junction
DSB	DNA double-strand break
DSBU	disuccinimidyl dibutyric urea
DTT	dithiothreitol
EDTA	ethylenediaminetetraacetic acid
EM	electron microscopy
EMSA	electron mobility shift assay
Fw	forward primer
GST	glutathione S-transferase
H3K4me3	trimethylation of lysine 4 of histone H3
HEPES	4-(2-hydroxyethyl)1-piperazineethanesulfonic acid
IEX	ion-exchange chromatography
IPTG	isopropyl-beta-D-thiogalactopyranosid
ITC	isothermal calorimetry
kb	kilobase
K_D	dissociation constant
LB	lysogeny broth
LB	lysogeny broth
MALS	multiangle light scattering
MBP	maltose-binding protein
MN	mononucleosomes

MRX	Mre11-Rad50-Xrs2
MST	microscale thermophoresis
NCO	non-cross-over
NCP	nucleosome core particle
OD	optical density
ON	overnight
PAGE	polyacrylamide gel electrophoresis
PBS	phosphate-buffered saline
PBST	phosphate-buffered saline with Tween
PEG	polyethylene glycol
PHD	plant homeodomain
RMM	Rec114-Mei4-Mer2
RT	room temperature
Rv	reverse primer
SDS	sodium dodecyl sulfate
SEC	size exclusion chromatography
ssDNA	single-stranded DNA
Strep	streptavidin
SUMO	small ubiquitin-like modifier
TAE	Tris, acetic acid, EDTA buffer
TB	terrific broth
TB	terrific broth
TBE	Tris, boric acid, EDTA buffer
TCEP	Tris(2-carboxyehyl)phosphine
TEMED	tetramethylenediamine
Tris	Tris(hydroxyethyl)aminomethane
Y2H	yeast two-hybrid assay

1 Introduction

The Japanese have a tradition of Kintsugi – repairing broken pottery with gold. The central premise of Kintsugi is that embracing flaws enables the creation of something new and beautiful. This idea of creating something unique from something broken is very old, reaching almost to the origins of life on earth, and even into our own development as a species. Our cells (as well as of other sexually reproducing organisms) introduce breaks and repairs into their genome to increase the viability and diversity of their offspring.

The cells of sexually reproducing organisms usually contain genetic information from both parents. During reproduction, a combination of one somatic cell from each parent would lead to polyploidy of the offspring, with potentially devastating effects. Therefore, the cells undergo specialized meiotic cell division during which they link and combine previously unconnected homologous chromosomes and create a unique genetic combination in the new haploid cells. Introducing breaks in the DNA and their subsequent repair is a crucial step in meiosis and sexual reproduction.

1.1 Meiotic cell division

Meiosis has two principal roles: an evolutionary and a mechanistic one. The evolutionary advantage of meiosis is in a reshuffling of the parental genome, which increases the genetic diversity of the population and thus can enhance the long-term fitness and adaptability of the species. The mechanistic

requirement is in creating a physical linkage between the homologous chromosomes, which enables their proper separation into new daughter cells (Hunter, 2015; Page and Hawley, 2003; Petronczki et al., 2003; Wilkins and Holliday, 2009). Although there are some exceptions (for example in *Caenorhabditis elegans* the recombination and the linkage of homologous chromosomes are uncoupled from one another (Garcia-Muse and Boulton, 2007)), the process is very conserved and mostly universal among sexually reproducing organisms, although the nomenclature of the involved proteins differs amidst species. Within this thesis, I will be referring to the proteins as named in *Saccharomyces cerevisiae*, for their homologs and orthologs from other species, please see the following Table 1.

Table 1: List of proteins required for meiotic DSB formation in different organisms (adapted from (Lam and Keeney, 2014). Regulatory enzymes are not shown.

S. cerevisiae	***S. pombe***	***Mus musculus***	***A. thaliana***
Spo11	Rec12	SPO11	SPO11-1/2/3
Spp1	Spf1	CXXC1	
Mer2/Rec107	Rec15	IHO1	PAIR1
Mei4	Rec24	MEI4	PRD2
Rec114	Rec7	REC114	PHS1
Mre11	Rad32	MRE11	MRE11
Rad50	Rad50	RAD50	RAD50
Xrs2	Nbs1	NBS1	
Hop1	Hop1	HORMAD1/2	ASY1
Red1	Rec10	SYCP2/3	ASY3/4

During meiosis, the cells undergo a single round of DNA replication followed by two rounds of cell division. This leads to

a reduction of the chromosome number, and the formation of four new haploid gametes from a single diploid cell (Figure 1). At the beginning of meiosis, the chromosomes are replicated and the sister chromatids are held together by cohesin (Smith and Roeder, 1997). After DNA replication, the cell introduces programmed breaks in the double-stranded DNA (DSBs). Normally those breaks would be repaired via the sister chromatid, but during meiosis, the usual repair mechanisms are modulated, and the breaks can be repaired via the homologous chromosomes leading to homologous recombination (reviewed in Subramanian and Hochwagen, 2014).

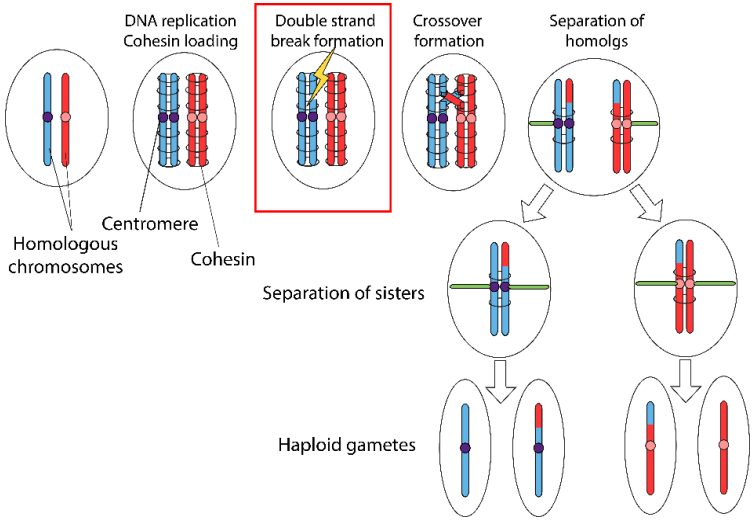

Figure 1: Overall mechanism of meiosis. At the beginning of meiosis, the homologous chromosomes are replicated and the cell introduces programmed DNA double-strand breaks (DSBs). Their repair via the homolog leads to the formation of crossovers, which serve as physical linkages between the homologs and allow them to be segregated into new daughter cells. The daughter cells undergo another round of division leading to the formation of four haploid gametes. Adapted from Weir lab.

DSBs are created by an evolutionary conserved topoisomerase Spo11 together with a group of proteins required for its activation and function (Bergerat et al., 1997; Keeney, 2008; Keeney et al., 1997; Lam and Keeney, 2014). After breaks are formed, Spo11 is covalently bound to the 5´-strands of both DNA ends until it is released by an endonucleolytic cleavage by Mre11, a component of the MRX complex (Mre11, Rad50, Xrs2) and Sae2 (Figure 2) (Neale et al., 2005). Following Spo11 release from the 5´-strand, the DNA ends are further resected by an exonuclease Exo1 to create a long single-stranded DNA tail first covered by RPA proteins and later bound by recombinases Rad51 and Dmc1 (Figure 2) (Garcia et al., 2011; Mimitou et al., 2017; Schiller et al., 2014; Sun et al., 1991; Symington, 2016; Zakharyevich et al., 2010). The nucleoprotein filament consisting of ss-DNA and recombinases invades the other chromosomes and identifies the homologous one by sequence similarity, which leads to the formation of a D-loop structure (Brown and Bishop, 2015; Hong et al., 2001; San Filippo et al., 2008). Once a stable D-loop is formed, the DNA break is repaired using the homologous chromosome as a repair template (Allers and Lichten, 2001; Bishop and Zickler, 2004; De Muyt et al., 2012; Hunter and Kleckner, 2001; Pyatnitskaya et al., 2019). This can lead to two different outcomes: a non-crossover (NCO) and a crossover (CO) (Figure 2).

Non-CO scenario happens when the invading strand is removed from the homologous chromosome and the DNA ends re-anneal. It results in a local transfer of a small part of the genetic

information from one homolog to the other one, but the exchange is not reciprocal (Martini et al., 2011; Palmer et al., 2003).

CO scenario follows stabilization and extension of the D-loop leading to the formation of a so-called double Holliday junction (dHJ), where both ends of the DSB are involved (Börner et al., 2004; Lynn et al., 2007; Pyatnitskaya et al., 2019). This intermediate is usually resolved into a crossover, where it leads to a reciprocal exchange of genetic information between the homologs (Gray and Cohen, 2016; Pyatnitskaya et al., 2019; Schwacha and Kleckner, 1995; Zakharyevich et al., 2012).

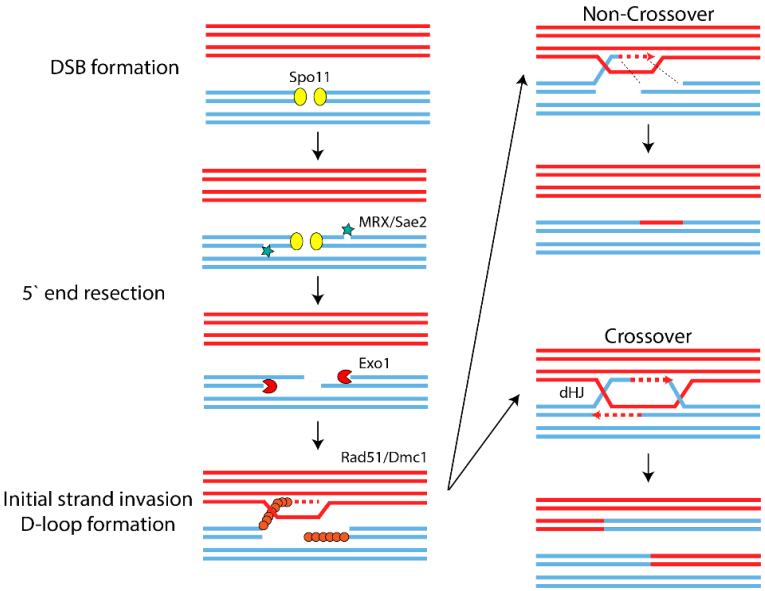

Figure 2: Homologous recombination. Meiotic recombination is initiated by the Spo11-introduced DSBs. They are resected first by action of MRX complex together with Sae2, followed by exonuclease Exo1. Single-stranded DNA, protected by RPA and later by Rad51/Dmc1, invades the homologous chromosome and forms a D-loop. It can be resolved in a crossover or non-crossover pathway. Adapted from Weir lab.

Once a link between the homologs is established, cohesin rings holding the sister chromatids connect also the homologs and a proteinaceous structure called synaptonemal complex connects them along their length (Kleckner, 2006; Zickler and Kleckner, 1999). It allows COs and recombination to complete until the homologous chromosomes are segregated into two new daughter cells at the end of the first meiotic division.

In the second meiotic division, the sister chromatids are segregated into new daughter cells without prior DNA replication, thus creating four haploid gametes with unique genomes.

1.2 DNA double-strand breaks

The introduction of DNA double-strand breaks (DSBs) is closely connected to a specialized architecture of the meiotic chromosomes. During meiosis, chromosomes are organized into a long nucleoprotein axis formed by proteins Hop1, Red1 and meiotic cohesin Rec8. Cohesin rings hold the sister chromatids together and extrude large DNA loops (Figure 3); in yeast, these loops can be up to 0.5 µm long, in mice they are roughly ten times bigger. The DSBs occur within those loops in hotspot regions marked with trimethylation of lysine 4 on histone H3 (H3K4me3) on nucleosomes (Borde et al., 2009; Pan et al., 2011; Tischfield and Keeney, 2012), to prevent splicing of the genes and destabilization of the genome. However, the DSB machinery (Spo11 complex) localizes in the proximity of the axis (Baudat and Nicolas, 1997; Buhler et al., 2007; Pan et al., 2011; Petes, 2001).

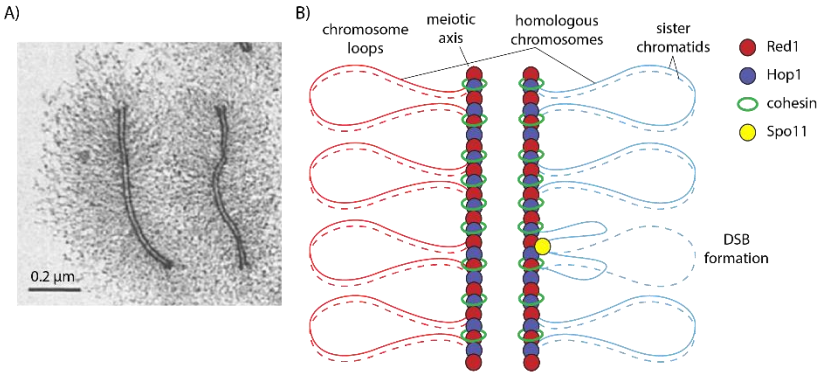

Figure 3: Loop-axis architecture of the meiotic chromosomes. A) Rotary shadowing electron-microscopy picture of the synapsed meiotic chromosome from moth *Hyalophora columbia*. Adapted from (Møens and Pearlman, 1988). B) Cartoon representation of two homologous chromosomes adopting meiosis-specific loop-axis organization. The sister chromatids are held together by meiotic cohesin Rec8, which extrudes large DNA loops from the axis. The break machinery (Spo11 complex) is localized by the axis, but the DSB hotspots are within the loops.

DSB formation requires a concerted effort of several proteins to create viable haploid cells. In *S. cerevisiae* it needs at least ten proteins: the Spo11 complex (Spo11, Ski8, Rec102, Rec104), the MRX complex (Mre11, Rad50, Xrs2) and the RMM proteins (Rec114, Mei4, Mer2) together with the regulatory enzymes which create the necessary post-translational modifications (PTMs; regulation of DSBs described in section 1.3) (Lam and Keeney, 2014). Without any of those players, DSB formation fails, leading to complete loss of meiotic recombination, failure to form synaptonemal complex, abnormal chromosomal segregation and ultimately to inviable spores (Ajimura et al., 1993; Cool and Malone, 1992; Engebrecht et al., 1990; Galbraith and Malone, 1992; Game et al., 1980; Gardiner et al., 1997;

Ivanov et al., 1992; Klapholz et al., 1985; Lam and Keeney, 2014; Malone et al., 1991; Malone and Esposito, 1981; Menees and Roeder, 1989; Pittman et al., 1998; Rockmill et al., 1995; Roeder et al., 1989).

1.2.1 Axial proteins Hop1 and Red1

The chromosomal axis in *S. cerevisiae* is formed by the HORMA-domain protein Hop1 (Hollingsworth et al., 1990), the core axial element Red1 (Smith and Roeder, 1997) and cohesin. During meiosis, the Scc1 kleisin subunit of cohesin is replaced by Rec8 (Klein et al., 1999), which localizes Hop1 and Red1 on gene ends and holds first the sister chromatids together (Panizza et al., 2011; Sun et al., 2015). Additionally, cohesin also connects the homologous chromosomes, once they are linked via crossovers (Brar et al., 2009) and plays a role in preventing DSBs in the centromeric region to maintain genome stability (Shonn et al., 2002).

Red1 contains a globular N-terminal domain, followed by a closure motif (CM; residues 340-352), a long unstructured region and a C-terminal coiled-coil responsible for Red1 tetramerization in a parallel-antiparallel configuration and filament formation (West et al., 2019, 2018). The CM in the centre of Red1 is responsible for interaction with the HORMA domain of Hop1 (West et al., 2018). Besides the N-terminal HORMA domain, Hop1 also contains an adjacent safety belt, a PHD domain zinc finger and a C-terminal closure motif (residues 585-605), which can interact in *cis* with the HORMA domain (West et al., 2018) thus creating a self-bound Hop1.

HORMA domains were first found in three proteins in *S. cerevisiae* (Hop1, Rev7 and Mad2) responsible for chromatin dynamics and structure (Aravind and Koonin, 1998). They can bind a closure motif and thus change their conformation and the position of the safety belt with respect to the HORMA. However, given that Hop1, as well as other meiotic HORMA-proteins from different organisms, contains a closure motif (CM) within its sequence (West et al., 2018), they can adopt an additional conformation. In this conformation its own CM is free, but the CM-binding site on the HORMA domain is occupied by a CM of another protein (Figure 4C). Within this thesis, I will be referring to those different conformations of Hop1 as unbuckled – no CM bound to the HORMA domain; closed – intramolecular HORMA-CM interaction; and exposed – extramolecular HORMA-CM interaction, its own CM is exposed and can interact with other binding partners (Figure 4).

The exposed conformation enables suggested head-to-tail oligomerization of Hop1, where a HORMA domain interacts with a CM of another Hop1 moiety and creates a long filament (Kim et al., 2014; West et al., 2019). This implied multimerization of Hop1 is supported by an *in vitro* observation, that the HORMA binds the Red1 CM with a higher affinity than its own CM (West et al., 2018). However, free Hop1 is almost exclusively in a closed conformation, where it binds its CM (West et al., 2018). This intramolecular interaction is difficult to break due to the high local concentration of the Hop1 CM. Therefore, the closed Hop1 found in cytoplasm or nucleoplasm has to be unbuckled by another player to be loaded on Red1 on the chromosomal axis

(Herruzo et al., 2021; Raina and Vader, 2020; Yang et al., 2020). Such a role is performed by a AAA+ ATPase Pch2 (TRIP13 in mammals), which opens both the closed Hop1 to load it on Red1, but also the Red1-bound Hop1 to remove it from chromosomes after DSBs are formed, upon synapsis. Removal of Hop1 from the axis effectively shuts down further DSB formation (Deshong et al., 2014; Subramanian et al., 2016).

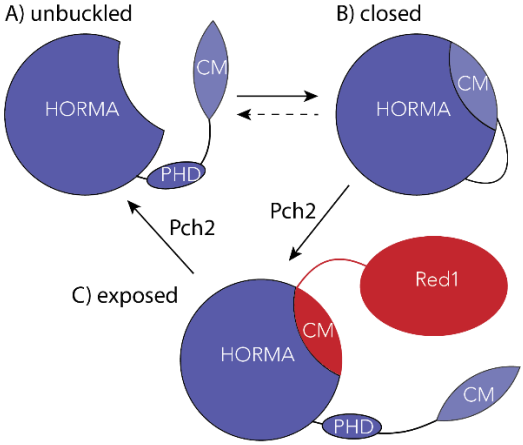

Figure 4: Hop1 conformations. A) Unbuckled Hop1, the HORMA domain does not interact with any CM. B) Closed Hop1, HORMA binds its CM. C) Exposed Hop1, HORMA binds a CM from another protein (in this case Red1, shown in red), its own CM is unbound.

Meiotic HORMA proteins are necessary to recruit an essential DSB formation protein Mer2 to chromosomes (Panizza et al., 2011). Fission yeast, *Schizosaccharomyces pombe*, and mouse homologs of Hop1 (Hop1 and HORMAD1) were shown to interact with homologs of Mer2 *in vivo* (Rec15 and IHO1; Table 1) (Kariyazono et al., 2019; Stanzione et al., 2016). Given that the chromatin association pattern of *S. cerevisiae* Hop1 is very

similar to that of Mer2, it is likely, that the budding yeast proteins interact as well (Panizza et al., 2011). However, this interaction was never detected *in vitro* nor confirmed in *S. cerevisiae*.

Even though Hop1 and Red1 are not strictly necessary for DSB formation, they both strongly promote it. The deletion of Red1 results in a 2.5-5-fold reduction in DSBs and deletion of Hop1 at least 10-fold (Blat et al., 2002; Kugou et al., 2009; Niu et al., 2005; Woltering et al., 2000). Their role is both to provide a structural scaffold for the DSB machinery (Murakami et al., 2020; Panizza et al., 2011), and also to stop the DSBs once the recombination took place and allow the cells to progress in the cell cycle.

1.2.2 Mer2 – an interactions platform protein

Mer2, also known as Rec107, is a highly divergent protein amongst the species originally found as a suppressor of the *mer1* phenotype (Engebrecht et al., 1991). It is expressed at low levels throughout the cell cycle, however, it includes an intron, which is spliced out only during meiosis in the presence of a meiosis-specific splicing factor Mer1 (Engebrecht et al., 1991; Nandabalan and Roeder, 1995), thus creating a functional protein essential for meiosis (Engebrecht et al., 1990).

At the beginning of meiosis, Mer2 is phosphorylated by S-phase specific cyclin-dependent kinase (S-CDK) within its N-terminal region and on C-terminal serine 271 and Dbf4-dependent kinase Cdc7 (DDK) on serine 29 (Henderson et al., 2006; Sasanuma et al., 2008; Wan et al., 2008). The phosphorylations on S29/30 are crucial for the assembly of the

DSB machinery by enabling the interaction with proteins Rec114 and Xrs2, part of the Spo11 activation mechanism and the MRX resection complex, respectively (Henderson et al., 2006; Sasanuma et al., 2008).

Rec114 together with Mei4 associates with Mer2 before DSB formation (Matos et al., 2008; Murakami and Keeney, 2014; Wan et al., 2008). Those three proteins are sometimes referred to as the RMM complex, based on their interaction in yeast two-hybrid assay, coimmunoprecipitation and partial foci overlap (Henderson et al., 2006; Li et al., 2006; Maleki et al., 2007). Interestingly, the chromatin localization of Rec114-Mei4 depends on Mer2, but Mer2 interacts with the axis even in absence of Rec114-Mei4 (Maleki et al., 2007; Panizza et al., 2011). Axis-bound Rec114-Mei4 interact with the Spo11 complex and play a role in its activation (Arora et al., 2004; Maleki et al., 2007; Prieler et al., 2005; Sasanuma et al., 2007). Even though the RMM is crucial for DSB formation, the complex was never observed *in vitro*. It can be explained by a recent suggestion, that rather than constituting a stoichiometric complex, the RMM proteins form a condensate on the chromosomal DNA (Claeys Bouuaert et al., 2021).

Another interaction partner of Mer2 is the MRX complex (Mre11, Rad50, Xrs2) (Arora et al., 2004; Henderson et al., 2006). Although MRX is a resection complex, it is also necessary for the DSBs to occur. Based on the yeast two-hybrid assay, Mer2 interacts with Xrs2 and weakly also with Mre11, thus bringing the resection machinery to the future break site. However, how is

this interaction facilitated or why is the resection machinery necessary for DSB formation is not known.

S. cerevisiae Mer2 is a homotetramer with a predicted coiled-coiled central domain between residues 165-232 (Acquaviva et al., 2013; Claeys Bouuaert et al., 2021; Sommermeyer et al., 2013). This core domain is responsible for interaction with protein Spp1 (Acquaviva et al., 2013; Sommermeyer et al., 2013), reader of the H3K4me3, DSB hotspot mark, on nucleosomes in the chromosomal loops (He et al., 2019; Miller et al., 2001). In the centre of the core domain of Mer2 lies valine 195; its mutation to aspartic acid disrupts Mer2 binding to Spp1 in yeast two-hybrid assay (Adam et al., 2018). However, this interaction was never shown *in vitro*.

Within the N-terminal region of Mer2 lies a surprisingly well-conserved patch (residues 52-72) (Tessé et al., 2017). Given its proximity to the N-terminal phosphorylations on Mer2 (Henderson et al., 2006), its role could correlate with an indicated phospho-dependent interaction with Rec114 and/or Xrs2 (Henderson et al., 2006). Interestingly, this region is also SUMOylated at the beginning of meiosis (Bhagwat et al., 2021) suggesting a SUMO-dependent interaction or conformational change. However, up to date, there is no data to explain the role of this region.

The C-terminal region of Mer2 was shown to play a role in DNA binding and DSB formation (Claeys Bouuaert et al., 2021), presumably by interacting with another binding partner. Even though many mechanistic details are missing, it is clear, that Mer2

serves as an interaction platform for the DSB machinery by connecting the DNA break site through its interaction with Spp1, the chromosomal axis possibly via Hop1 and the Spo11 machinery via its interaction with Rec114.

1.2.3 Spp1 – a nucleosome binder

Spp1 recognizes methylated nucleosomes (He et al., 2019; Miller et al., 2001) via its N-terminal PHD (plant homeodomain) zinc finger domain (residues 19-78). PHD domains have a specialized histone sequence reading ability, which is modulated by histone modifications (Sanchez and Zhou, 2011). The PHD domain of Spp1 has a preference for H3K4me3 peptide (K_D of 1.7 µM) over H3K4me2 (K_D of 3.8 µM) or mono- and non-methylated H3 (16.7 µM and no detectable binding, respectively) (He et al., 2019). Even though the affinities to di- and tri-methylated peptides are similar *in vitro*, the Spp1 preference for H3K4me3 *in vivo* is much stronger (Miller et al., 2001).

The interaction between the Spp1 and H3K4me2/3 is also regulated by other histone modifications. Phosphorylation of the N-terminus of H3 (H3T3ph, H3T6ph) completely disrupts or severely reduces Spp1 binding to nucleosomes (He et al., 2019) and asymmetric dimethylation of arginine 2 (H3R2me2assym) reduces Spp1 binding 2-fold (He et al., 2019; Kirmizis et al., 2007). The preferred combination of H3 modifications is found only at the first nucleosomes of the gene; therefore, it limits Spp1 binding to the transcription origin.

A crystal structure of the N-terminus of Spp1 (aa 1-124) bound to an H3K4me3 peptide (He et al., 2019) revealed, that the PHD

domain of Spp1 adopts a canonical Cys4-His-Cys3 fold (Figure 5A, shown in yellow) (Musselman and Kutateladze, 2011) stabilized by two zinc atoms (Figure 5A, shown in green). The C-terminal hydrophobic patch of the PHD domain is additionally stabilized by an adjacent C3H zinc finger domain (Figure 5A, shown in orange) (He et al., 2019), which includes another zinc. Although the C3H domain has a crucial role in the stabilization of the PHD domain, the structure suggests, that it does not directly contribute to the recognition of the modified histone tail (Figure 5A) (He et al., 2019).

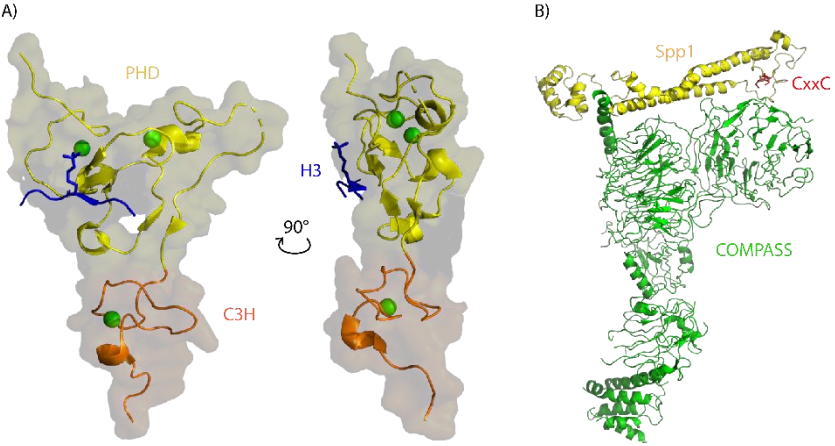

Figure 5: Structure of Spp1. A) Crystal structure of the PHD-C3H (yellow and orange respectively) domain in complex with H3 (blue). Zinc atoms are shown in green. From PDB: 6J2P (He et al., 2019) B) Cryo-electron microscopy structure of the COMPASS with the C-terminal part of Spp1 (yellow). CxxC motif is shown in red. From PDB: 6BX3 (Qu et al., 2018).

The C-terminal region of Spp1 is responsible for binding to COMPASS (Complex of Proteins Associated with Set1), an evolutionary conserved (Dou et al., 2006) complex of seven proteins associated with a catalytic protein Set1 (Briggs et al.,

2001; Roguev et al., 2001). COMPASS is responsible for the introduction of H3K4 methylations in vegetative cells in most mammals (Baudat et al., 2010; Myers et al., 2010; Parvanov et al., 2010) or in yeast also in meiosis (Borde et al., 2009; Sollier et al., 2004). The methyltransferase activity of Set1 is regulated by the associated proteins (Takahashi et al., 2011), particularly by Spp1. It promotes trimethylation, likely by opening up the catalytic site of Set1 and thus obtaining more space to accommodate the trimethylated lysine (Dehé and Géli, 2006; Takahashi et al., 2009). Its loss decreases H3K4me3 both *in vitro* (Kim et al., 2013; Takahashi et al., 2009) and *in vivo* (Dehé et al., 2006; Morillon et al., 2005; Schneider et al., 2005).

Based on the structure of COMPASS, the C-terminal region of Spp1 consists of four short stacked helices (aa 117-175) followed by two long intertwined helices (aa 187-349) (Figure 5B, shown in yellow) (Qu et al., 2018). However, the C-terminal region of Spp1 also interacts with the central coiled-coil domain of Mer2, which makes the Spp1 interactions with Mer2 and COMPASS mutually exclusive (Acquaviva et al., 2013; Sommermeyer et al., 2013). The interaction with Mer2 is impaired upon mutating an evolutionary conserved CxxC motif found in the loop between the two long helices of Spp1 (Figure 5B, shown in red) (Acquaviva et al., 2013). This motif gave the name to the mammalian homolog of Spp1, CXXC1 (Table 1).

During meiosis, Spp1 occurs in the cell in two distinct pools; as a part of the COMPASS and as a part of the DSB machinery, bound to Mer2. Interestingly, Spp1 in complex with Mer2 has a longer residence time on the nucleosomes compared to Spp1 in

COMPASS (Karányi et al., 2018), which suggest additional stabilization of the nucleosome-Spp1 interaction by Mer2. However, Spp1 itself is not crucial neither for DSB levels (Rockmill et al., 1995) nor for H3K4me3 levels (reduction by ~20%) (Sommermeyer et al., 2013), although its deletion significantly reduces both and leads to a change in the pattern of break formation. Presumably, Spp1 in meiosis provides the specificity of the DSB hotspot recognition, via its interaction with H3K4me3, and localizes the DSB machinery at the promoter regions.

The Spp1 homologs from *S. pombe* and mice both contain an N-terminal PHD domain, which regulate the function of the COMPASS also in those organisms (Brown et al., 2017; Lee and Skalnik, 2005; Mahadevan and Skalnik, 2016). Additionally, both of those proteins specifically recognize H3K4 (di- and tri) methylation on nucleosomes (He et al., 2019).

1.2.4 Nucleosomes and the H3K4me3 mark

Nucleosomes are the basic structural unit of eukaryotic chromatin. They consist of a histone octamer, formed by two copies of proteins H2a, H2b, H3 and H4, wrapped with two rounds of chromosomal DNA (Figure 6). Even though nucleosomes are very tightly packed, they are also highly dynamic, as they "slide" along the DNA (Pennings et al., 1991). Even though this dynamic behaviour complicates structural studies due to increased background noise and lack of regular crystal lattice, there are multiple structures available. The majority of nucleosome crystal structures consist of a nucleosome

core particle (NCP) with 146 or 147 bp of DNA, which does not contain any DNA overhangs (Figure 6). For structural and biochemical *in vitro* studies, the nucleosomes from *Xenopus laevis* appear to be the most stable and due to extremely high conservation of histones are commonly used also in interaction studies with proteins from different organisms. However, the histones exist also in different specialized variations, like CENPA, a centromeric version of H3, or H2AZ and H2AX, which reduces nucleosome stability and is associated with DNA repair, respectively (Felsenfeld and Groudine, 2003).

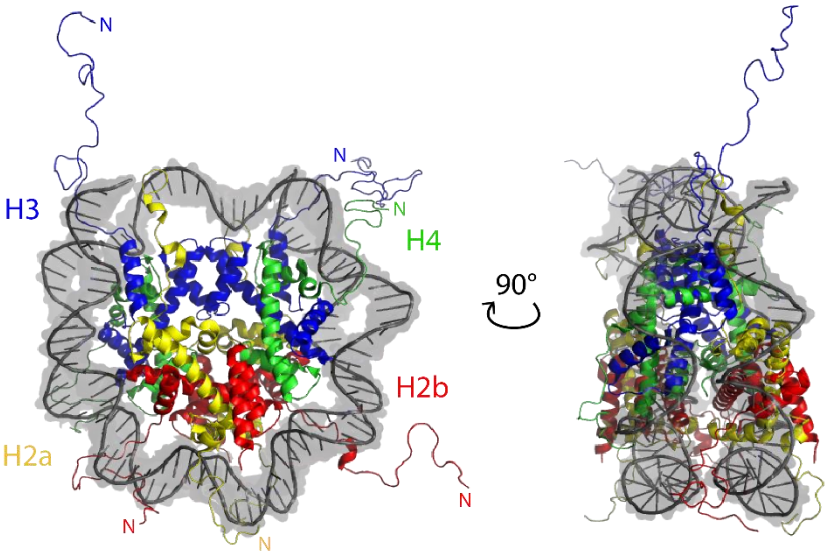

Figure 6: Structure of the nucleosome core particle (PDB: 1KX5) (Davey et al., 2002). The histone octamer consisting of two copies of H2a (yellow), H2b (red), H3 (blue) and H4 (green) is wrapped with two rounds of DNA (grey).

The core of the histone octamer is formed by the C-termini of the histone proteins, while the N-terminal tails are exposed to the solvent and can be heavily post-translationally modified. Those

modifications strongly determine the chromatin organization and affect transcription (Allfrey et al., 1964). Di- and tri-methylations of H3K4 occur in the proximity of transcriptionally active genes and probably allow transcription by recruiting nucleosome remodelling complexes and histone modifiers or by preventing transcription repressors to bind to chromatin (Ruthenburg et al., 2007; Smith and Shilatifard, 2010). In meiosis, H3K4me3 enables normal DSB levels by marking the DSB hotspots.

In most mammals, H3K4me3 is introduced either by COMPASS (in vegetative cells) or by a meiosis-specific methyltransferase Prdm9 (Baudat et al., 2010; Myers et al., 2010; Parvanov et al., 2010). Yeast, however, are lacking this protein and COMPASS is responsible for H3K4 methylations also during meiosis (Borde et al., 2009; Sollier et al., 2004).

1.3 Regulation of DSBs

To ensure at least one crossover per homologous chromosome pair, the cells introduce hundreds of DSBs into their genome (Kauppi et al., 2013; Keeney, 2008; Pan et al., 2011; Sun et al., 1989). However, a random formation of DNA breaks would have a devastating effect on the genome integrity and function. Therefore, there are several levels of very stringent control involved in DSB formation: spatial, temporal and numerical.

1.3.1 Spatial control

The spatial control of DSBs is closely connected to the loop-axis architecture of the meiotic chromosomes (Figure 3), where the DSB machinery is localized by the axis, but the DSB hotspots

lie within the DNA loops. The positions of the hotspots correlate with nucleosome-depleted regions at promoters (Pan et al., 2011) marked by trimethylation of lysine 4 on histone H3 (H3K4me3) (Borde et al., 2009; Pan et al., 2011; Tischfield and Keeney, 2012). Additionally, there is a sequence specificity, as the hotspots tend to be AT-rich (Borde et al., 2009; Pan et al., 2011; Tischfield and Keeney, 2012) and Spo11 has a preference for cleavage 3′ of a cytosine (Murakami and Nicolas, 2009; Pan et al., 2011). Conversely, the regions of telomeres and centromeres are protected from DSBs to maintain chromosome stability (Baudat and Nicolas, 1997; Blat et al., 2002; Blitzblau et al., 2007; Borde et al., 1999; Buhler et al., 2007; Gerton et al., 2000; Pan et al., 2011; Petes, 2001).

However, while the DSB hotspots are within the loops, the DSB machinery (Spo11 complex) lies in the proximity of the chromosomal axis formed by Hop1, Red1 and cohesin (Blat et al., 2002; Kim et al., 2010; Kleckner, 2006; Panizza et al., 2011). The current model (tethered loop-axis model; Figure 7) suggests proteins Spp1, an H3K4me3 mark reader, and Mer2, a chromosome axis-bound protein, to directly interact and thus be the key players in establishing the connection between break site and break machinery (Acquaviva et al., 2013; Sommermeyer et al., 2013). Mer2 connects the tethered loop to the Spo11 complex likely via its interaction with Rec114 and Mei4 and allows DSBs to occur (Maleki et al., 2007; Panizza et al., 2011).

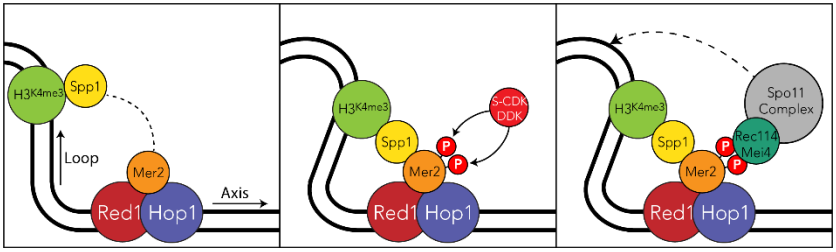

Figure 7: The loop-axis tethered model. In the early S-phase, Spp1 reads the H3K4me3 mark on nucleosomes and interacts with Mer2 loaded on the chromosomal axis. Mer2 is phosphorylated by S-CDK and DDK, which presumably allows it to bind Rec114-Mei4. That leads to the activation of the Spo11 complex and the formation of a DSB.

1.3.2 Temporal control

Temporal control guarantees, that the DSBs occur only after the chromosome replication is complete to prevent destabilization of the genome. It is ensured by meiosis-specific expression of DSB proteins (Spo11, Rec102, Rec104, Rec114, Mei4), meiosis-specific splicing (Mer2) (Keeney, 2008) and by the action of several kinases, which coordinate DSBs with the cell cycle progression (Borde et al., 2000; Henderson et al., 2006; Murakami and Keeney, 2014; Wan et al., 2008).

The beginning of the DSB formation correlates and is dependent on the activity of S-phase specific cyclin-dependent kinase (S-CDK) and Dbf4-dependent kinase Cdc7 (DDK) (Benjamin et al., 2003; Henderson et al., 2006; Masai and Arai, 2002; Matos et al., 2008; Wan et al., 2008). Amongst their targets belongs also protein Mer2, which is phosphorylated on several residues, but serines 29 and 30 were shown to be essential for DSB formation (Sasanuma et al., 2008; Wan et al., 2008). Those phosphorylations are necessary for Rec114-Mei4 loading onto

the axis and Mer2 interaction with the resection protein Xrs2 (Henderson et al., 2006; Panizza et al., 2011; Wan et al., 2008). While S-CDK functions globally in the whole nucleus, DDK is bound to the replisome (Matsumoto et al., 2005; Murakami and Keeney, 2014), thus it can phosphorylate only Mer2 located on the replicated parts of the chromosome and is limiting DSBs to those regions. After DNA replication, there is about a 90 min lag, presumably needed to construct the DSB machinery (Borde et al., 2000; Murakami and Keeney, 2014), since it is assembled before DSB formation.

However, DNA replication does not only facilitate DSB formation, it can also limit it by activation of Mec1 kinase (=ATR), which inhibits DDK. That leads to hypophosphorylation of Mer2 and limited loading of Rec114 and Mei4 on the chromosomal axis (Blitzblau and Hochwagen, 2013; Keeney et al., 2014). The temporal control mechanism is likely universal, it was shown, that blocking DNA replication in *S. pombe* also prevents DSB formation (Ogino and Masai, 2006). Additionally, early replication in *S. pombe* and mouse increases DSB levels as well (Pratto et al., 2021; Wu and Nurse, 2014).

1.3.3 Numerical control

Once a DSB is made, the cell has to ensure, that there will be no more breaks introduced in its proximity to maintain genome stability. This is controlled by the activation of several kinases and is closely related to the temporal control of DSBs. There are two mechanisms, which prevent too many DSBs from occurring: hotspot competition and DSB interference. The important

difference is that the first happens before DSB formation, whereas the latter after.

Hotspot competition is observed, when one strong hotspot suppresses DSB formation in its proximity (Keeney et al., 2014; Wu and Lichten, 1994; Xu et al., 1995). It is likely caused by competition for a limiting factor needed for DSB formation. Such a limiter could be the RMM proteins, due to their localization at the chromosomal axis, which reduces their mobility (Panizza et al., 2011). However, the exact mechanism of the hotspot competition remains unclear.

DSB interference limits DSB formation in the vicinity of an existing break. It is controlled by a kinase Tel1 (=ATM), which is activated as a response to DNA damage (Mohibullah and Keeney, 2017). Xrs2 (part of the resection MRX complex) contains a Tel1 binding domain (Shima et al., 2005), which likely directs Tel1 to the DSB site and allows it to phosphorylate Rec114, which probably results in disassembly or deactivation of the DSB machinery. Tel1 activity prevents further breaks not only in the proximity of an existing break on the same DNA molecule (within ~100 kb from an existing break) but also on the same locus of the sister chromatid (Fowler et al., 2018; Garcia et al., 2015; Zhang et al., 2011). Conversely, the absence of Tel1 promotes DSB formation (Garcia et al., 2015), presumably to ensure at least one CO per chromosome pair.

Additionally, there is also a DSB interference between homologous chromosomes, which ensures, that the DSBs do not occur at the same loci of the homologs. However, the mechanism

underlying this process is unclear (Zhang et al., 2011). Furthermore, recombination or synapsis defects (e. g. decreased Spo11 activity) activate kinase Mek1, which extends the window of opportunity for DSBs to ensure CO is formed (Acosta et al., 2011; Gray et al., 2013; Prugar et al., 2017).

Both hotspot competition and DSB interference have been observed also in *S. pombe* (Fowler et al., 2018). Additionally, *Drosophila* oocytes and mice defective in Tel1/ATM showed an increase in DSB formation (Joyce and McKim, 2010; Lange et al., 2011). This suggests, that the numerical control of DSBs is conserved amongst species.

DSBs are stopped by the formation of the synaptonemal complex (SC), which removes Hop1 from the chromosomal axis (Börner et al., 2008; Chen et al., 2014). This triggers the disassembly of many of the DSB proteins from the axis and allows all existing breaks to be repaired (Carballo et al., 2013; Kee et al., 2004; Li et al., 2006; Maleki et al., 2007; Mu et al., 2020; Panizza et al., 2011).

1.4 Research aims

The control process of introducing DSBs into the genome during meiosis is critical, but so far, this mechanism has predominantly been investigated *in vivo*. In such a setup, the large number of uncontrollable variables can lead to interference and problems with interpreting the data. Therefore, my principal aim is to study the crucial process of DSB control *in vitro* to gain a clearer insight into the molecular details of this process. To

achieve this, I investigate several aspects of DSB control, all bound to Mer2 as a key player in meiotic DSB formation.

Firstly, what is the role of Mer2 regarding its binding partner Spp1? Although it is suggested that Mer2 and Spp1 interact, the requirements to create an Spp1-Mer2 complex remain unclear. Both Spp1 and Mer2 are phosphorylated and SUMOylated during meiosis and surrounded by several other proteins. It is thus possible that a posttranslational modification or an additional binding partner is necessary to enable the Spp1-Mer2 interaction.

Secondly, how does Mer2 affect Spp1 interaction with nucleosomes? Spp1 interacts both with nucleosomes and with Mer2. But the order and dynamics of those interactions are unknown. Does Spp1 need to be bound to nucleosomes to interact with Mer2 or *vice versa*?

Thirdly, how is the connection between the break site and the break machinery established? The breaks occur within the DNA loop, but the break machinery is localized by the chromosomal axis. It has been suggested that Mer2 binds to Hop1, which is adopting a closed conformation when in the cytoplasm and an exposed conformation when loaded on the axis. However, it is not clear, how, if at all, Mer2 specifically recognizes the axial Hop1 and whether this Mer2-Hop1 interaction is enough to pull the Mer2-bound Spp1 with the nucleosome to the axis to allow breaks to be formed.

Finally, what are the roles of the conserved N- and C-terminal regions of Mer2? Mer2 sequence is very diverse amongst its homologs from other organisms except for two conserved

patches, one within each terminus. This could be explained by its interaction with a more evolutionary conserved partner. The necessity to keep this interaction throughout the evolution would keep the conserved regions of Mer2 from changing as quickly as the rest of the protein. However, these mysterious conserved binding partners remain unidentified.

2 Results

2.1 Analysis of the Spp1-Mer2 interaction

2.1.1 Design of Spp1 and Mer2 truncations and their purification

In vivo studies indicated, that Spp1 and Mer2 interact during meiosis and suggested, which domains are important for the interaction (Acquaviva et al., 2013; Sommermeyer et al., 2013). However, it is not entirely clear, whether the proteins interact directly and also in the absence of other cellular elements and whether the suggested interaction domains are the only ones responsible for binding or only contribute to it. These questions can be answered by a deeper *in vitro* analysis in a controlled environment. To provide means for further investigating the Spp1-Mer2 complex formation, I first designed several truncations of both proteins.

Spp1 contains a PHD and C3H domain within its N-terminus, which serves as a nucleosome binding domain (He et al., 2019; Miller et al., 2001), and a C-terminal α-helical domain, responsible for COMPASS interaction (Figure 8) (Qu et al., 2018). This α-helical domain was also suggested to interact with Mer2 (Acquaviva et al., 2013; Sommermeyer et al., 2013; Figure 8). To reveal the Mer2-interaction domain, I created two truncations of Spp1. The first comprises its PHD domain with an adjacent C3H domain and a small overhang ($Spp1^{N\text{-}170}$) and the second is its presumed Mer2 interaction domain with an N-terminal overhang ($Spp1^{169\text{-}C}$) (Figure 8 and Figure 10A).

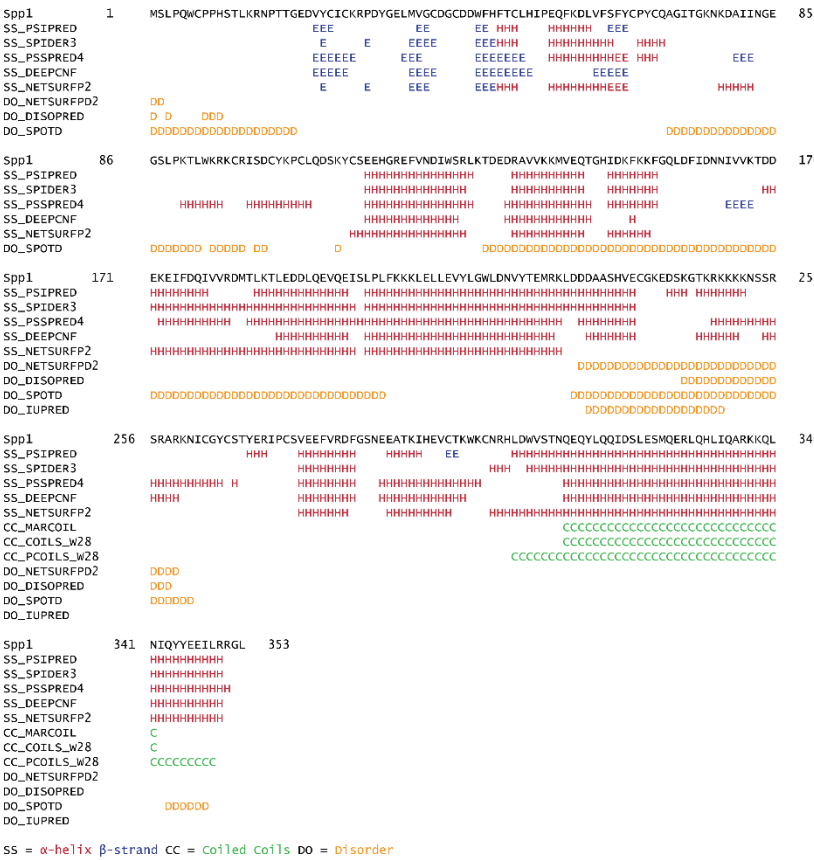

Figure 8: Secondary structure prediction of Spp1. Created using MPI Bioinformatics Toolkit (Zimmermann et al., 2017)

Mer2 contains an evolutionary conserved α-helical core domain, specifically residues 165-232 (Figure 9) (Acquaviva et al., 2013; Claeys Bouuaert et al., 2021; Sommermeyer et al., 2013), surrounded by largely unstructured terminal regions. The core of Mer2 was suggested to interact with Spp1 *in vivo* (Acquaviva et al., 2013; Sommermeyer et al., 2013), but the role of the Mer2 terminal regions on the interaction with Spp1 (if they do have any) is unclear. Therefore, I created several truncations:

the core itself (Mer2$^{140-256}$, referred to as Mer2^{core}), the N-terminal region of Mer2 without and with the core domain (Mer2^{N-139} and Mer2^{N-256}, referred to as Mer2$^{\Delta C}$), and the C-terminal region of Mer2 without and with the core domain (Mer2^{256-C} and Mer2^{140-C}, referred to as Mer2$^{\Delta N}$) (Figure 10B).

Figure 9: Secondary structure prediction of Mer2. Created using MPI Bioinformatics Toolkit (Zimmermann et al., 2017)

Both Spp1 and Mer2 are SYMOylated during early meiosis (Bhagwat et al., 2021) and Mer2 is additionally phosphorylated during the early S-phase by S-CDK and DDK (Henderson et al., 2006; Murakami and Keeney, 2014) (analysis of Mer2 phosphorylation in fraction 2.5). To exclude the possible effect of

the post-translational modifications (PTMs) on the Spp1-Mer2 complex formation, the proteins and their truncations were produced in *E. coli*. This resulted in a homogenous population without any PTMs. The proteins were purified in three steps: affinity chromatography, ion exchange and size-exclusion chromatography (Figure 11).

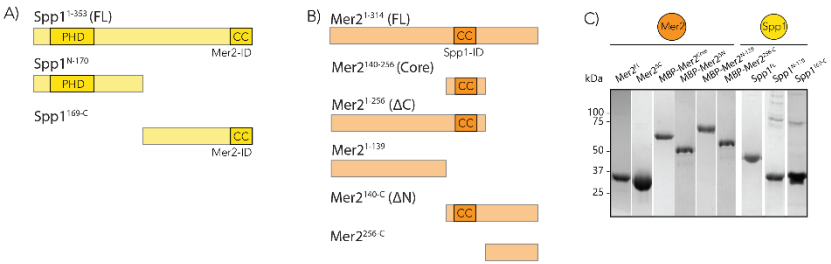

Figure 10: Truncations used in this study. A-B) Domain diagram of Spp1 and Mer2 and their truncations. A) Spp1 contains an N-terminal PHD domain and a C-terminal predicted coiled-coil, likely responsible for Mer2 interaction. B) Mer2 contains a central predicted coiled-coil, presumably responsible for Spp1 interaction. C) Purified Spp1 and Mer2 constructs on SDS-gel stained with InstantBlue.

To increase yield and solubility, they were produced with a cleavable N-terminal MBP- or GST-tag (unless specified differently in the text). In the case of $Mer2^{FL}$ and $Mer2^{\Delta C,}$ the tag could be removed with the 3C protease of HRV. The tag-cleavage from $Mer2^{core}$ and $Mer2^{\Delta N}$ was not possible, presumably due to steric hindrance of the cleavage site to the protease. To increase the stability, the terminal constructs, $Mer2^{N-139}$ and $Mer2^{255-C}$, also contain the N-terminal MBP-tag. All of the proteins could be purified to a high level of homogeneity and were stored at -80 °C for further analyses (Figure 10C).

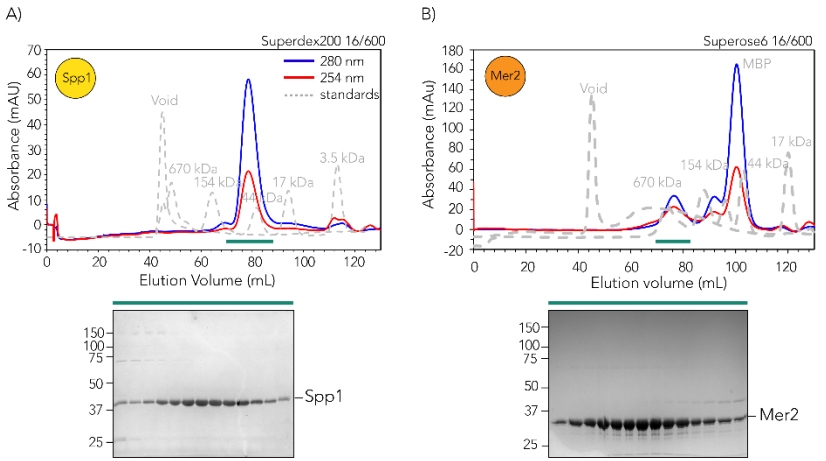

Figure 11: Purification of Spp1 and Mer2. Size-exclusion chromatogram and a 10 % SDS-gel of fractions containing untagged A) Spp1 or B) Mer2. A) GST was cleaved before loading on the column and was caught by a GST-column attached after the SEC column. In the early fraction are visible weak bands corresponding to non-cleaved GST-Spp1 and GST alone B) MBP was cleaved before loading on the column as well and was separated on SEC without an additional column. In the Mer2 fractions is visible slight degradation. The relative absorbance of the complex at 280 and 260 nm shows that it is free of any significant nucleic acid contamination. Molecular weight markers are shown in grey.

2.1.2 Characterization of the Spp1-Mer2 complex

Once the purification conditions for the proteins were established, the next step was to test their interaction. Co-expression can enhance complex formation because it gives the proteins time to interact while they are still in the cell. However, co-expression of Spp1 and Mer2 failed to produce both the complex and the individual proteins. Therefore, I tried to express the proteins separately and co-lyse them, which yielded a substantial amount of the untagged Spp1-Mer2 complex (Figure

12A). Interestingly, the complex eluted almost at the same elution volume as the 670 kDa globular marker, suggesting either that the complex adopts a higher-order stoichiometry, and/or that the complex is very elongated and thus travels faster within the chromatography column, and elutes earlier than globular proteins used for markers.

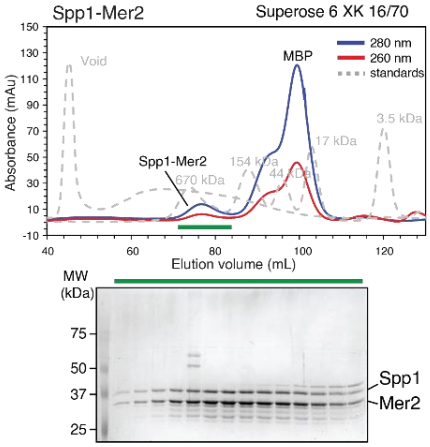

Figure 12: Purification of the Spp1-Mer2 complex. A complex of full-length Spp1 and Mer2 was purified to homogeneity with a slight degradation of Mer2. N-terminal MBP-tags were removed before loading on the size-exclusion chromatography column. Molecular weight markers are shown in grey.

To reveal the stoichiometry of the complex, the proteins were analyzed both individually and in complex using size-exclusion chromatography coupled with multi-angle light scattering (SEC-MALS) (Figure 13). Mer2 constructs were used as MBP-fusions to better differentiate the oligomerization stage. While the theoretical size of a full-length MBP-tagged Mer2 is 78.5 kDa, the measured size was 316 kDa, which suggests that Mer2 is a tetramer. The same also applied to the MBP-Mer2^{core}, where the

calculated size is 56.5 kDa, but the measured size was 222 kDa. On contrary, neither of the Mer2 terminal regions proved to be tetrameric, with the N-terminal region of Mer2 (Mer2^{N-139}) being only 68 kDa (calculated size is 58 kDa) and the C-terminal region of Mer2 (Mer2^{140-C}) 120 kDa (calculated size is 53 kDa) (Figure 13A and D). These findings are in agreement with the recently published data (Claeys Bouuaert et al., 2021), that Mer2 forms a tetramer, but additionally demonstrate, that the core of Mer2 is exclusively responsible for the tetramerization, with the terminal regions not contributing to the oligomerization of the protein.

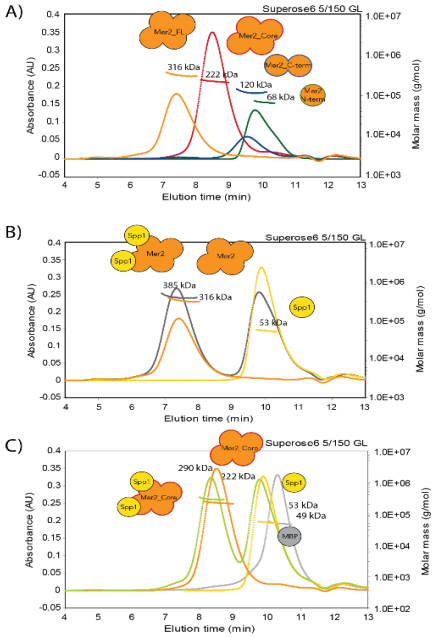

D) SEC-MALS experiments summary

Sample	SEC-MALS MW (kDa)	Stoichimetry	Calc. MW (kDa)
MBP-Mer2^{FL}	316	tetramer	314
MBP-Spp1	92	monomer	90
Spp1	53	monomer	42
Spp1+ MBP-Mer2^{FL}	385	2 x Spp1 4 x Mer2	397
Spp1+ MBP-Mer2$^{140-256}$	290	2 x Spp1 4 x Mer2	309
MPB-Spp1+ MBP-Mer2$^{40-271}$	417	2 x Spp1 4 x Mer2	389
MBP-Mer2$^{140-256}$	222	tetramer	226
MBP-Mer2^{N-139}	68	monomer	58
MBP-Mer2^{255-C}	120	dimer	106

Figure 13: SEC-MALS of the Spp1-Mer2 complex. A) MBP-Mer2 constructs with cartoons of measured oligomerization state. B) MBP-Mer2^{FL} with untagged Spp1. C) MBP-Mer2^{core} with untagged Spp1 and MBP as a control. D) Summary of the SEC-MALS experiments. Coloured dots refer to respective profiles in A-C

Spp1 alone is a monomer (calculated size is 42 kDa and measured 53 kDa), but upon interaction with full-length Mer2, it forms a large complex of 385 kDa (Figure 13B and D), suggesting that a Mer2 tetramer binds two copies of Spp1. Additionally, I tested whether the implied Spp1-interaction domain of Mer2 (residues 165-232) localized within the core of Mer2 is sufficient to form a stable complex with Spp1. Indeed, I observed a large complex of 290 kDa of Spp1 with $Mer2^{core}$ (Figure 13C and D). It confirms, that the $Mer2^{core}$ is sufficient for binding to Spp1 in a 2:4 stoichiometry. Additionally, these data show, that Spp1 and Mer2 form a size-exclusion stable complex independently on any PTM.

Even though it is clear, that the $Mer2^{core}$ is enough to create a stable complex with Spp1, it remains unknown whether the terminal regions of Mer2 play any role in Spp1 binding. To investigate this, I fluorescently labelled Spp1 and analyzed its binding to different truncations of Mer2 via microscale thermophoresis (MST; Figure 14A). Since not all Mer2 constructs could be prepared without an MBP-tag, I used all Mer2 versions as MBP-tagged fusions to ensure comparable data should Spp1 unspecifically interact with MBP. Results showed that Spp1 indeed interacts with the $Mer2^{core}$ with a very high affinity of 137 nM ± 4 (Figure 14A – red trace). However, $Mer2^{FL}$ proved to have an even stronger affinity for Spp1 (24 nM ± 2; Figure 14A – orange trace), suggesting either that there is an additional contribution of Mer2 terminal regions to the Spp1 interaction, or that the interaction domain is larger than the $Mer2^{core}$ truncation. Both Mer2 terminal regions interact with

Spp1 only very weakly, similarly to MBP control alone, but their faint contribution can explain the difference between the affinities of Spp1-Mer2^{FL} and Spp1-Mer2^{core}.

To confirm the strength of the Spp1-Mer2 interaction, John Weir performed isothermal calorimetry (ITC). Given that this method requires a substantial amount of initial material, Mer2^{core} was used, which was expressed in larger quantities than the full-length protein. The measured affinity was 36.7 nM ± 11.4 (Figure 14B), slightly higher than the affinity determined by MST. This marginal discrepancy could be explained by different experimental conditions, pipetting error or an effect of the Spp1 labelling. Regardless, both analyses confirmed that Spp1 interacts remarkably strongly with the core of Mer2.

The Mer2-interaction domain of Spp1 has been suggested to lie within its C-terminal region (Acquaviva et al., 2013; Sommermeyer et al., 2013). To confirm the localization of the binding motif on Spp1, I performed a pulldown with Strep-tagged Mer2 and full-length Spp1 or its truncations, in which were deleted either the suggested C-terminal Mer2-binding domain (Spp1$^{N\text{-}170}$) or the N-terminal PhD domain (Spp1$^{169\text{-}C}$) (Figure 14C). As expected, only the Spp1^{FL} and Spp1$^{169\text{-}C}$, containing the C-terminal domain, interacted with Mer2, confirming previous *in vivo* data *in vitro*.

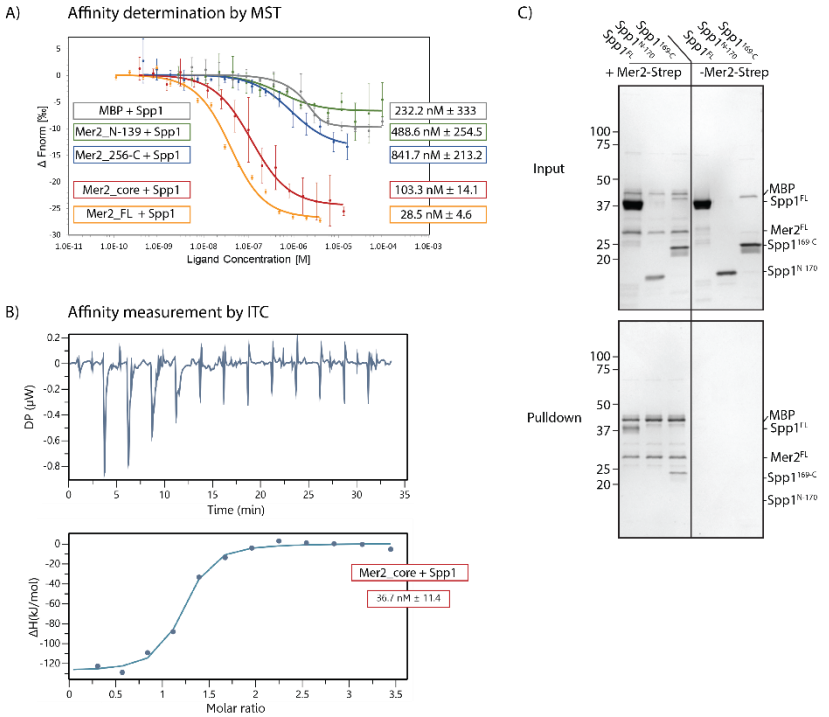

Figure 14: Determination of the affinity between Spp1 and Mer2 and identification of their interaction domains. A) Affinity measurement between MBP-tagged Mer2 constructs and labelled Spp1 determined via MST. Error bar, SEM; n=3 B) Affinity measurement between MBP-tagged Mer2^{core} and full-length Spp1 via ITC. C) Pulldown of Spp1 truncations with Strep-tagged Mer2^{FL} analyzed on 10-20 % SDS-gel. In the elution sample is visible excess of MBP coming from the Spp1 samples, which unspecifically interacts with Mer2.

Taken together, these data confirm *in vitro* that the C-terminal region of Spp1 directly interacts with the helical core of Mer2 as previously reported *in vivo* (Acquaviva et al., 2013; Sommermeyer et al., 2013). Additionally, they demonstrate, that the Mer2^{core} is solely responsible for the tetramerization of the

protein. Furthermore, the data reveal a 2:4 stoichiometry of the Spp1-Mer2 complex and the affinity as low nanomolar.

2.1.3 Structural analysis of the Spp1-Mer2 complex

The data from the previous chapter show that the Spp1-Mer2 complex adopts a 2:4 stoichiometry (Figure 13). However, apart from the general reciprocal binding regions, it is unclear how the proteins are organized within the complex. To reveal the spatial coordination of the complex, I crosslinked Mer2 separately and in complex with Spp1 with disuccinimidyl dibutyric urea (DSBU; 11 Å spacer) and Franziska Müller with Petra Janning (Max Planck Institute of Molecular Physiology, Dortmund) analyzed the samples by mass-spectrometry (Figure 15A).

The crosslinking pattern of Mer2 alone and in complex with Spp1 were very similar, suggesting no significant conformational changes in Mer2 upon binding to Spp1. Additionally, there were many cross-links in Mer2 between the same residue which confirms Mer2 oligomerization, consistently with the SEC-MALS analysis (Figure 13) and recent publication (Claeys Bouuaert et al., 2021).

The Spp1 domain that interacts with Mer2 lies within its C-terminal region as shown by a pulldown (Figure 14C) and *in vivo* studies (Acquaviva et al., 2013; Sommermeyer et al., 2013). However, the crosslinks between Spp1 and Mer2 localized instead rather within the N-terminal region and the centre region of Spp1. These data suggest that although Spp1 interacts with Mer2 via its C-terminal helical domain (Figure 14), there might an additional contribution of the N-terminal region of Spp1.

Although the interaction provided by the N-terminal part of Spp1 is not strong enough to form a stable complex of $Spp1^{N-170}$ with Mer2 *in vitro*, it can further stabilize the Spp1-Mer2 complex. Additionally, it has to be considered, that the crosslinkers are connecting the proximal residues independently on whether they interact with each other or not.

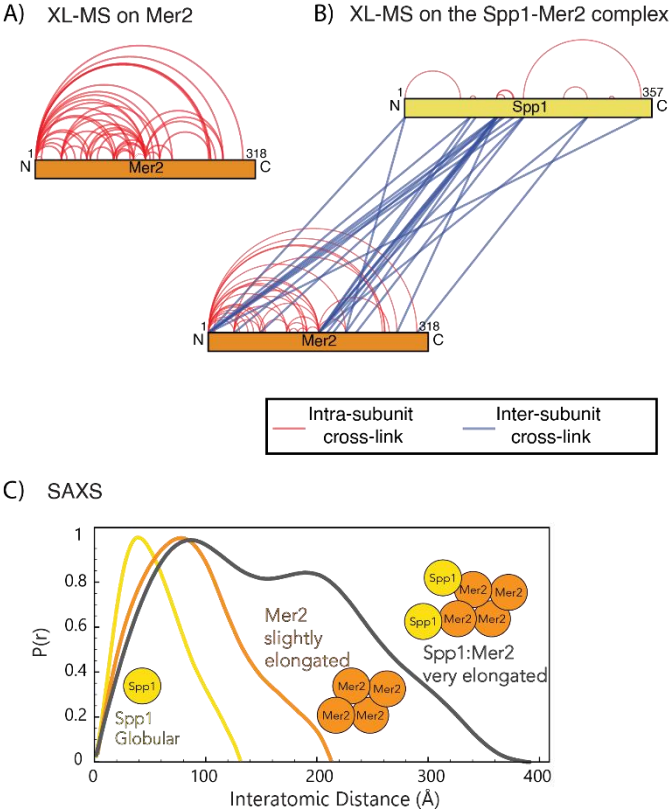

Figure 15: Biophysical analysis of the Spp1-Mer2 complex. A-B) Crosslinking mass-spectrometry pattern of A) Mer2 alone and B) in complex with Spp1. Intra-subunit cross-links are marked in red, inter-subunit cross-links in blue. Crosslinks were filtered to give a 1 % false discovery rate and visualized by xVis (Grimm et al., 2015). C) SAXS analysis of the Spp1-Mer2 complex and

its subunits alone revealed an elongated shape of Mer2 and the Spp1-Mer2 complex.

To further investigate the organization of the Spp1-Mer2 complex, it was analyzed using size-exclusion chromatography coupled with small-angle x-ray scattering (SAXS) (Figure 15B). This experiment revealed Spp1 to be a rather globular protein (~13 nm in diameter), as expected based on the secondary sequence prediction (Figure 8), while Mer2 adopted an elongated shape (~21 nm long) consistently with both the secondary structure prediction (Figure 9) and its early elution from the size exclusion chromatography column (Figure 11B). However, the Spp1-Mer2 complex is even more elongated by comparison (~38 nm long). This suggests that there is either a conformational change in Mer2 upon binding to Spp1, which is unlikely bearing in mind that the XL-MS profiles of Mer2 alone and in complex with Spp1 were very similar (Figure 15A), or that the PHD domains of Spp1 are reaching out of the core of the complex alongside the $Mer2^{core}$, thus extending the rod-like shape of Mer2.

To further reveal the organization of the Spp1-Mer2 complex, I aimed to determine the structure experimentally. To do this, I tried three different approaches: crystallization (summarized in Table 2), negative staining electron-microscopy and cryo-electron microscopy (Figure 16). Unfortunately, none was successful.

Generally, the samples suitable for crystallization are small molecules or complexes, which are rigid, stable and lack flexible domains or regions. I initially attempted to crystalize the Spp1-

Mer2 complex using $Spp1^{FL}$ and MBP-$Mer2^{core}$ lacking the flexible terminal regions to improve the rigidity of the complex. The body of such a complex is formed nearly exclusively by a stable α-helical bundle of four copies of $Mer2^{core}$ and two copies of the $Spp1^{C\text{-}term}$. Based on the XL-MS data, the PHD domain of Spp1 is in proximity to Mer2 (Figure 15A), hence it might adopt a stable conformation in respective to the $Mer2^{core}$. The MBP-tag on this truncation of Mer2 cannot be cleaved, likely due to sterical hindrance compounded by oligomerization. MBP-tags are known to increase the solubility of the fusion partner, which is undesired during crystallization. However, this issue can be overcome by increasing the concentration. The optimal crystallization concentration of the proteins determined by a pre-crystallization screen was 10.45 mg/ml for the Spp1-Mer2 complex and 20-50 mg/ml for Mer2 alone. To increase the chance of obtaining diffraction-quality crystals, I used eight different crystallization screens for the Spp1-Mer2 complex and five for Mer2 along with three different protein:precipitant ratios, followed by an increase of concentration of $Mer2^{core}$ (summarized in Table 2). However, neither Spp1-Mer2 nor Mer2 alone produced any usable crystals. It may have been caused by the flexibility of the proteins or the solubilization effect of the uncleavable MBP-tag on Mer2.

An alternative solution to solving the structure of the Spp1-Mer2 complex is crystallizing the complex from another organism. My former student David Liedtke tried to obtain a crystal structure of Spp1-Mer2 from *Kazachstania nagashii* during his bachelor thesis (Liedtke, 2020). Unfortunately, although this approach provided at least some microcrystals of

Spp1-Mer2, no diffraction data could be acquired due to the longer time required for crystallization optimization.

Table 2: Crystallization of Mer2 and Spp1-Mer2 complex

Construct	**Concentration**	**Screens**
Spp1/MBP-Mer2^{core} (co-lysed)	10.45 mg/ml 20 mM HEPES pH 7.5, 150 mM NaCl, 5 % glycerol, 1 mM TCEP	Classic I Classic II PEG I PEG II Protein Complex JCSG+ Cryos Morpheus
MBP-Mer2^{core}	21.7 mg/ml 25 mM HEPES pH 7.5, 150 mM NaCl, 5 % glycerol, 0.5 mM TCEP	Classic PEG I PEG II JSCG+ Morpheus
MBP-Mer2^{core}	40 mg/ml 20 mM HEPES pH 7.5, 150 mM NaCl, 5 % glycerol, 1 mM TCEP	PEG I PEG II Morpheus
MBP-Mer2^{core}	110 mg/ml 20 mM HEPES pH 7.5, 150 mM NaCl, 5 % glycerol, 1 mM TCEP	PEG I PEG II Morpheus

Higher flexibility and the presence of an MBP-tag do not necessarily pose a problem for electron microscopy (EM). For this method, the main limitation is the size of the specimen. To obtain a sufficiently good final resolution, the particles should be at least 100 kDa. The 2:4 Spp1-Mer2 complex, with both proteins full-length and untagged, is 228 kDa and therefore suitable for EM analysis. Negative staining EM requires a very little sample,

only 4 µl of 20-50 µg/ml, and can thus be used for a broad screening e.g., to check the quality of a protein. After several attempts, I obtained acceptable staining of an Spp1-Mer2 sample (Figure 16A), but it appeared as though the complex had partially precipitated, probably due to the staining procedure. Such a decrease in protein stability during staining is a relatively common problem, which can be overcome by optimization of the staining or the buffer composition. However, in this case, I decided against lengthy optimization of the negative staining EM and instead moved on to cryoEM, which uses an unstained native sample.

The main advantage of cryoEM over negative staining EM is the final resolution obtained. Negative staining EM can reach a resolution up to ~18-20 Å, which is sufficient to determine the overall shape of the specimen but does not provide enough details to build the model of the protein. Nevertheless, it can be used to model previously known parts of the structure into the final form and to give an overall idea about the shape and organization of the specimen. By contrast, cryoEM can reach subatomic resolution and thus can be used to determine structure *ab initio*. However, in comparison to negative staining, it requires higher concentrations of the sample and is less tolerant to high salt and detergents.

Given that Mer2 is more stable in high-salt buffers with glycerol and Spp1 is stabilized by zinc, the buffer composition had to be greatly optimized to stabilize both of the proteins and satisfy the demands of the technique. In the end, I used 0.1 mg/ml Spp1-Mer2 complex in 10 mM HEPES pH 7.5, 150 mM NaCl,

1 mM $MgCl_2$, 10 mM $ZnCl_2$, 1 mM TCEP and copper grids for cryoEM. This yielded micrographs with visible C-shaped elongated protein complex (Figure 16B). Although the complex is not homogeneous enough, and cannot, therefore, be used for data collection and structure determination, it confirms the previous observations that the Spp1-Mer2 complex is very elongated and suggests, that it is rather flexible (Figure 13A and Figure 15B).

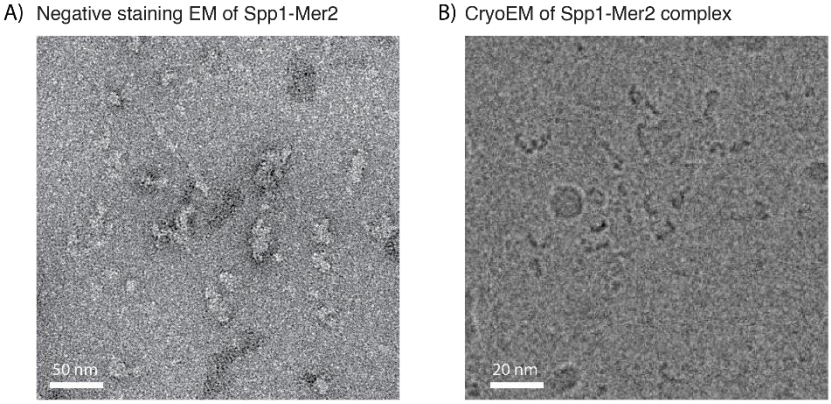

Figure 16: Electron microscopy of the Spp1-Mer2 complex. A) Negative staining microscopy of the Spp1-Mer2 complex. B) CryoEM micrograph of the Spp1-Mer2 complex revealed C-shaped particles.

A more homogeneous sample could be obtained by increasing the rigidity of the complex. The PHD domain of Spp1 likely moves rather freely, since it lacks stabilization by its binding to the nucleosome. Moreover, Mer2 interacts with Spp1 via its core, hence the position of the Mer2 terminal regions can vary and increase the heterogeneity of the complex on the grids. Although the XL-MS data suggested additional interaction between Spp1 and Mer2 also outside of their binding motifs (Figure 15A), the

affinity between those additional binding motifs might be too weak to stabilize the complex under used conditions. Therefore, using truncations of Spp1 and/or Mer2 might improve the rigidity and homogeneity of the complex in grids.

The flexibility of the complex and the specific demands on the buffer composition complicate the structural analysis of the Spp1-Mer2 complex. To solve its structure, one could create a complex containing only the C-terminal α-helical part of Spp1 and $Mer2^{core}$ with a longer linker between the MBP-tag and the protein to enable the tag cleavage. In principle, such a complex would contain only an alpha-helical bundle of Spp1 and Mer2. In that case, it has to be considered, how informative is such a structure. To obtain a structure of the whole complex, electron microscopy seems like a more realistic option given the size of the full-length complex (228 kDa) and its flexibility. Since there are distinct particles on the grid (Figure 16B), the biggest problem is the high flexibility of the complex. That can be overcome by mild cross-linking or by a change in the buffer composition. However, the buffer suitable for the Spp1-Mer2 is already rather complex to satisfy both of the binding partners, therefore mild-crosslinking and an increase in the concentration is a coherent step toward the structure of the Spp1-Mer2 complex.

Nevertheless, the SAXS data and the XL-MS alone provide valuable insight into the organization of the Spp1-Mer2 complex. They suggest that the complex is very elongated with the PHD domains of the two copies of Spp1 facing outwards alongside the helical core of Mer2. Furthermore, the data implies, that there is an additional weak interaction between the N-terminal PHD or

C3H domain of Spp1 and Mer2. Altogether, even though I was not able to solve the structure of the Spp1-Mer2 complex, the additional biophysical analysis combined with the biochemical data shed a light on the architecture of the complex.

2.2 Interaction of Spp1-Mer2 with nucleosomes

2.2.1 Spp1-Mer2 binding to H3K4me3 nucleosomes

Spp1 serves as a nucleosome H3K4me3-reader during meiosis. To study this interaction and how it may be influenced by Mer2, I prepared synthetic recombinant modified mononucleosomes (MN) using the methyl-lysine analogue method (Simon et al., 2007). The naturally occurring cysteine in the sequence of histone H3 was mutated to alanine (C110A) and the desired methylated lysine was mutated to cysteine (K4C). Purified mutated histone was subsequently converted to a trimethyl-lysine analogue via reaction with an alkylating agent (Simon et al., 2007). The histone was then reconstituted into octamers and wrapped with 145 and 167 bp of Widom sequence DNA (Lowary and Widom, 1998) to result in a nucleosome core particle (NCP) and a mononucleosome (MN), respectively. This approach gave me full freedom to prepare different versions of nucleosomes with or without modifications and to test their interaction with other proteins.

The nucleosome has an intrinsic two-fold symmetry; it includes two copies of each of the histones. Since Spp1 is dimerized upon binding to Mer2, I hypothesized that this dimerization could strengthen Spp1 interaction with

nucleosomes. To test this hypothesis, I performed an electron mobility shift assay (EMSA) with H3K4me3 nucleosomes and monomeric Spp1, dimerized Spp1 via an N-terminal GST-tag and also dimerized Spp1 via interaction with Mer2 (Figure 17A). Dimerization via GST increased the apparent binding of Spp1 to nucleosomes, but interestingly, Spp1 dimerized via its interaction with Mer2 appeared to have an even stronger affinity to the modified nucleosomes. However, one has to keep in mind that EMSA experiments are performed at very low salt, therefore hydrophobic interactions are strongly favoured over electrostatic ones, which can provoke misleading interpretations.

To confirm the apparent increase in affinity to nucleosomes upon Spp1 dimerization in a more natural environment, I performed a pulldown with commercial biotinylated modified and unmodified nucleosomes as bait and Spp1, GST-Spp1 and Spp1-Mer2 as prey (Figure 17B). Since Spp1 specifically recognizes the H3K4me3 mark on nucleosomes (He et al., 2019), the unmodified nucleosomes served as a control for the unspecific binding of the Spp1 variants. The results of the pulldown were consistent with the EMSA. Monomeric Spp1 was barely visible on the gel, whereas dimerized GST-Spp1 interacted stronger with the modified nucleosomes. The Spp1-Mer2 complex also showed strong binding to the modified nucleosomes, however, I also observed an additional binding of Mer2 to unmodified nucleosomes in the control line. This could have been caused by an unspecific binding of Mer2 either to the beads or the nucleosomes, or it could be a sign of interaction between Mer2 and nucleosomes (further analysis in section 2.2.2).

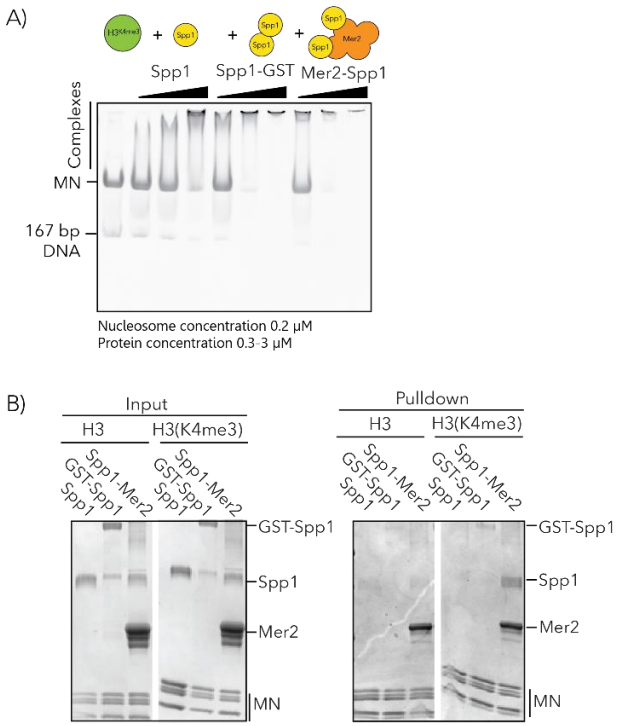

Figure 17: Interaction of the Spp1-Mer2 complex with H3K4me3 nucleosomes. A) EMSA with modified nucleosomes and monomeric Spp1 or Spp1 dimerized via GST-tag or Mer2 interaction. B) Pulldown with biotinylated nucleosomes analyzed on 10-20 % SDS-gel and stained with InstantBlue. As bait were used the same proteins as in A).

Next, I tested whether Spp1-Mer2 could form a stable complex with the nucleosomes in solution. 5 µM Spp1-Mer2 complex was mixed with 5 µM H3K4me3 nucleosomes and incubated for 1 hour on ice to allow the complex to assemble and reach an equilibrium. The reaction was then analyzed on an analytical size-exclusion column (Figure 18) and eluted fractions were loaded on a 10-20 % SDS-gel. Even though the absorbance peak was not very sharp, presumably due to suboptimal buffer composition, a

clear shift in the elution volume could be observed, confirming the ability of Spp1-Mer2 to form a stable complex with modified nucleosomes.

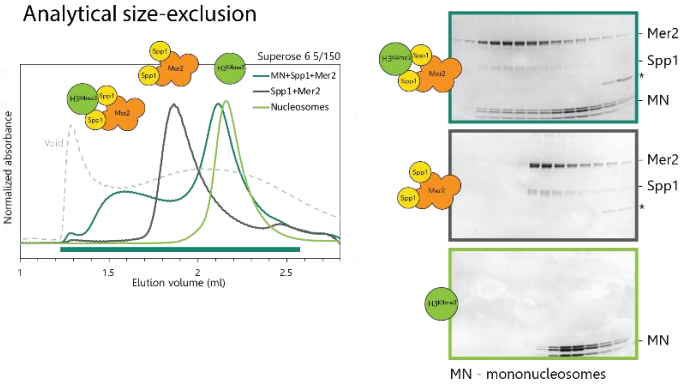

Figure 18: Analytical size-exclusion chromatogram of the nucleosome-Spp1-Mer2 complex. On the left side is a chromatogram with normalized absorbances, fractions marked in petrol blue were analyzed on 10-20 % SDS-gels. The void marker is shown as a grey dashed line.

The biochemical data consistently show that Spp1-Mer2 forms a stable complex with the nucleosomes and that the dimerization of Spp1 increases its affinity to H3K4me3 mononucleosomes (MN). To gain an insight into the organization of the Spp1-Mer2-MN assembly, the complex was cross-linked with DSBU (11 Å spacer) and analyzed by mass-spectrometry (XL-MS) (Figure 19A). The XL-MS revealed many more internal Spp1 crosslinks than were observed in the analysis of the Spp1-Mer2 complex without nucleosomes (Figure 15A). Given that only the proximal residues can be crosslinked, it suggests that the two Spp1 moieties come closer to one another in the MN-Spp1-Mer2 complex than in the Spp1-Mer2 complex possibly due to conformational or sterical rearrangement of Spp1 upon binding to nucleosomes. In

the absence of nucleosomes, the PHD domains of the two Spp1 moieties in the Spp1-Mer2 complex are rather flexible, but after interaction with nucleosomes, the PHD domains bind the histone H3 tails, which decreases their flexibility and brings them closer to one another.

There were only very few crosslinks detected between Spp1 and nucleosomes, although Spp1 is an established nucleosome binder (He et al., 2019). This could be caused simply by the fact, that the Spp1-MN interaction interface is relatively small (only the PHD domain of Spp1 interacts with the H3 tail) and therefore does not include many residues available for crosslinking. Strikingly, several crosslinks between Mer2 and nucleosome were identified. This reveals that, as well as Spp1, Mer2 is also in proximity to the nucleosome and therefore might interact with it. Such an interaction could explain Mer2 binding to nucleosomes in a pulldown (Figure 17B). Based on the XL-MS pattern, the nucleosome-binding interface of Mer2 constitutes the whole protein, without a distinct binding domain. However, this apparent lack of a specific binding domain on Mer2 could be caused by the low number of detected crosslinks and the flexibility of Mer2. The nucleosomal crosslinked residues were modelled on a previously determined structure of a mononucleosome, PDB: 1kx5 (Davey et al., 2002) (Figure 19B). Crosslinks were located mainly around the DNA entry/exit site on the nucleosomes, which could be explained by a larger Mer2:nucleosome binding interface and/or flexibility of Mer2. Taken together, these data imply that Mer2 not only strengthens the interaction between Spp1 and nucleosomes via Spp1

dimerization but also that it directly contributes to the interaction with nucleosomes.

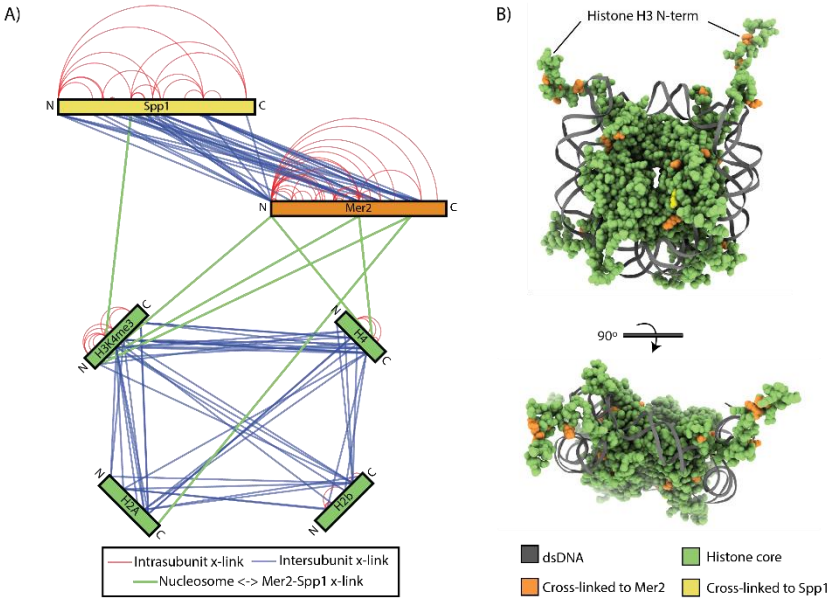

Figure 19: Cross-linking mass-spec analysis of the nucleosome-Spp1-Mer2 complex. A) Nucleosome-Spp1-Mer2 complex crosslinked with DSBU and analyzed by mass spectrometry. Crosslinks were filtered to give a 1 % false discovery rate and visualized by xVis (Grimm et al., 2015). B) Nucleosome crosslinks from A) modelled onto a structure of a *X. laevis* nucleosome (PDB: 1kx5 (Davey et al., 2002)).

2.2.2 Mer2 interaction with nucleosomes in absence of Spp1

Previous data implied that Mer2 binds nucleosomes (Figure 17B, Figure 19). To test whether this interaction could occur even in the absence of Spp1, an analytical SEC was performed with an untagged Mer2^{FL} and unmodified nucleosomes (Figure 20). The chromatogram shows a clear elution shift when both Mer2 and nucleosomes are present, confirming that Mer2 forms a stable

complex with nucleosomes in solution. The chromatogram also indicates that the Mer2-MN complex has a distinct stoichiometry.

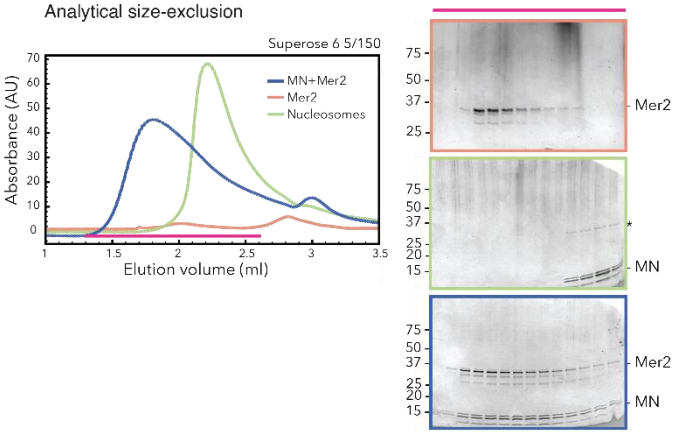

Figure 20: Analytical size-exclusion of the nucleosome-Mer2 complex. Fractions marked with magenta in the chromatogram were analyzed on 10 % (in case of Mer2) and 10-20 % SDS-gel (in case of MN and MN-Mer2).

To determine the stoichiometry of Mer2-MN, the assembly was first tested on a mass photometer (MP). This technique determines the molecular mass in solution at very low concentrations (~20-100 nM) based on light scattered by single molecules as they are landing on a test glass (Young et al., 2018). The experiment resulted in three main peaks (Figure 21A) of sizes corresponding to Mer2 tetramer (measured at 127 kDa, theoretical size 142 kDa), nucleosomes (measured at 187 kDa, theoretical size 202 kDa) and the Mer2-MN complex (measured at 303 kDa). The measured size of the complex corresponds best to the size of a Mer2:MN complex with a 4:1 stoichiometry (one Mer2 tetramer binds one nucleosome), which is 344 kDa (sizes summarized in Figure 21C). The size distribution suggests, that less than 50% of proteins formed a complex at the given

concentration of 60 nM. Given that under equilibrium at the protein concentration equal to the complex dissociation constant (K_D) one should observe a 50% complex formation, I assume that the K_D of the Mer2-MN complex is likely slightly higher than 60 nM. However, the samples are diluted 10-times immediately before measurement and measured for a very short time (1 min), hence the experiment is not performed under equilibrium and the suggested K_D is only tentative.

To confirm the 4:1 stoichiometry of the Mer2-MN complex determined by the MP and to detect the possible formation of larger oligomers at higher concentration, the sample was analyzed on SEC-MALS at 1 mg/ml concentration (Figure 21B). I observed a complex of 341 kDa, which almost perfectly corresponds to a theoretical size of a complex consisting of one Mer2 tetramer bound to one nucleosome, as suggested by the MP (Figure 21B, summarized in Figure 21C). Additionally, I detected a 10.96 MDa peak, which could correspond to a higher-order assembly of Mer2 alone, with nucleosomes or with free DNA. Recently Mer2 was suggested to form condensates on DNA (Claeys Bouuaert et al., 2021), which could also explain such a large assembly.

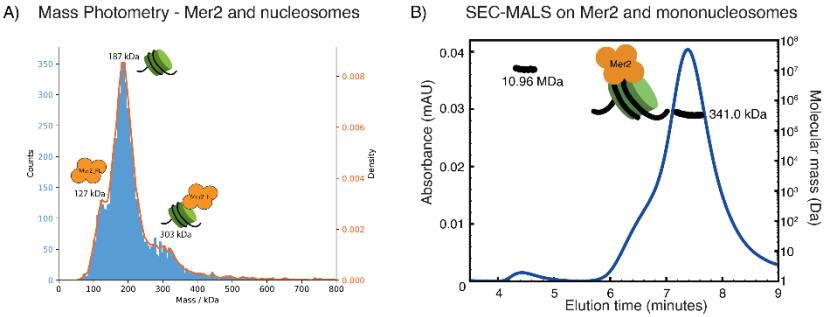

C)

	Theoretical	Measured mass SEC-MALS	Measured mass MP
Mer2^{FL} tetramer	142 kDa	-	127 kDa (10%<)
Mono-nucleosome	202 kDa	-	187 kDa (7%<)
1:1 complex	344 kDa	341 kDa (1%<)	303 kDa (12%<)

Figure 21: Mer2 interaction with nucleosomes A) Mass photometry and B) SEC-MALS of the Mer2-MN complex. C) Summary of theoretical and measured molecular mass values of nucleosomes, Mer2^{FL} and the Mer2-MN complex.

Based on the XL-MS data, Mer2 interacts with nucleosomes at the DNA entry/exit site (Figure 19). For the XL-MS analysis as well as analytical SEC, SEC-MALS and MP, nucleosomes with 167 bp DNA containing small free DNA overhangs were used. Therefore, Mer2 could also be simply binding to the DNA overhangs of the nucleosomes instead of specifically recognizing the nucleosome itself. To test this, analytical EMSAs were performed (Figure 22). They revealed that Mer2 interacts with a 6-fold higher apparent affinity to mononucleosomes than to the same 167 bp DNA used for nucleosome reconstitution (5 nM vs 30 nM, Figure 22A – top and middle panel). The discrepancy between the apparent K_D determined by MP and EMSA could be due to the experimental conditions, both analyses are non-equilibrium experiments and EMSAs are carried out at very low

salt (Fried and Bromberg, 1997). Nevertheless, it is clear, that Mer2 is a very strong nucleosome binder. To test the effect of the DNA overhangs on Mer2 binding, a nucleosome core particle (NCP; with 147 bp DNA without any DNA overhangs) was used in the same analysis with Mer2. The lack of DNA overhangs on nucleosomes decreased ~8-fold the affinity of Mer2 to NCP in comparison to MN with 167 bp DNA (to 40 nM; Figure 22A – bottom panel).

The common binding site of the nucleosome is an "acidic patch" on H2A. Therefore, I tested whether mutation of this binding site (E56T, E61T, E64T, D90S, E91T, E92T) (Kalashnikova et al., 2013) has any effect on Mer2 binding. To enable better detection of any difference in binding, the EMSA was performed with NCP. However, no significant difference in binding was detected (Figure 22B – middle panel). Next, I prepared tailless NCPs (lacking the N-terminal tails of the histones) to test whether Mer2 recognizes the histone tails. Surprisingly, Mer2 bound very tightly to the tailless NCPs, with an apparent K_D ~ 5 nM (Figure 22B – bottom panel). This might be due to the low salt conditions of an EMSA, in which the highly basic histone tails shield the histone core or the acidic DNA and interfere with Mer2 binding. Altogether, these data suggest that Mer2 specifically recognizes the nucleosomal DNA at the entry/exit point of a nucleosome and also interacts with the histones themselves.

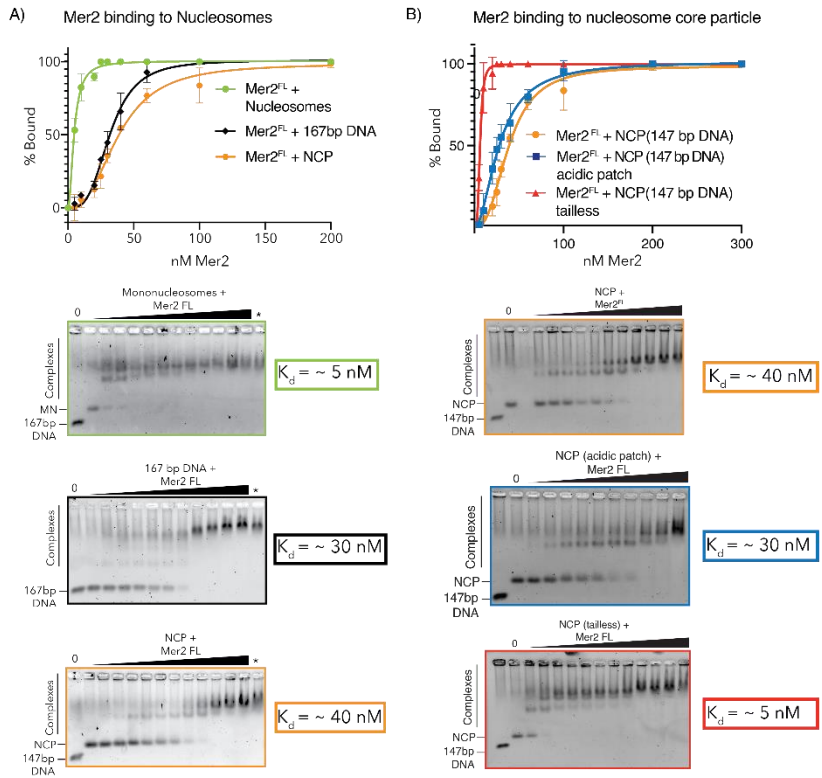

Figure 22: Identification of the interaction domains of Mer2 with nucleosomes. A-B) EMSA of untagged full-length Mer2 with A) nucleosomes (green), nucleosomal DNA (black) and nucleosome core particle (NCP; orange) or B) NCP with acidic patch mutation (blue) and tailless NCP (red). Error bars, SEM; n=4.

The XL-MS data of the MN-Spp1-Mer2 complex (Figure 19) failed to reveal any obvious nucleosome-binding domain in Mer2. To test whether there is a specific part of Mer2, which recognizes nucleosomes, I performed another set of EMSAs. In this case, tetrameric Mer2 truncations containing the core were used to prevent discrepancies caused by different oligomerization stages of Mer2 constructs. Deletion of either of the Mer2 terminal

regions led to a decrease in affinity to nucleosomes (Mer2$^{\Delta C}$ binds with a K_D ~12.5 nM and Mer2$^{\Delta N}$ with a K_D ~30 nM; Figure 23A – top and middle panel) and Mer2^{core} did not exhibit any binding at all (Figure 23A – bottom panel). This suggests, that both Mer2 terminal regions contribute to the nucleosome binding. To confirm this observation, a pulldown with commercial biotinylated nucleosomes and tetrameric Mer2 truncations was performed (Figure 23B). Advantageously, pulldown can be performed in a more physiological buffer, although a high local concentration of the bait on beads may cause misleading results. The pulldown confirmed that both Mer2^{FL} and Mer2$^{\Delta N}$ interact with nucleosomes. However, unlike in the EMSA, Mer2$^{\Delta C}$ did not show any binding, suggesting that the main Mer2-nucleosome interaction is largely mediated by the C-terminal part of Mer2, with some possible contribution from the N-terminal region.

Taken together, my data suggests that Mer2 not only strengthens the interaction between Spp1 and nucleosomes through Spp1 dimerization but is also a true nucleosome binder as it interacts via its C-terminal region with the histones and the nucleosomal DNA on the DNA entry/exit site of a nucleosome.

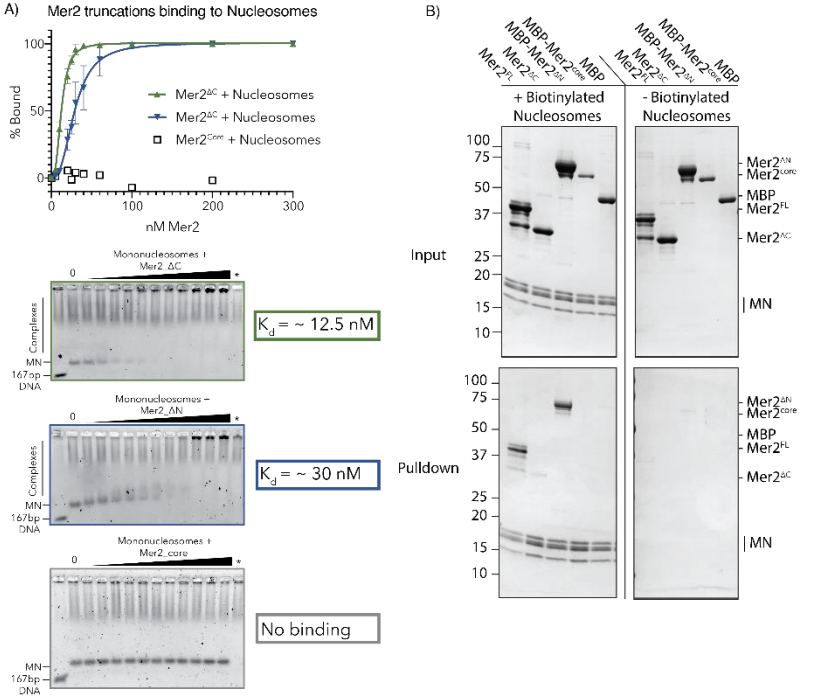

Figure 23: Mer2 truncations interacting with nucleosomes. A) EMSA of untagged truncations of Mer2 with the nucleosome. Error bars, SEM; n=4. B) Pulldown of Mer2 construct with biotinylated nucleosomes on 10-20 % SDS-gel stained by InstantBlue.

2.2.3 EM analysis of Spp1-Mer2 on nucleosomes

While the biochemical analysis enabled me to determine which parts of Spp1 and Mer2 interact with nucleosomes, a deeper structural analysis could provide helpful insights into the organization of the complex. The whole 1:2:4 MN-Spp1-Mer2 complex is roughly 430 kDa in size and probably somewhat flexible (as suggested by attempts to solve the structure of the Spp1-Mer2 complex – section 2.1.3). Given the size and the flexibility of the complex, I aimed to obtain the structure of the

MN-Spp1-Mer2 complex by electron microscopy (EM), first by negative staining EM followed by cryoEM. However, neither of the methods resulted in high-quality micrographs, which could be used for a structural study.

The negative staining EM can provide an insight into the behaviour and shape of the MN-Spp1-Mer2 complex. However, similarly to the Spp1-Mer2 complex, I was not able to obtain good quality micrographs with well-defined homogeneous particles that could be used for further analysis (Figure 24A). From the micrographs, it appeared that the particles were partially precipitated, likely due to the grid preparation at room temperature and the staining procedure. Hence, I decided to proceed with cryo-electron microscopy (cryoEM) to determine whether the instability of the particles would improve under cryo-conditions.

CryoEM on nucleosome complexes is generally quite complicated because of the dynamic behaviour of the nucleosomes (Luger, 2003). Therefore, I tried to optimize simultaneously both the nucleosome sample alone and the MN-Spp1-Mer2 complex sample to gain an insight into the handling of the nucleosome sample.

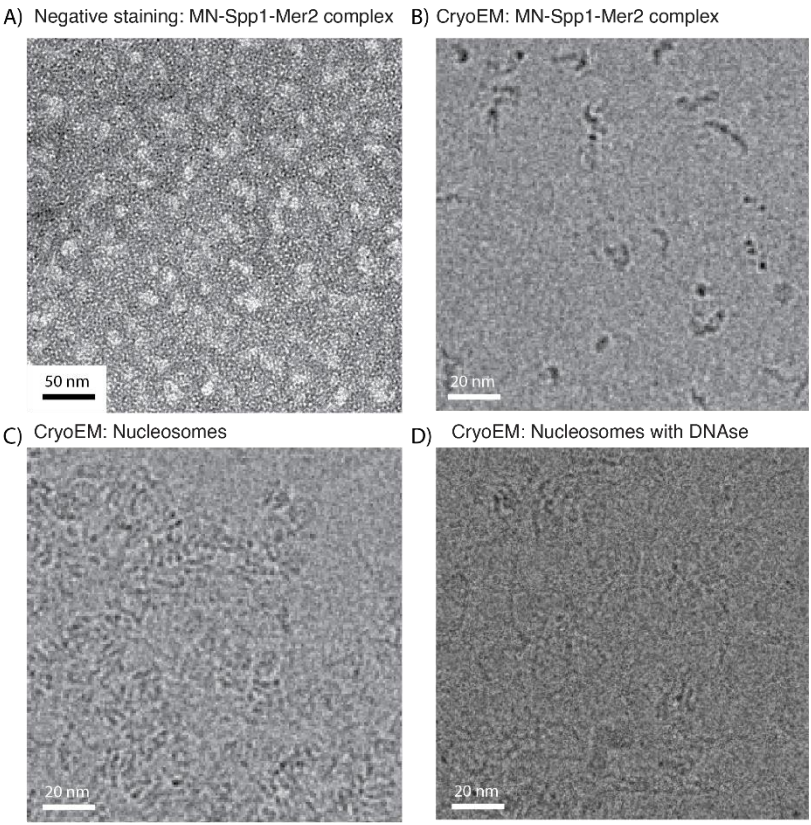

Figure 24: CryoEM of the nucleosome-Spp1-Mer2 complex. A) Negative staining micrograph of the nucleosome-Spp1-Mer2 complex with 1 % uranyl acetate. Scale bar 50 nm. B-D) CryoEM micrographs of B) the nucleosome-Spp1-Mer2 complex, C) nucleosomes alone and D) nucleosome treated with DNAse. Scale bars are 20 nm.

The initial micrographs of the nucleosome sample indicated a strong preference for side views of the nucleosomes and a tendency of the particles to form crowds with considerable quantities of free DNA in the sample (Figure 24C). It could be caused by the disassembly of the nucleosomes during grid preparation or by an imprecise reconstitution of the histone

octamers with DNA, where more DNA was added than necessary. Given that free DNA increases the background noise, the structural studies of the complex would benefit from using a nucleosome sample without free DNA. To eliminate it, the nucleosomes were treated with 10 µg/ml DNAse I (BioFroxx), which should have been able to digest only the free DNA, as it is not protected by the nucleosome. However, treatment with DNAse led to disassembly of the nucleosomes, and could therefore not be used (Figure 24D). Another possibility to improve the homogeneity of the sample would be to clean it with a size-exclusion (SEC) column before grid preparation.

To analyze the MN-Spp1-Mer2 complex, the nucleosomes were mixed with Spp1 and Mer2 and purified on SEC to obtain a homogenous sample containing the tripartite complex. On the micrographs are visible C-shaped particles (Figure 24B), similar to the ones observed in the Spp1-Mer2 complex in absence of the nucleosome (Figure 16B). However, the particles are not homogeneous and many of them are precipitated, Furthermore, I did not see any particles with nucleosomes, suggesting, that the complex fell apart during preparation.

Therefore, to improve the stability of the complex, I attempted to mildly crosslink the sample using the gradient fixation (GraFix) method (Stark, 2010). As a crosslinker, I used paraformaldehyde, which can link both proteins and DNA, thus stabilizing the MN-Mer2 binding interface. I applied the sample on a glycerol and paraformaldehyde gradient (10-35% of glycerol, 0-4% of paraformaldehyde). However, this also failed to yield any high-quality micrographs.

To obtain a structure of the MN-Spp1-Mer2 complex, the buffer composition has to be optimized as well as the complex formation and its stabilization via crosslinking. All three components comprising the complex have very specific requirements on the buffer composition; Spp1 requires zinc because of its PHD domain, Mer2 high salt to improve its stability and nucleosomes low salt and EDTA to prevent nucleosome stacking. Despite many attempts, I was unable to find a buffer composition in which all proteins would be stable enough, would interact with one another and would be compatible with the demands of the method.

Nonetheless, the biochemical data together with the XL-MS experiment provide an insight into the organization of the MN-Spp1-Mer2 complex. Most importantly, they identified Mer2 as a true nucleosome binder; it interacts strongly via its terminal regions (especially the C-terminal one) with the DNA entry/exit site of the nucleosome. The SEC-MALS and MP experiments confirmed that one Mer2 tetramer binds to one nucleosome, suggesting that the stoichiometry of the whole MN-Spp1-Mer2 complex is 1:2:4. Furthermore, the biochemical assays show, that the dimerization of Spp1 driven by Mer2 increases the affinity of Spp1 to modified nucleosomes. Taken together, the data imply that Spp1 contributes the specificity in binding to nucleosomes and Mer2 delivers the strength. Altogether, the data provide an insight into the functional arrangement of the MN-Spp1-Mer2 complex and can be used as a base for further structural and biochemical studies.

2.3 Mer2 interaction with Hop1

2.3.1 Localization of Mer2 to the axis

Hop1, a meiotic HORMA domain protein, contains a closure motif (CM) in its own C-terminal region. As a result, it can exist in three different conformations: a closed one – the CM binds to its HORMA domain, an unbuckled one – the CM is not bound to the HORMA and exposed – the HORMA interacts with a CM of another protein (section 1.2.1, Figure 4) (West et al., 2018). Free Hop1 is usually in a closed conformation, bound to its CM. On the axis, Hop1 interacts with the closure motif of Red1, a process that presumably requires that its own CM is first displaced, likely by the catalytic activity of the AAA+ ATPase Pch2 (Raina and Vader, 2020). Once on the axis, the C-terminal CM of Hop1 is thus displaced, which may allow binding to other factors. It has been suggested that this might allow additional Hop1 molecules to bind, forming a "beads on a string" type assembly (West et al., 2019), but there is currently no direct evidence for this.

Meiotic HORMA proteins, as a part of the axis, are necessary for Mer2 recruitment to the chromosomes (Panizza et al., 2011; Stanzione et al., 2016). Mer2 homologs from mouse and fission yeast (IHO1 and Rec15) have been shown to associate with Hop1 homologs *in vivo* (HORMAD1 and Hop1) (Kariyazono et al., 2019; Stanzione et al., 2016), however, there is no *in vitro* data to support it.

To understand the molecular basis of the interaction between Mer2 and the chromosomal axial, I performed a pulldown assay with Mer2 and the axial proteins. Given that Red1 has been

shown to form filaments via its C-terminal motif (West et al., 2019), I made use of a Red1 point mutant (I743R), which is tetramerizing, but not able to form filaments. In a pulldown assay, I used untagged Mer2^{FL} as prey and Strep-Hop1 from *E. coli* or Red1^{I743R}-MBP with and without Strep-Hop1 expressed in insect cells (by Saskia Funk and Veronika Altmannová) as a bait (Figure 25A) and quantified the amount of pulled Mer2 (Figure 25B).

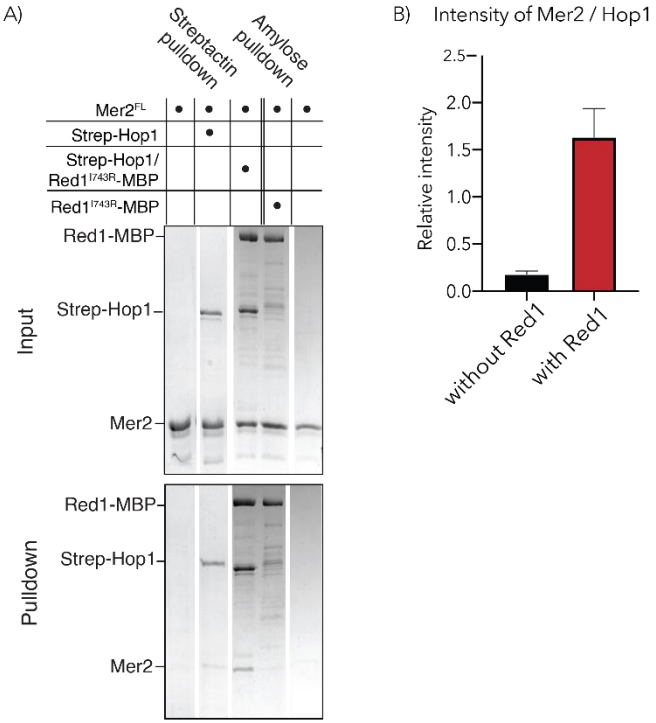

Figure 25: Interaction of Mer2 with Hop1 and Red1. A) Pulldown of full-length untagged Mer2 with Strep-Hop1, Red1^{I743R}-MBP or Hop1-Red1 complex on Streptavidin or amylose beads on SDS-gel stained with InstantBlue. B) Quantification of A); error bars, SEM; n=3.

Consistently with data from other organisms (Kariyazono et al., 2019; Stanzione et al., 2016), the budding yeast Mer2 appears to directly interact with Hop1 (Figure 25A – second lane). Interestingly, the quantity of pulled Mer2 increases about eight times, when Red1 is also present (Figure 25A – third lane, Figure 25B), although, there is no detectable interaction between Mer2 and Red1 alone (Figure 25A – fourth lane). Given that the Hop1 in the Hop1-Red1 complex should be exclusively in the exposed conformation, whereas the free Hop1 is largely in a closed conformation, the data implies, that Mer2 interacts specifically with the exposed conformation of Hop1.

2.3.2 Identification of the interaction regions

The initial data suggested that Mer2 interacts specifically with an exposed Hop1 (Figure 25). There is a described mutation in the closure motif of Hop1 – K593A (Niu et al., 2005), which is known to disrupt the interaction between the HORMA domain and the closure motif, thus resembling the unbuckled and in a way also exposed conformation of Hop1 (West et al., 2018). However, it has to be mentioned, that the $Hop1^{K593A}$ is not identical to the axial exposed Hop1, it only mimics it.

To verify that Mer2 interacts with the unbuckled conformation of Hop1, I performed a pulldown with $Mer2^{FL}$ and three different versions of Hop1: wild-type, $Hop1^{K593A}$ (unbuckled Hop1) and Hop1 without the HORMA domain ($Hop1^{256\text{-}C}$, from here on referred to as $Hop1^{\Delta HORMA}$) (Figure 26A). However, the results were not very clear, it appeared as if Mer2 interacts with both wild-type Hop1 and $Hop1^{K593A}$ with the same apparent affinity,

which might be caused by the use of unbuckled Hop1 instead of exposed one. But an additional quantification of the intensity of the Mer2 signal relative to Hop1 confirms that Mer2 interacts stronger with Hop1^{K593A} (~1.35 Mer2/Hop1 ratio) than with wild-type Hop1 (~0.9 Mer2/Hop1) (Figure 26B), thus validating the hypothesis, that Mer2 interacts preferentially with the unbuckled Hop1. Additionally, there was no detectable binding between Mer2 and Hop1$^{\Delta HORMA}$, which suggests that Mer2 interacts with the N-terminal HORMA domain of Hop1, preferentially when it is accessible in an unbuckled/exposed conformation.

Next, I aimed to determine, which part of Mer2 is required for the binding to Hop1. To test this, I used full-length Mer2 and its several tetrameric truncations missing either of the terminal regions in a pulldown with unbuckled Hop1^{K593A} and confirmed the presence of Mer2 in the eluate via αMer2 western blot. The results demonstrate, that partially the Mer2^{core}, but mainly its C-terminal region are responsible for Mer2 binding to Hop1 (Figure 26C).

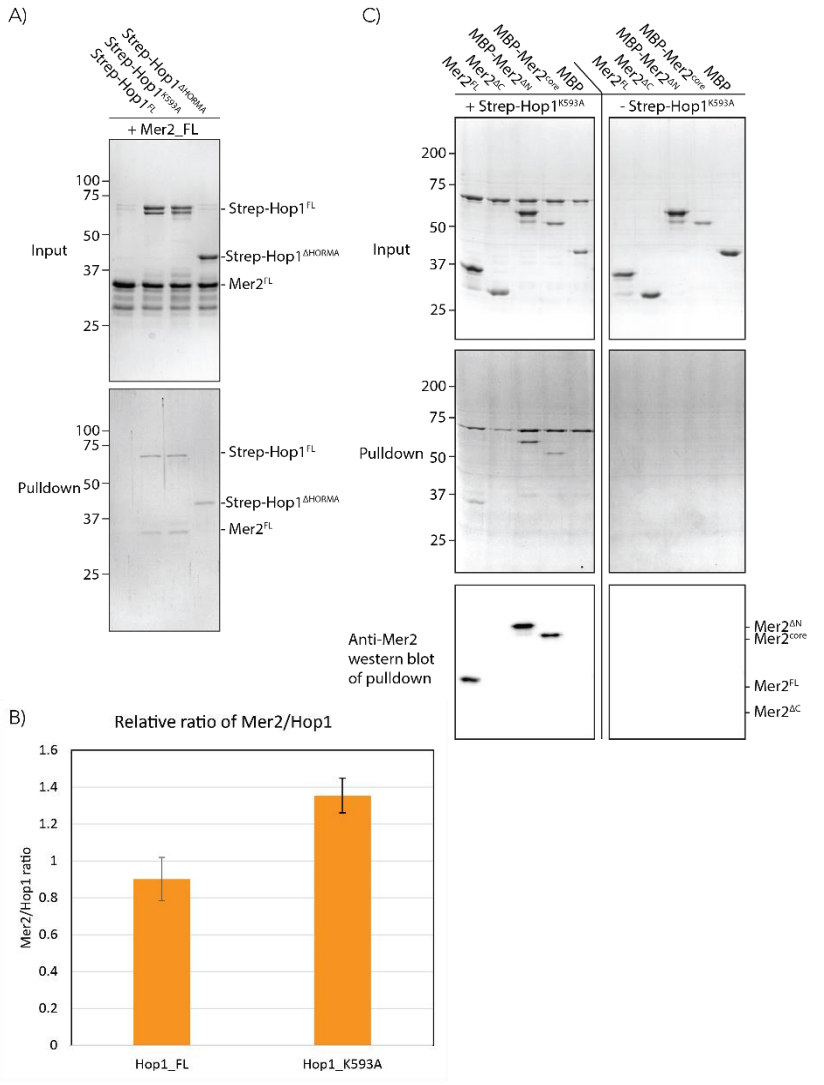

Figure 26: Identification of the binding domains of Mer2 and Hop1. A) StrepTactin pulldown of untagged Mer2^{FL} with Strep-tagged truncations of Hop1. Quantification in B); error bars, SEM; n=3 C) Reciprocal pulldown of Mer2 truncations with Strep-Hop1^{K593A}. Pulled Mer2 was detected both on SDS-gel stained with InstantBlue and an αMer2 western blot.

After a closer inspection, we found a novel conserved patch at the complete C-terminal region of Mer2 (Figure 27A). Since Mer2 is overall a very degenerate protein, the presence of such a conserved patch suggests, that it interacts with a conserved binding partner, such as Hop1. To test whether the conserved patch within the C-terminal region of Mer2 interacts with Hop1, I created a new truncation of Mer2, where the 19 conserved C-terminal residues were deleted ($Mer2^{N-295}$), and carried out a pulldown experiment with the same versions of Hop1 as previously ($Hop1^{WT}$, $Hop1^{K593A}$ and $Hop1^{\Delta HORMA}$) (Figure 27B). Strikingly, there was no detectable Mer2, which confirms, that the conserved C-terminal patch of Mer2 is responsible for interaction with Hop1.

I demonstrated, that Mer2 interacts directly with Hop1, Spp1 and nucleosomes. To confirm, whether those interactions are compatible with one another or whether any of them prevents another one to occur, I combined all of the components and performed a pulldown on Strep-tagged $Hop1^{K593A}$ (Figure 27C). Interestingly, all of the proteins are pulled down in large amounts, suggesting that the interactions within the MN-Spp1-Mer2-Hop1 complex are stabilizing one another and that the assembly might be cooperative.

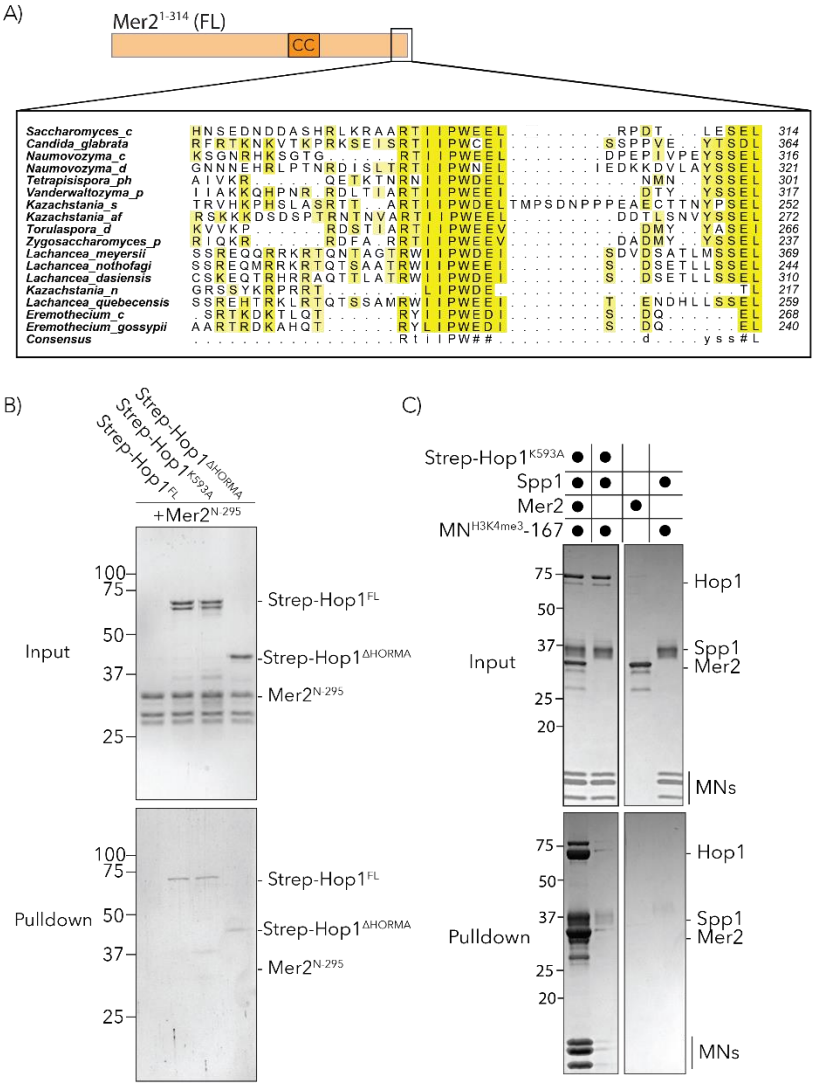

Figure 27: The conserved C-terminal patch of Mer2 and its role. A) Sequence alignment of Mer2 orthologs revealed a conserved patch within its C-terminus. B) StrepTactin pulldown of the Mer2 truncation missing the 19 conserved C-terminal residues (Mer2$^{N\text{-}295}$) with Strep-Hop1 constructs. C) Pulldown of the MN^{H3K4me3}, Spp1 and Mer2 on Strep-Hop1^{K593A}.

To gain an insight into the structural organization of the Mer2-Hop1 assembly, the complex was crosslinked with DSBU and subsequently analyzed by mass-spectrometry (Figure 28A). The analysis revealed many Mer2-Hop1 crosslinks localized within the C-terminal regions of both proteins and also within the HORMA domain of Hop1 and the core of Mer2. Interestingly, the more abundant Mer2-Hop1 crosslinks (>5 observations) were localized only on one "face" of the HORMA domain, when mapped on a model of $Hop1^{HORMA}$ (based on open Mad2, PDB: 1duj (Luo et al., 2000) created by John Weir), whereas the other "face" was essentially crosslink-free.

Strikingly, the suggested Mer2-binding interface on $Hop1^{HORMA}$ is in line with a model of $Hop1^{HORMA}$, $Mer2^{254\text{-}C}$, $Red1^{N\text{-}400}$ created using AlphaFold Multimer (Evans et al., 2021; Jumper et al., 2021; Varadi et al., 2022) by John Weir (Figure 28C) without any prior structural information on either on the components. In this model, not only Mer2 consistently with the XL-MS data interacts only with one "face" of HORMA, but also it reveals, that the other "face" is occupied by Red1 CM (aa 340-365). Additionally, Mer2 is proximal to the Hop1-Red1 binding interface, suggesting it might be affected by Red1. A weak interaction of Mer2 with Red1 could stabilize the Mer2-Hop1 interaction, even though it is not strong enough to be detected in a pulldown. It would also explain the increase in Mer2 binding to Hop1 in the presence of Red1 in comparison to Hop1 alone (Figure 25).

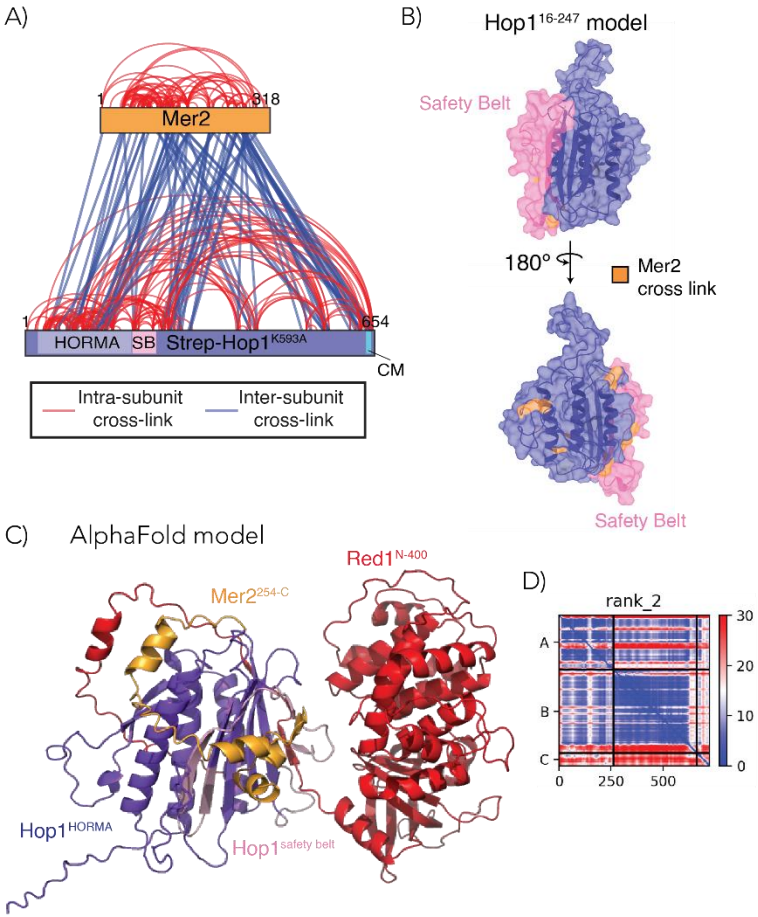

Figure 28: Structural analysis of the Mer2-Hop1 complex. A) Crosslinking pattern of Mer2-Hop1 complex. Crosslinks were filtered to give a 1 % false discovery rate and visualized by xVis (Grimm et al., 2015) B) Homology model of Hop1^{HORMA} using open Mad2 (PDB: 1duj) (Luo et al., 2000) as a template with highlighted abundant crosslinks (>5 observations) model are localized only on one "face" of HORMA. C) AlphaFold model of the C-terminal regions of Mer2 (orange) with Hop1^{HORMA} (blue) and Red1^{N-400} (red). The safety belt of Hop1 is highlighted in pink. D) PAE plot of the AlphaFold model of Hop1(A), Red1 (B) and Mer2 (C). High confidence areas are shown in blue, low confidence in red.

Taken together, all of this data consistently confirms, that Mer2 binds to the chromosomal axis through the interaction with Hop1 in the exposed conformation. This interaction is likely further stabilized in the presence of Red1. The conserved 19 C-terminal residues of Mer2 interact with the HORMA domain of Hop1 both in the presence and absence of Spp1 and nucleosomes. Mer2 thus creates a direct connection between the DSB site within the chromosomal loop and the chromosomal axis.

2.3.3 Interaction of the Hop1 PHD domain with nucleosomes

Hop1 contains a recently discovered PHD domain C-terminally adjacent to the HORMA domain (Ur and Corbett, 2021). Its function is unknown, however, PHD domains are often responsible for binding to modified (and especially to di- and trimethylated) nucleosomes. There are many possible modifications, that Hop1 could be interacting with, but during meiosis, H3K4me3 and in mammals also H3K36me3 (Lange et al., 2016; Yamada et al., 2017) are especially important.

Therefore, I prepared nucleosomes with either of those modifications and with wild-type nucleosomes as control and performed a pulldown with Strep-tagged Hop1 in a closed or unbuckled conformation. Surprisingly, Hop1 interacts with both trimethylated nucleosomes, but not with the wild-type ones. Even though this result does not show specificity for a certain modification on the nucleosome, it implies that Hop1 has a preference for trimethylation and can serve as a basis for further studies.

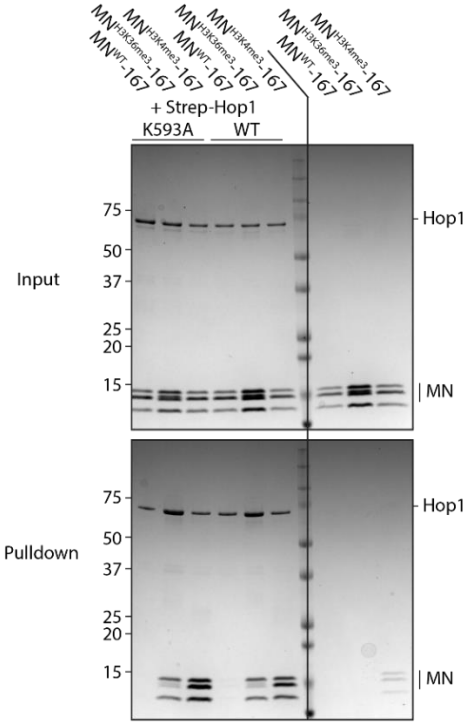

Figure 29: Hop1 interaction with nucleosomes. StrepTactin pulldown of Strep-Hop1 in unbuckled or closed conformation with modified trimethylated nucleosomes analyzed on 10-20 % SDS-gel.

2.4 Role of the conserved N-terminal patch of Mer2

2.4.1 *In vivo* phenotype of Mer2_3A and 4A mutations

In the Mer2 sequence, there is not only a conserved patch within the C-terminal region, responsible for binding to Hop1 (Figure 27) but also an additional conserved region within its N-terminal part (Figure 30A) (Tessé et al., 2017). To reveal the role of this region, I created two mutants of Mer2 with either three (W58, K61 and L64) or four (D52, E68, R70 and E71) residues from the conserved patch mutated to alanine, from now on

referred to as Mer2^{3A} and Mer2^{4A}. Based on the sequence alignment (Figure 30A) and secondary structure prediction (Figure 9), all the residues appear to be part of the same α-helix, where all the conserved residues face the same side of the helix. The residues mutated in the 3A mutant are more conserved than the ones in the 4A mutant, therefore it is possible that the effect of the 3A mutations is stronger, or that the 4A mutant might perturb a different set of interactions, not universally conserved through evolution.

To identify the role of the conserved patch of Mer2, our collaborators (Vivek Raina and Vaishnavi Nivsarkar from Vader laboratory, MPI Dortmund and Cancer Centre Amsterdam) tested the effect of the 3A and 4A mutations *in vivo* (full analysis in (Rousová et al., 2021)). Interestingly, they found out, that while the Mer2$^{3A/4A}$ mutants were expressed at levels comparable to Mer2^{WT}, the cells with mutated Mer2 produced almost completely unviable spores (Figure 30B), which phenotypically copied *mer2Δ* strains. Such a strong phenotype can have several explanations, including problems with DSB formation or resection. A co-immunoprecipitation (co-IP) followed by a western blot analysis revealed that although Mer2 mutants are still normally associated with the axis (αHop1 signal, Figure 30D), they are hyperphosphorylated (especially Mer2^{3A}) and are not removed from the axis after three hours of meiosis, as is the case for Mer2^{WT}. Given that Mer2 is phosphorylated by CDK and DDK before break formation and is removed from the axis after the DNA breaks are resected, the results imply a problem with the introduction of DSBs. Additionally, after DNA break formation,

kinase Mek1 is activated and among other targets phosphorylates also histone H3 on threonine 11 (H3T11) (Subramanian et al., 2016), which serves as a control for DSB formation. The cells with mutated Mer2 failed to phosphorylate H3T11, which also suggests that the Mer2$^{3A/4A}$ prevent DSBs and thus lead to unviable spore formation.

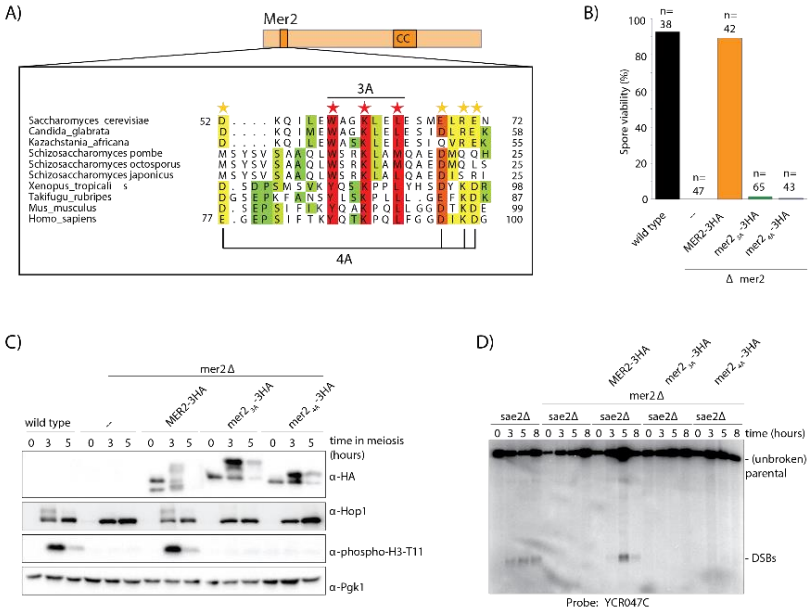

Figure 30: *In vivo* analysis of the Mer2$^{3A/4A}$ mutants. A) Sequence alignment of Mer2 orthologs revealed a conserved patch within the N-terminal region of Mer2. Mutation of three (red starts) or four (yellow stars) residues to alanines resulted in Mer2^{3A} and Mer2^{4A} mutants. B) Quantification of spore viability in indicated strains. C) Western blot analysis of meiotic yeast culture of same strains as in B). D) Southern blot analysis comparing DSB levels in indicated strains in *saeΔ* background strains. Cells were collected at the indicated time after induction of meiosis. Faster migrating DNA species indicate DSBs.

A southern blot in the *sae2Δ* background confirmed, that the Mer2$^{3A/4A}$ mutants prevent DSB formation (Figure 30D). Sae2 is part of the resection machinery, in its absence, DNA breaks cannot be repaired and therefore can be visualized. However, there are no detectable DSBs in cells with Mer2$^{3A/4A}$ mutants, which strengthens the arguments, that those conserved residues are necessary for DSB formation.

2.4.2 Mer2$^{3A/4A}$ binding to nucleosomes

The conserved N-terminal patch of Mer2 plays a crucial role in DSB formation probably by establishing a critical connection to another binding partner. Disruption of interaction with Hop1 can be excluded because the conserved C-terminal residues of Mer2 are responsible for binding to Hop1 (Figure 26) and because Mer2$^{3A/4A}$ mutants normally bind to Hop1 (Figure 30C). Moreover, the Hop1 deletion has a milder phenotype (Blat et al., 2002; Niu et al., 2005; Woltering et al., 2000) than the mutations of the conserved N-terminal patch of Mer2. The interaction between Mer2 and Spp1 is established via the core of Mer2 (Figure 14) and, as in the case of Hop1, the deletion of Spp1 has only a mild effect on DSB formation (Rockmill et al., 1995). Another known interaction partners of Mer2 are the Rec114-Mei4 complex. However, those proteins are very difficult to work with and I was not able to obtain a stable enough complex to study their interaction with Mer2 (further information in section 2.6).

To detect, which interaction is perturbed by the Mer2 mutations, Veronika Altmannová performed a co-IP mass-spectrometry analysis from yeast with wild-type Mer2 or the

Mer2^{4A} mutant, since there was some difficulty in making the appropriately tagged Mer2^{3A} strain. In addition, since it was established that Mer2^{3A} and Mer2^{4A} both disrupt DSB formation, all strains for co-IP MS were in addition deficient for Spo11 activity (Spo11 Y135F).

The co-IP MS analysis revealed, that the Mer2^{4A} is deficient in nucleosome binding (Figure 31A). In particular, the interaction with H3 (Hht1) and H4 was strongly affected, which is in line with the model, that Mer2 binds to the DNA entry/exit site of the nucleosomes formed by H3 and H4 (Figure 19). To confirm the decrease of affinity between Mer2 and nucleosomes upon mutating the conserved N-terminal patch of Mer2, I purified the mutants and performed a pulldown with biotinylated nucleosomes (Figure 31B), however, there is no detectable difference in binding. Based on the co-IP MS, the Mer2-nucleosome interaction is weakened but not abolished by the mutation hence the difference in the affinity might not be big enough to manifest in a pulldown experiment. Therefore, I aimed to reveal the affinity of Mer2^{3A} to nucleosomes by an EMSA (Figure 31C) with the same setting as previously (section 2.2.2) to obtain comparable results. The data showed that the Mer2^{3A} mutant has a roughly five-times lower affinity to the nucleosome than wild-type Mer2 (25 nM vs. 5 nM). The decrease in the apparent affinity upon mutating Mer2 is in line with the pulldown results; the protein concentrations are much higher in a pulldown (1-3 µM) than the affinity of either Mer2 construct to the nucleosomes, therefore the concentration of all binding partners in a pulldown is high enough to provide stable binding.

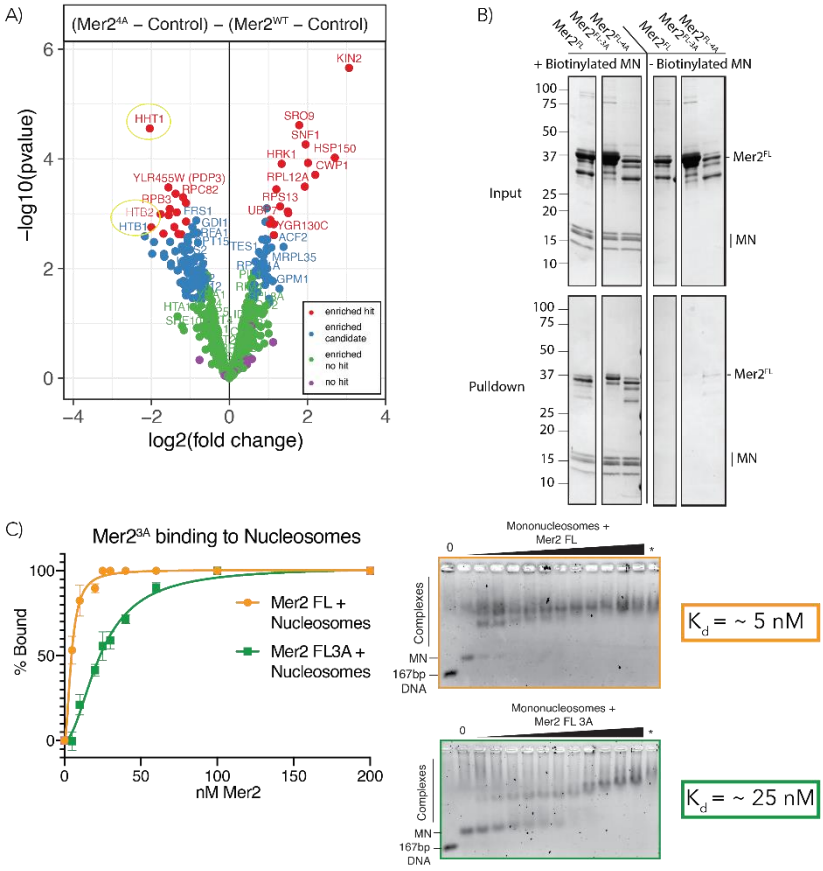

Figure 31: The role of Mer2$^{3A/4A}$ in nucleosome interaction. A) Volcano plot of co-IP MS of Mer2^{WT} and Mer2^{4A}. Proteins are grouped into hits (red) and candidates (blue) based on the fold change and p-value. Proteins on the left side are decreased in Mer2^{4A} compared to Mer2^{WT}, whereas proteins on the right side are increased. Histones H3 (Hht1) and H2b (Htb1/Htb2) are circled in yellow. B) Pulldown of Mer2^{WT} and Mer2$^{3A/4A}$ with biotinylated nucleosomes. C) EMSA of Mer2^{WT} and Mer2^{3A} with mononucleosomes shows a five-fold decrease in binding upon mutation. Error bars, SEM; n=4

The mutation of the conserved N-terminal patch of Mer2 reduces the binding to nucleosomes in a co-IP MS experiment as well as in an EMSA. Nonetheless, it can have a very severe effect

in vivo. Additionally, my previous *in vitro* data suggested, that the interaction between Mer2 and nucleosomes is established rather via the C-terminal region of Mer2 (Figure 23). Therefore, it is possible, that the Mer2$^{3A/4A}$ are not clear mutants and are affecting several phenomena, not only Mer2 binding to the nucleosomes.

2.4.3 Mer2 binding to Mre11

To determine, if another interaction is disturbed by the Mer2 mutations, Veronika Altmannová performed a yeast two-hybrid assay (Figure 32A). It confirmed that interaction with neither Spp1 nor Hop1 is affected by the mutation, as suggested above (full analysis in (Rousová et al., 2021)). Additionally, it revealed Mre11 as a binding partner of wild-type Mer2, as implied by (Arora et al., 2004; Henderson et al., 2006), but not of the Mer2 mutants. Mre11 is a part of an MRX complex formed by Mre11-Rad50-Xrs2 responsible for the resection of DSBs once they are formed (Neale et al., 2005). To confirm, whether the interaction between Mer2 and Mre11 (and loss thereof) appears also *in vitro*, I performed a pulldown with a C-terminally Strep-tagged Mre11 as a bait (purified by Veronika Altmannová) and the Mer2 mutants as a prey (Figure 32B). The quantification of the pulled Mer2 signal revealed, that there is nearly a 50 % decrease in binding of Mer2^{3A} versus the wild-type and about 90 % decrease when Mer2^{4A} is used (Figure 32B). Please note that the purified Mer2^{4A} construct is less stable, which can cause such a dramatic decrease in affinity.

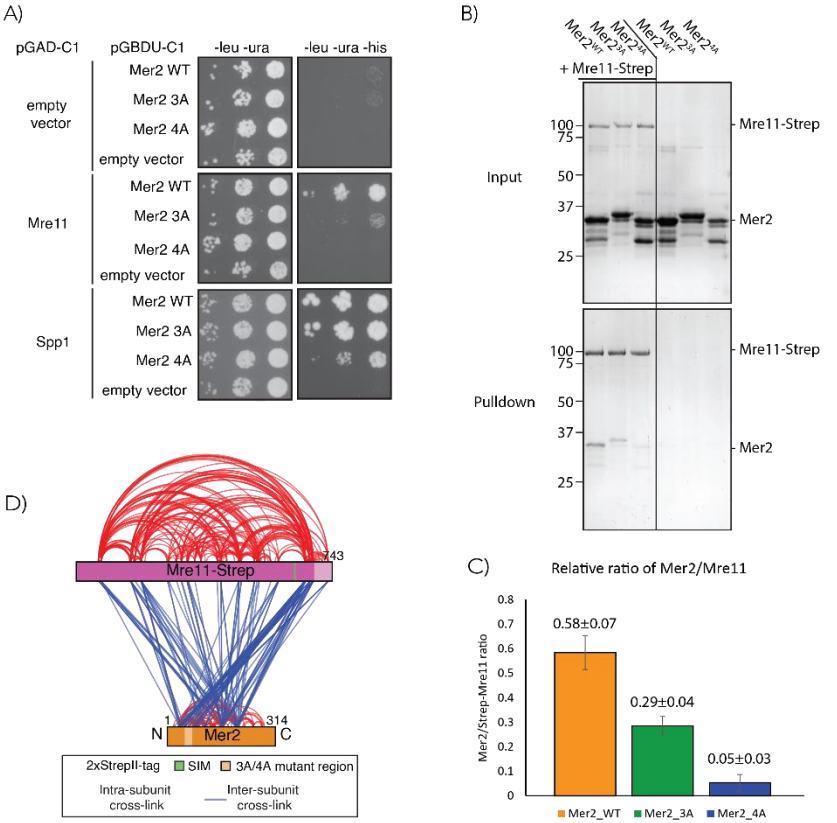

Figure 32: The role of Mer2$^{3A/4A}$ in binding to Mre11. A) Yeast-two-hybrid assay with Mer2^{WT} and Mer2$^{3A/4A}$. Yeast were transformed with the pGAD-C1 (activation domain) and pGBDU (DNA binding domain) plasmids. Cells were pipetted onto non-selective (left) or selective (right) plates at three serial concentrations. B) Pulldown of Mer2^{WT}, Mer2^{3A} and Mer^{4A} with C-terminally Strep-tagged Mre11, quantified in C). Error bars, SEM; n=3 D) Crosslinking pattern of Mer2-Mre11 revealed many links between the N-terminal region of Mer2 in the proximity of the conserved residues and the C-terminal part of Mre11 in the proximity of a SUMO-interaction motif (SIM). Crosslinks were filtered to give a 1 % false discovery rate and visualized by xVis (Grimm et al., 2015).

To confirm the interaction regions of Mer2 and Mre11, the complex was crosslinked by DSBU and analyzed by mass-spectrometry (Figure 32D). There are many crosslinks between the N-terminal region of Mer2 (proximal to the conserved patch) and the C-terminal part of Mre11 (close to the SUMO-interaction motif; SIM), which is in line with the previous experiments. Additional crosslinks between the core of Mer2 and Mre11 can be hinting at a larger interaction interface or can be caused by the high flexibility of Mer2. The difference between the strong *in vivo* and weaker *in vitro* effect of the mutations can be caused by the lack of post-translational modifications on both proteins or the lack of other binding partners.

The conserved patch within the N-terminal region of Mer2 is essential for DSB formation. It plays a role in the interaction with the nucleosome and, additionally, it is responsible for binding to the resection machinery protein Mre11, which suggests, that breaks can only occur when the means to repair them are nearby.

2.5 Mer2 phosphorylation

During early meiosis, Mer2 is phosphorylated by DDK on serine 30 and heavily by S-CDK within its N-terminal region and on serine 271 in the C-terminus (Henderson et al., 2006; Murakami and Keeney, 2014). According to *in vivo* studies (Sasanuma et al., 2008; Wan et al., 2008), S-CDK phosphorylation is necessary for DDK to be active on Mer2 and the phosphorylations of serines 29 and 30 are necessary for DSBs to occur. The phosphorylations were implied to enable Mer2 interaction with Rec114 and Xrs2 (part of MRX), however,

currently, there is very little data to support it (Henderson et al., 2006; Sasanuma et al., 2007).

To test whether recombinant Mer2 can at all be phosphorylated *in vitro*, we obtained plasmids containing genes for S-CDK and DDK for yeast expression generously gifted by John Diffley (Francis Crick Institute, London). John Weir successfully purified DDK out of yeast but had technical difficulties with purifying an active S-CDK. Because the S-CDK phosphorylation is priming DDK to phosphorylate Mer2 (Wan et al., 2008), I prepared phospho-mimicking mutants of Mer2 with serines 29/30 mutated to aspartic or glutamic acid and to alanine as a negative control to imitate the S-CDK phosphorylation and allow DDK to act on Mer2.

Saskia Funk performed the kinase assays with radioactive ATP and revealed that although wild-type $Mer2^{FL}$ is phosphorylated by DDK, both phospho-mimicking mutations (especially $Mer2^{S29/30D}$) are increasing the level of phosphorylation, while the amount of phosphorylation of $Mer2^{S29/30A}$ copies one of the wild-type (Figure 33A). This confirms, that the phospho-S29/30 are indeed priming further phosphorylation, but some sites can be phosphorylated even in the absence of the priming phosphorylation. To check, where the phospho-sites are located, another set of kinase assays was performed, this time with $Mer2^{core}$ and Mer2 truncations lacking the 40 N-terminal residues, including the S29/30 ($Mer2^{40\text{-}C}$). There was no detectable phosphorylation of $Mer2^{core}$, which is consistent with the previously suggested locations of phospho-sites within the terminal regions of Mer2. Given that $Mer2^{40\text{-}C}$ is

lacking the priming phosphorylation within the N-terminal region, one would expect not to see any phosphorylation. However, Mer2$^{40\text{-}C}$ was phosphorylated heavier than full-length wild-type Mer2 and Mer2$^{S29/30A}$.

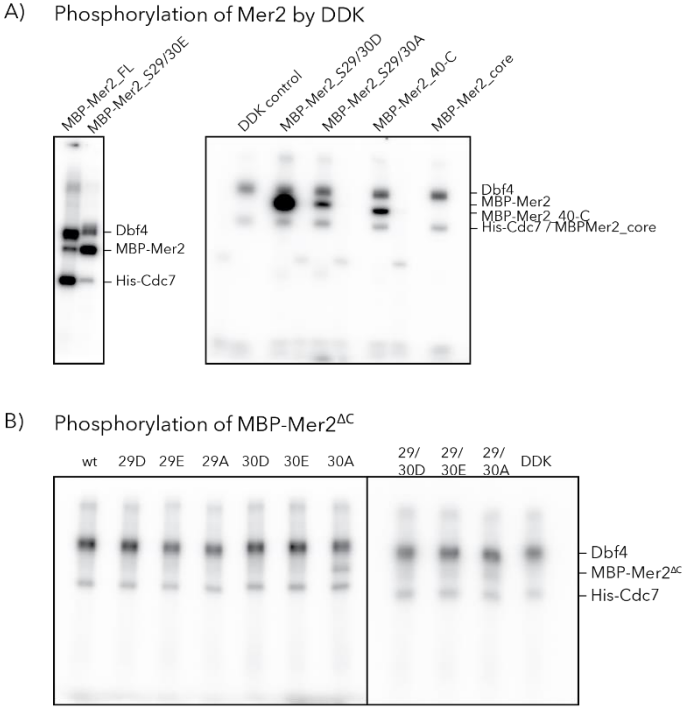

Figure 33: Phosphorylation of Mer2 variants A) Kinase assay with Mer2 constructs (as indicated) and DDK performed by Saskia Funk with radioactive ATP. B) Kinase assay with DDK and Mer2$^{\Delta C}$ construct with phospho-mimicking (S29D/E, S30D/E) or non-phosphorylatable (S29A, S30A) mutation

To determine, which Mer2 residues are phosphorylated in different Mer2 constructs, the samples were analyzed using mass-spectrometry by Tanja Bange (Ludwig-Maximilians Universität München; Figure 34). Surprisingly, there were many new

phospho-sites found within the C-terminal regions of Mer2, especially in Mer2 constructs with phospho-mimicking residues on position 29/30; the C-terminal phosphorylation pattern was nearly identical in the $Mer2^{40\text{-}C}$ construct. The results confirm, that indeed the priming phosphorylation on S29/30 (or its phospho-mimicking mutants) supports further phosphorylation of Mer2, especially within its C-terminal region, however, it can be overcome by deletion of the 40 N-terminal residues (Figure 34). Interestingly, The $Mer2^{WT\_FL}$ construct was lacking any phosphorylation within its C-terminal region, while the $Mer2^{S29/30D}$ was partially deficient in N-terminal phosphorylation. This could be caused by an interplay of the terminal regions, where the priming phosphorylations allow the kinases to act on the C-terminal region, possibly by a conformational change.

To further study the priming phosphorylations on the N-terminus of Mer2, I prepared a set of Mer2 variants, all based on $Mer2^{\Delta C}$ (=$Mer2^{N\text{-}256}$) truncation, lacking the C-terminal part. The variants include a mutation in either of the priming phospho-sites on serine 29 and/or 30 to glutamate or aspartate as phospho-mimicking residues or to non-phosphorylatable alanine, as a negative control (Figure 33B). Since some of the Mer2 variants included one or two of the priming phospho-mimicking residues (and they were proven effective as shown in the previous paragraph), I expected, that at least some of those variants will be phosphorylated within their N-terminal region to the same level as their full-length variants. However, this was not the case and none of the $Mer2^{\Delta C}$ was phosphorylated, except for $Mer2^{S30A}$ and $Mer2^{S29/3A}$, which is peculiar, given that alanine is a non-

phosphorylatable mutant and there was no phosphorylation detected previously with another construct containing S30A mutation. When analyzed on MS, both Mer2^{S30A} and Mer2$^{S29/3A}$ show a similar phosphorylation pattern within the N-terminal region as the Mer2^{WT_FL} construct. However, these data were obtained from a single experiment and therefore can serve rather as a starting point than a final result.

Figure 34: Mass-spectrometry analysis of the phospho-Mer2 variants. The sequence of Mer2^{FL} with detected phosphorylations in different constructs with the priming phospho-sites S29/30 marked with a red rectangle and the core domain marked in grey. Borders of constructs are marked with an arrow and the number of the residue.

Taken together, the data show that the priming phosphorylation of Mer2 on serines 29 and 30 increases the level of phosphorylation by DDK *in vitro*. However, the necessity for these priming phosphorylations can be overcome by the deletion of the N-terminal region. Even though the level of

phosphorylation was not tested with S-CDK, but with phospho-mimicking mutants, the data suggest, that the C-terminal region of Mer2 largely enhances any phosphorylation of Mer2, especially in the presence of phospho-mimicking mutants.

2.6 Mer2 interaction with Rec114 and Mei4

Mer2 was also suggested to interact with Rec114 and Mei4 *in vivo* (Henderson et al., 2006; Li et al., 2006; Maleki et al., 2007) in a phospho-dependent manner (Sasanuma et al., 2008). However, a recent *in vitro* study implied, that those proteins form rather a DNA-dependent phase separation (Claeys Bouuaert et al., 2021), than a stoichiometric complex. My students Leonie Konopka and Kristina Sturm during their bachelor's (Konopka, 2019) and master's (Sturm, 2020) thesis, respectively, tried to shed a light on the Mer2-Rec114-Mei4 (RMM) complex. They successfully purified the Rec114-Mei4 complex expressed in insect cells and also their truncations in *E. coli*. However, despite many attempts, they did not manage to create a stable RMM complex. For further details, please see their respective theses.

3 Discussion

3.1 Formation of the Spp1-Mer2 complex

It was implied by *in vivo* studies that the nucleosome binder Spp1 interacts directly with protein Mer2 (Acquaviva et al., 2013; Sommermeyer et al., 2013). However, currently, there is lacking detailed understanding of this interaction at the molecular level. Therefore, I aimed to shed light on this interaction *in vitro* in the absence of other cellular elements, which could uncontrollably influence the interaction.

Simultaneously with recently published findings (Claeys Bouuaert et al., 2021), I observed that the *S. cerevisiae* Mer2 forms a tetramer (Figure 13). Additionally, I revealed, that the $Mer2^{core}$ construct (aa 140-256), containing the predicted coiled-coil (aa 165-232) (Acquaviva et al., 2013; Sommermeyer et al., 2013), is responsible for the oligomerization (Figure 13A). This was previously implied based on the secondary structure prediction (Figure 9), but it was never demonstrated. My data show, that the Mer2 terminal constructs lacking the core domain ($Mer2^{N\text{-}139}$ = $Mer2^{N\text{-}term}$ and $Mer2^{256\text{-}C}$ = $Mer2^{C\text{-}term}$) alone are not able to tetramerize. Interestingly, Mer2 is phosphorylated within its terminal regions, especially at serines 29 and 30, which are essential for DSB formation (Henderson et al., 2006). Given that the Mer2 terminal regions ($Mer2^{N\text{-}term}$ and $Mer2^{C\text{-}term}$) surrounding the α-helical core are largely unstructured (Figure 9), these findings suggest that the tetrameric $Mer2^{core}$ has a rather structural function and is surrounded by flexible terminal regions with regulatory function.

Moreover, I demonstrated, that the Mer2^{core} interacts directly with the C-terminal α-helical domain of Spp1 (Spp1$^{169\text{-}C}$) and serves as a dimerization scaffold for Spp1 (Figure 13B-D and Figure 14). The interaction regions of Spp1 and Mer2 are consistent with the domains suggested by *in vivo* studies (Acquaviva et al., 2013; Sommermeyer et al., 2013) including a central valine 195 in the Mer2^{core}, whose mutation to aspartic acid disrupts the interaction with Spp1 (Adam et al., 2018). I revealed, that the interaction takes place even in the absence of any posttranslational modification or an additional factor at low nanomolar affinity (Figure 14). This implies, that the Spp1-Mer2 interaction is likely to be constitutive also *in vivo*.

My data from crosslinking experiment (DSBU, 11 Å spacer) coupled with mass spectrometry (XL-MS) further characterized the Spp1-Mer2 complex (Figure 15A). The crosslinking pattern on Mer2 alone is consistent with the published crosslinking pattern on full-length Mer2 with DSS crosslinker (disuccinimidyl suberate, 11 Å spacer) (Claeys Bouuaert et al., 2021), although I observed more crosslinks outside of the core domain of Mer2 (Figure 15A and Figure 35). This could be caused by the use of a different crosslinker, although the length of the spacer is the same (DSBU vs. DSS), purification procedure (MBP affinity vs. NiNTA affinity) or storage buffer (500 mM NaCl vs. 300 mM NaCl SEC buffer) resulting in a slightly different organization of the flexible terminal regions of Mer2. In both crosslinking datasets, there are many crosslinks to the same residues on another copy of Mer2, but also between very distant residues. This led to the suggestion of an antiparallel-parallel organization

of the Mer2 core (Claeys Bouuaert et al., 2021). However, given the tetramerization of Mer2, other organizations of the oligomer would also satisfy the observed crosslinks. One of them is a parallel configuration possibly with a bent within the core. Such a conformation is also supported by the presence of a predicted short loop or unstructured region in the core of Mer2 (Figure 9). However, without additional structural information, both suggestions remain speculative.

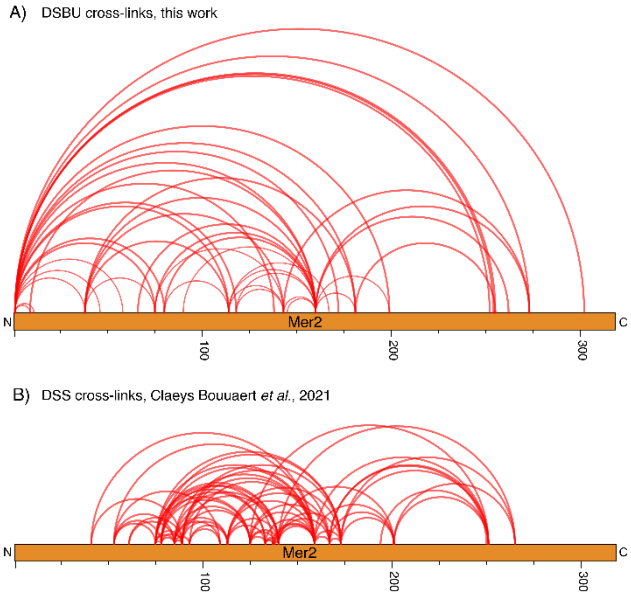

Figure 35: Comparison of crosslinking patterns on Mer2. A) Mer2 crosslinked with DSBU in this thesis. B) Mer2 crosslinked with DSS in (Claeys Bouuaert et al., 2021).

Upon binding Spp1, the crosslinking pattern of Mer2 does not exhibit any significant changes, suggesting that the interaction does not lead to a significant conformational change in Mer2. The structure of Mer2 is not known, however, there is structural

information about Spp1. Even though it is not clear how the domains of Spp1 interact with one another, the structures of the separate parts of Spp1 have been determined. Its N-terminal PHD and domain together with the C3H domain are globular (He et al., 2019), whereas the helical C-terminal domain, responsible for binding to COMPASS or Mer2 is extended (Qu et al., 2018). My SAXS analysis confirmed a globular shape of Spp1 (Figure 15B), consistently with the known substructures of Spp1.

Given that Mer2 is largely α-helical protein, it is not surprising, that the SAXS data implied a very elongated shape of the protein (~ 21 nm long), consistently with the early elution volume of Mer2 from SEC (Figure 11B). Interestingly, the Spp1-Mer2 complex is even more elongated than Mer2 alone (~ 38 nm long). Mer2 tetramerization core region interacts with the C-terminal α-helices of Spp1, therefore one could imagine, that the two helices of Spp1 lie on the α-helical bundle of the Mer2^{core} while the globular PHD domains face away from one another alongside the α-helical bundle, thus elongating the structure of the complex. This arrangement is likely if the Mer2 core is antiparallel-parallel helices, as suggested by Claeys Bouuaert et al. (Claeys Bouuaert et al., 2021).

However, as mentioned earlier, due to Mer2 tetramerization, it is not clear, whether Mer2 adopts this arrangement or if it is rather a parallel one. In that case, it would be unlikely, that the Mer2 core would include two asymmetric binding sites for Spp1 to allow the PHD domains of Spp1 to face away from each other. It would be much more likely, that both PHD domains would be extended to the same side. Nevertheless, this arrangement would

be compatible with the very elongated shape of the Spp1-Mer2 complex as well. Additionally, it would also allow for both Spp1 moieties in the Spp1-Mer2 complex to interact with the same nucleosome, as is likely the case. In either case, it is clear, that the core of the complex is very elongated and formed by the α-helical bundle of Mer2 and Spp1 likely with the V195 of Mer2 positioned at the centre.

3.2 Mer2 localization by the chromosomal loops

Given that the N-terminal PHD domain of Spp1 serves as a nucleosome H3K4me3 mark reader, its dimerization through Mer2 is compatible with the 2-fold symmetry of the nucleosome. An EMSA experiment and a pulldown with biotinylated mononucleosomes (MN; reconstituted with 167 bp DNA resulting in short free DNA overhangs) revealed, that the dimerization of Spp1 boosts Spp1 affinity to the H3K4me3 nucleosomes (Figure 17). Dimerization via Mer2 increases Spp1 affinity to the modified nucleosomes even more, suggesting Mer2 increases the Spp1-MN binding not only by dimerization of Spp1 but also by direct interaction with nucleosomes. This increase in affinity may be essential for proper DSB formation since the interaction between COMPASS-bound Spp1 and H3K4me3 is rather weak (He et al., 2019), whereas the association of the DSB machinery is a more stable event (Karányi et al., 2018).

XL-MS of the nucleosome-Spp1-Mer2 complex showed more crosslinks between the Spp1 units than in the absence of the nucleosome (Figure 15A and Figure 19). It implies, that the units are getting closer to one another, which supports the idea, that

both Spp1 moieties are bound to the same nucleosome and can explain the increase in the Spp1-H3K4me3 affinity upon dimerization via Mer2. Interestingly, the crosslinking data revealed some crosslinks between Mer2 and the nucleosome, especially with histones H3 and H4. After closer examination, I found out, that Mer2 is a very strong nucleosome binder (apparent K_D determined by EMSA ~ 5 nM) (Figure 22A). It interacts with both the DNA and with the nucleosome core particle (NCP; a histone octamer wrapped with 146 bp of DNA, resulting in a lack of free DNA overhangs). Additionally, I revealed, that the interaction is not dependent on histone modifications, the histone tails or the acidic patch of the nucleosome – the typical binding interface of the nucleosome (Figure 22B). Altogether, these data suggest, that Mer2 specifically recognizes the DNA entry/exit site on the nucleosome. Interestingly, it is consistent with the observation from fission yeast, where Rec15, a functional homolog of Mer2, is localized both at the chromosomal axis and also at the DSB hotpots (Miyoshi et al., 2012).

Given that the Spp1 affinity for the H3 tail is low micromolar (He et al., 2019), my observation further explains, why is the residence time of Mer2-bound Spp1 on nucleosomes longer than that of COMPASS (Karányi et al., 2018). Mer2 likely strengthens the Spp1-nucleosome interaction, not only by the dimerization of Spp1 but also by direct interaction with the nucleosome. This leads to the formation of a stable complex at the DSB site, where Spp1 provides the specificity and Mer2 the strength of the interaction.

Additionally, these new findings can explain, why neither Spp1 nor H3K4me3 is strictly necessary for DSB formation (though they are necessary for normal patterning). Mer2 can be imagined to bind stochastically to nucleosomes within the chromosome loops and connect them with the chromosomal axis. Presumably, Mer2 does not have a preference for a specific type or location of the nucleosome, therefore, many Mer2-bound nucleosomes would not be available for Spo11 cleavage, but only some would. This would reduce the number of DSBs and change their pattern, as is observed in the absence of Spp1 or H3K4me3 mark (Acquaviva et al., 2013; Karányi et al., 2018; Sommermeyer et al., 2013).

I revealed that the Mer2 terminal regions, especially the C-terminal part, are responsible for the interaction with nucleosomes (Figure 23), while the Mer2^{core} does not show any binding. This is consistent with previous findings (Claeys Bouuaert et al., 2021), that the C-terminal region of Mer2 is interacting with DNA. However, Mer2 has a significantly higher affinity for nucleosomes over free DNA (5 nm vs. 30 nm) and also interacts with the nucleosome core particle (NCP), which lacks any DNA overhangs. Consistent with my XL-MS data, this strengthens the argument, that rather than being a promiscuous DNA binder, Mer2 has a strong preference for the nucleosomal DNA at the entry/exit site of the nucleosome. Moreover, I observed, that the Mer2-MN complex is SEC stable with a distinct stoichiometry of one nucleosome per one Mer2 tetramer (Figure 21). Altogether, these findings suggest that although

Mer2 *can* interact also with naked DNA, in a cell it presumably rather forms a very specific complex with nucleosomes.

It was implied that Mer2 forms a DNA-dependent condensate together with Rec114 and Mei4 (Claeys Bouuaert et al., 2021), although it was also previously suggested that this interaction is phospho-dependent (Henderson et al., 2006; Murakami and Keeney, 2014; Wan et al., 2008). However, liquid-liquid phase separation of the RMM proteins brings up several questions. First of all, what would stop all of the RMM proteins to create one large condensate instead of being spread among the chromosomes, as we can observe? Additionally, once DNA breaks are made, the phosphorylation of Rec114 likely prevents further DSB formation. If the RMM interaction truly was phase separation dependent, how would the DSBs be stopped? Even though the proteins are migrating within the condensate and thus can be phosphorylated on the surface of the droplet, would the reaction be fast enough to prevent further DNA breaks in the proximity of an existing DSB? Another issue with this hypothesis lies within the used method. A positively charged protein or DNA binding protein will bind a negatively charged DNA and will form a condensate in the presence of a crowding agent independently of the biological relevance. Lastly, all of the other known protein interactions involved in the DSB formation have a distinct stoichiometry. I also observed, that Mer2 forms a stoichiometric complex with nucleosomes and that it has a strong preference for the nucleosomes over free DNA. Therefore, it is unlikely, that such a precise and convoluted system with defined

complexes would rely on an uncontrollable phase separation event.

It is however possible, that the Mer2-Rec114-Mei4 interaction is dependent on DNA, but rather than forming a condensate, it likely requires also proper previously described PTMs of the involved proteins and/or other binding partners. In meiosis, many key players are phosphorylated and SUMOylated (Bhagwat et al., 2021; Henderson et al., 2006), without those modifications, DSBs cannot be introduced and meiosis cannot proceed. Therefore, it is likely, that they affect crucial interactions of the meiotic DSB proteins; one of those interactions could be the one between the RMM proteins. Given that Mer2 also directly interacts with the nucleosomes, the axial Hop1 and with the resection machinery, it is conceivable, that any or all of those proteins need to be assembled on the axis to facilitate a structural change in Mer2 that might allow posttranslational modification and/or subsequent Rec114-Mei4 interaction and ultimately activation of Spo11.

3.3 Mer2 localization to the chromosomal axis

It is crucial to establish a connection between the DSB proteins and the chromosomal axis not only to physically link the DSB hotspot with the Spo11 complex but also to be able to regulate and stop the break formation. Here, I show for the first time, that Mer2 is responsible for linking the DSB hotspot to the axis via direct interaction with Hop1 without any prior modification on either of the binding partners (Figure 25 and Figure 26). Such an interaction was already suggested in mammals and also in fission

yeast, but was never confirmed in budding yeast nor *in vitro* (Kariyazono et al., 2019; Stanzione et al., 2016).

I revealed that Mer2 interacts directly with Hop1, although the interaction seems to be strengthened by the presence of Red1 (Figure 25). This effect is likely caused by both a conformational change of Hop1 caused by Red1 binding and by direct interaction between Red1 and Mer2.

Red1 changes the conformation of the HORMA domain of Hop1 upon binding the closure motif (CM) of Red1 with the assistance of Pch2 (Herruzo et al., 2021; Raina and Vader, 2020; West et al., 2018; Yang et al., 2020). Given that Hop1 contains a CM in its sequence, it can exist in three different conformations: closed – HORMA binds the Hop1 CM, unbuckled – HORMA does not interact with any CM and exposed – HORMA binds CM of another protein (e. g. Red1) and the Hop1 CM is free for interaction with another partner (Figure 4). The free Hop1 in the nucleoplasm is mostly in a closed conformation, whereas Hop1 on the axis adopts exposed conformation. The unbuckled and exposed conformations have a very similar fold to the HORMA domain; hence I used the unbuckled Hop1 ($Hop1^{K593A}$) to mimic the axial exposed Hop1. I found out, that the budding yeast Mer2 specifically interacts with the unbuckled conformation of Hop1 over the closed one (Figure 26). This mechanism provides an additional level of control, as it limits the DNA break machinery to the chromosomal axis. Without this limitation, Mer2 could interact with the free closed Hop1 in the nucleoplasm, which would lead to an assembly of the DSB machinery around the loop and uncontrollable DSB formation.

Moreover, the preference of Mer2 for the axial Hop1 can explain how breaks are shut down by chromosome synapsis. SC formation leads to the recruitment of Pch2, which removes Hop1 from the axis causing a conformational change of the HORMA domain from exposed to closed. Since Mer2 prefers unbuckled (and likely also exposed) Hop1, it would be removed from the axis too, effectively shutting down the DSB formation (Chen et al., 2014; Raina and Vader, 2020; Subramanian et al., 2016; Vader, 2015; West et al., 2018; Yang et al., 2020).

The Mer2 homolog from fission yeast (Rec15) is directly interacting both with Hop1 (Hop1) and Red1 (Rec10) (Miyoshi et al., 2012). Although I did not detect any binding between Mer2 and Red1 in a pulldown setup (Figure 25), the AlphaFold model of the HORMA domain of Hop1 ($Hop1^{HORMA}$), the N-terminal globular domain of Red1 (including its closure motif; $Red1^{N\text{-}400}$) and the C-terminal region of Mer2 ($Mer2^{254\text{-}C}$) implies a direct Red1-Mer2 interaction (Figure 28C). Even though the affinity is not strong enough to be detectable in a pulldown, once the Hop1-Mer2 interaction is established, Red1 can further stabilize it. Importantly, the position of the $Mer2^{C\text{-}term}$ in the model is consistent with the Hop1 residues crosslinked to Mer2 (Figure 28B). The XL-MS data showed, that Mer2 interacts with one "face" of the HORMA domain of Hop1 (Figure 28A). The other "face" is likely occupied by Red1, as is suggested by the AlphaFold model (Figure 28C), therefore unavailable for Mer2 binding.

Additionally, Red1 is a tetramer and likely tetramerizes Hop1 upon binding, thus increasing its local concentration (West et al.,

2019), although formal proof of this is lacking. This can strengthen the Hop1-Mer2 interaction by avidity. In the pulldown, I used a monomeric Hop1 immobilized on beads to mimic the high local concentration, however, it might not be the perfect mimic.

Furthermore, the Hop1-Red1 complex used in a pulldown was purified from insect cells, which introduce some post-translational modifications, but the Hop1 by itself is unmodified from *E. coli*. It was shown, that all three of those proteins, Mer2, Hop1 and Red1 are phosphorylated and SUMOylated during meiosis (Bhagwat et al., 2021; Henderson et al., 2006). Those modifications are likely regulating the meiotic recombination and can affect the interaction. However, this was not yet studied in detail, but through my thesis work, I have established the tools necessary to allow these questions to be directly addressed.

Even though Mer2 is a very divergent protein, it contains a surprisingly conserved patch within the last 19 residues. I revealed, that this region is responsible for Mer2 binding to Hop1 (Figure 26). The C-terminal region of Mer2 was previously shown to play a role in DNA binding and DSB formation (Claeys Bouuaert et al., 2021), however, without a known mechanism. My findings explain this observation and, given the high conservation of the Mer2 patch, imply, that the corresponding region of Mer2 homologs will interact with the respective HORMA domain protein as well.

Adjacent to the HORMA domain of Hop1 lies a zinc finger domain recently established as a PHD (plant homeodomain). Its

role is a source of speculation. In fission yeast, this domain was shown to be involved in Mer2 interaction (Kariyazono et al., 2019). However, in budding yeast, I showed that the C-terminal part of Hop1 (including the PHD domain) was not able to interact with Mer2, but the deletion of the HORMA lead to disruption of the interaction (Figure 26). This suggests that the HORMA is responsible for Mer2 binding, consistent with the AlphaFold model (Figure 28C). Given that PHD domains are often interactors of nucleosome modifications, I tested this hypothesis with two different trimethylations on histone H3, concretely H3K4me3 and H3K36me3 and revealed, that Hop1 specifically recognizes trimethylated nucleosomes (Figure 29). Given that HORMA-proteins in other organisms lack the PHD domains, it is possible, that the role of the Hop1 PHD is taken over by another protein or the pathway was adapted and does not require Hop1 PHD anymore. Either way, this observation raises an interesting question about the role of the PHD of Hop1 and opens the door for further studies.

3.4 Mer2 association with the resection machinery

It is established that the resection machinery, the MRX complex, is generally necessary for DSB formation (Ajimura et al., 1993; Johzuka and Ogawa, 1995), although some mutations of the proteins result in successful meiosis. However, the mechanism of this requirement is unknown.

With the help of our collaborators (Vader laboratory), I showed that Mre11 directly interacts with the conserved N-terminal patch of Mer2. Adjacent to the serines 29/30 of Mer2,

which are critical for DSB formation, lies a second conserved patch (residues 52-71) (Tessé et al., 2017), predicted to be α-helical (Figure 9). One side of the helix is very conserved, suggesting, that it is involved in an interaction with a conserved binding partner. Our collaborators revealed, that the mutation of the conserved residues to alanine (resulting in Mer2^{3A} or Mer2^{4A}) led to the formation of unviable spores due to failure in DSB formation (Figure 30).

Additional yeast two-hybrid assay performed by Veronika Altmannová revealed, that the mutations of Mer2 completely abolished the interaction with Mre11 (Figure 32A). I confirmed the direct interaction of Mer2 and Mre11 also *in vitro* by a pulldown (Figure 32B), however, both Mer2 mutants still retained some binding to Mre11. Such a difference could be explained by the absence of post-translational modification in the pulldown experiment.

Recently it was observed, that Mer2 is heavily SUMOylated during meiosis (Bhagwat et al., 2021). One of the SUMOylated residues is also a lysine (K61), part of the conserved N-terminal patch of Mer2, mutated in Me2^{3A}. Interestingly, based on the GPS-SUMO prediction software (Zhao et al., 2014), Mre11 contains three SUMO-interaction motifs (SIMs), two within its N-terminal region and another in the C-terminal area. It was shown, even before the discovery of those SIMs, that the deletion of the C-terminal region of Mre11 disrupts meiosis but does not affect vegetative DNA repair (Furuse et al., 1998). It suggests, that the C-terminal SIM of Mre11 is responsible for a meiosis-specific interaction, crucial for DSBs. My XL-MS data on the

Mer2-Mre11 complex revealed many crosslinks between the N-terminal region of Mer2 and the C-terminal part of Mre11, in the proximity of the SIM, thus supporting the idea of a SUMO-dependent interaction of Mer2 and Mre11 (Figure 32C).

A previous *in vivo* study based on a yeast two-hybrid assay already suggested that the MRX complex is connected with the DSB machinery via Mer2 (Arora et al., 2004; Henderson et al., 2006). However, the results implied, that the main interactor is Xrs2, whereas Mre11 bound Mer2 only weakly. Put together with my observations, it is likely, that the main localization of the MRX complex is through Mer2-Xrs2, but Mre11 plays a rather regulatory role, which, upon SUMOylation of Mre11, somehow enables the DSB formation through interaction with Mer2.

I found out, that the conserved N-terminal patch of Mer2 also plays a role in the nucleosome interaction. Both IP-MS and an EMSA showed a decrease in binding (Figure 31), although neither was diminished. It confirms the importance of Mer2 terminal regions for nucleosome binding (as discussed in 3.2) and suggests, that the mutations are not pure separation of function mutants. They disrupt more functions of Mer2, likely by disturbing the fold of the α-helix. Nevertheless, it is clear, that the conserved patch plays an important role in binding both the nucleosome and Mre11, likely driven by SUMOylation.

3.5 Relationship of the Mer2 terminal regions

Mer2 is heavily phosphorylated by S-CDK and DDK within its N-terminal region with an additional S-CDK phospho-site in the C-terminal area of Mer2 (Henderson et al., 2006). These

phosphorylations (or at least the ones on serines 29 and 30) are necessary for a proper DSB formation, supposedly by enabling the interaction with Rec114 and Xrs2 (Boekhout et al., 2019; Henderson et al., 2006; Li et al., 2006; Panizza et al., 2011; Wan et al., 2008). It was suggested, that the S-CDK phosphorylation on S30 serves as priming phosphorylation, which enables DDK to act on Mer2 *in vivo* (Henderson et al., 2006; Murakami and Keeney, 2014). However, it was never studied in depth, nor in vitro, how those phosphorylations affect one another or if the S-CDK phosphorylations are truly necessary for DDK to act on Mer2.

With help from Saskia Funk, I showed, that the recombinant DDK is very active on Mer2 *in vitro* even in absence of S-CDK. Using mass-spectrometry, I found many residues phosphorylated by DDK within the N-terminal region of Mer2, which were never observed before (Figure 34). Strikingly, both S29 and S30, which are necessary for DSB formation, remained unphosphorylated. Mutating those serines to mimic phospho-serines ($Mer2^{S29/30D}$ and $Mer2^{S29/30E}$) strongly increased the number of phosphorylated residues and resulted in a heavily phosphorylated C-terminal region of Mer2 (Figure 33A and Figure 34). Interestingly, the deletion of 40 N-terminal residues ($Mer2^{40\text{-}C}$) gave roughly the same pattern of C-terminal phosphorylation as $Mer2^{S29/30D}$ (Figure 34). However, the deletion of the C-terminal region ($Mer2^{\Delta C}$) led to an almost complete loss of phosphorylation (Figure 33B and Figure 34).

These findings suggest a complex interplay between the two kinases and imply two types of DDK phosphorylation on Mer2:

one is dependent on S-CDK (like S29) and the other one is not. Additionally, there is a convoluted effect of the Mer2 terminal regions, where the C-terminal part somehow actively enables the N-terminal phosphorylation. It is conceivable, that one of the effects of the S29/30 phosphorylation is in enabling the C-terminal region to be phosphorylated which in turn allows the phosphorylation of the rest of the N-terminal region. Such a complex interplay between the kinases and Mer2 terminal sections likely provides another level of control of DSBs. Full phosphorylation of Mer2 might change the conformation of the protein and thus facilitate its interaction with other binding partners.

It is clear, that Mer2 is a tetramer with an α-helical core surrounded by largely unstructured terminal regions (Figure 9 and Figure 13). However, it is not known, how are the subunits of Mer2 organized and what is the position of the terminal parts in respect to one another. In any case, due to high flexibility, it is conceivable, that the terminal segments are very close to one another and therefore can affect each other's post-translational modifications and behaviour. Even though there are still many question marks in the mechanism and role of Mer2 phosphorylation, it is clear, that it is far more complex, than thought previously. Additionally, it is possible, that the phosphorylation pattern of Mer2 changes once Mer2 binds nucleosomes and/or Hop1. It is also conceivable, that not only the interaction with Rec114 but also with Hop1 or nucleosomes is modulated by phosphorylation or SUMOylation. Up to date, however, there is no data to study such an effect. My data opens

a door for further studies with the possibility of a strong interplay between the terminal regions of Mer2 and the effect of the phosphorylation on the Mer2 interactions and *vice versa*.

4 Conclusion and outlook

In this thesis, I biochemically and structurally dissected the meiotic protein Mer2. I identified its novel binding partners, nucleosomes and Mre11, the resection machinery protein. Additionally, I deepened our understanding of its interaction with Spp1 and Hop1, binding partners suggested by *in vivo* studies. Given that none of those interactions was studied *in vitro*, my data provides a basis for further studies of the meiotic DSB control and formation.

I confirmed, that Mer2 forms a complex with Spp1, as was suggested *in vivo* (Acquaviva et al., 2013; Sommermeyer et al., 2013) (Figure 12 and Figure 13). I revealed, that the complex is very stable and does not require any other factor or a post-translational modification. The C-terminal region of Spp1 and the core domain of Mer2 interact with a very strong affinity (low nanomolar; Figure 14) in a 2:4 stoichiometry (Figure 13). I confirmed previous observation, that Mer2 is a tetramer (Figure 13A) (Claeys Bouuaert et al., 2021) and showed, that the core domain is responsible both for tetramerization and also for Spp1 binding.

I revealed, that one role of the Spp1 dimerization via Mer2 is in increasing its affinity to nucleosomes (Figure 17). It was shown, that Spp1 in complex with Mer2 has a longer residence time on nucleosomes in comparison to Spp1 in COMPASS (Karányi et al., 2018), however without any mechanistic clarification. My data explain this observation, as dimerized Spp1 binds stronger to nucleosomes. Furthermore, I revealed that Mer2

itself specifically interacts with the DNA entry-exit site of the nucleosome via its terminal regions (Figure 23 and Figure 24). Given that the Mer2-nucleosome interaction is very strong (low nanomolar), the data clearly shows, that Mer2 is a true nucleosome binder, a role, which was never observed or suggested before. Altogether, my data suggest a complex interplay between the proteins, where Mer2 tetramer interacts with Spp1 via its core and thus dimerizes it and strengthens its interaction with the H3K4me3 nucleosome. Mer2 then "locks" the complex by binding the DNA entry/exit site via its terminal regions.

Even though it is very likely that both Spp1 moieties and also Mer2 interact with the same nucleosome, there is currently no formal proof. I revealed, that one Mer2 tetramer binds one nucleosome (Figure 21), however, it is also possible, that Mer2 interacts with the nucleosomes within the axis, instead of the ones in the loop, where Spp1 binds. This hypothesis could be tested by analyzing the MN-Spp1-Mer2 complex on SEC-MALS. The sizes and stoichiometries of the separate components (and even the Spp1-Mer2 and MN-Mer2 subcomplexes) are known (Figure 13 and Figure 21), however, to obtain clear results, a buffer optimization might be needed.

Structural studies on Spp1-Mer2 and MN-Spp1-Mer2 were extremely challenging, likely due to the high flexibility of the proteins and suboptimal buffer composition. I could observe distinct particles of the Spp1-Mer2 complex on cryoEM (Figure 16), however, they were not homogenous enough. To improve the sample homogeneity, the complex could be mildly crosslinked or

one could use a Mer2 truncation without the flexible terminal regions. To obtain a structure of the MN-Spp1-Mer2 complex, a thorough buffer optimization and potentially also mild crosslinking would be necessary. Nevertheless, the biochemical and biophysical data together with known structures of nucleosomes and parts of Spp1 provide valuable insight into the organization of the MN-Spp1-Mer2 complex.

For the first time, I showed that Mer2 directly interacts with the axial protein Hop1 via its conserved C-terminal patch *in vitro* and without any prior modification (Figure 27). Interestingly, I revealed, that Mer2 favours the unbuckled or exposed conformation of Hop1 (Figure 26). Mer2 strongly preferred Hop1 bound to Red1 (hence in the exposed conformation) over free closed Hop1 (Figure 25). This suggests, that Red1 additionally contributes to the Hop1-Mer2 binding, even though I did not detect any direct interaction between Mer2 and Red1 in a pulldown. However, it is consistent with the AlphaFold model of the Mer2-Hop1-Red1 truncations (Figure 28C).

The additional contribution of Red1 to the Hop1-Mer2 interaction could be detected by quantifying the affinities of the proteins in the presence and absence of Red1. However, given that wild-type Hop1 and Red1 purified separately fail to interact (Saskia Funk, personal communication), the unbuckled Hop1^{K593A} would have to be used. Nevertheless, such a quantification could provide a useful insight into the arrangement of the axial protein with Mer2. Furthermore, it is possible, that there is an effect of Hop1 oligomerization upon Red1 binding (suggested by the structural analysis in (West et al., 2019, 2018)),

which increases its affinity to Mer2. Hence, it is possible, that Mer2 prefers not only unbuckled/exposed conformation of Hop1, but also a tetramerized Hop1. As such, it would provide an additional level of control to DSBs. A further structural study and a thorough biochemical analysis might provide an answer to this question.

Additionally, I demonstrated, that the MN-Spp1-Mer2-Hop1 interactions are mutually compatible (Figure 27C). In the future, it would be interesting to study the complex in a bigger depth. In the pulldown, there is more Mer2 pulled in the MN-Spp1-Mer2 pulled than in the Mer2 alone sample. It is likely, that the interactions strengthen one another, similar to what I observed in the MN-Spp1-Mer2 complex. However, this hypothesis has to be tested further. Moreover, it would be interesting to test the stoichiometry of the assembly. The MN-Spp1-Mer2 is very likely a 1:2:4 complex and Red1 is a tetramer. Therefore, it is conceivable, that Hop1, although a monomer by itself, is tetramerized both by Mer2 and by Red1. This would be consistent with the AlphaFold model of Mer2-Hop1-Red1 truncations (Figure 28C), which contains one copy of each protein. Further studies of the MN-Spp1-Mer2-Hop1 will likely require a thorough buffer optimization, however, once in an optimal buffer, the whole complex, potentially even in the presence of Red1 could be analyzed by SEC-MALS and by cryoEM. Such a project is very ambitious and will require a large time investment, yet it could provide answers to many questions, which arose within this thesis.

I revealed for the first time, that Hop1 specifically recognizes trimethylated nucleosomes, possibly via its PHD domain (Figure 29). Up to date, there is no role assigned to this domain and given that PHD domains often recognize modified nucleosomes, it is feasible, that it also plays a role in such an interaction. However, this would have to be further confirmed by the use of Hop1 truncations in EMSAs and pulldowns with methylated nucleosomes. Additionally, although my data clearly shows the preference of Hop1 for trimethylated nucleosomes, I cannot exclude any binding to di- or monomethylated nucleosomes. Hence, a broader analysis with more types of histone modifications could reveal, whether Hop1 has a preference for a certain nucleosome modification or if it is a general trimethylation binder.

I unveiled a novel direct interaction of Mer2 with Mre11. It was suggested, that those proteins might weakly interact in a yeast two-hybrid assay (Arora et al., 2004; Henderson et al., 2006), however, it was never studied nor shown *in vitro*. With our collaborators (Vader lab), I showed, that the conserved N-terminal patch of Mer2 is responsible for Mre11 binding (Figure 32). Mutations of this conserved region of Mer2 abolished the Mre11 *in vivo*, however, the effect was not as prominent *in vitro*. That might be caused by the absence of posttranslational modifications on Mer2. Given that the conserved region of Mer2 is SUMOylated during meiosis (Bhagwat et al., 2021) and that Mre11 has three predicted SUMO interaction motifs (SIM), it is very likely, that the interaction is SUMO-dependent. However, further analysis is necessary to provide evidence for the role of

SUMO in the Mer2-Mre11 interaction. *In vitro,* SUMOylation assay followed by an interaction study could support this hypothesis. Alternatively, reciprocal mutation of the SIM of Mre11 followed by pulldown with Mer2 could be sufficient to prove the SUMO-dependent Mer2-Mre11 interaction. Additionally, given the conservation of the Mre11-binding region of Mer2, it is likely, that their homologs from different organisms interact as well. However, the Mer2-Mre11 interaction was never tested in other organisms.

The phosphorylation of Mer2 plays a crucial role in DSB formation, however, the role of the phosphorylation is not clear. It was suggested, that DDK acts on Mer2 only on serine 29 and only after S30 is phosphorylated by S-CDK (Henderson et al., 2006; Wan et al., 2008). Here, I provide a possible explanation for the role of the S29/30 phosphorylation. My data show, that only in the presence of those phosphorylations (or their phosphomimicking mutants), the C-terminal region of Mer2 can be phosphorylated by DDK. DDK phosphorylation of the C-terminal segment of Mer2 was never observed before, but I demonstrated, that it is necessary for further N-terminal phosphorylation of Mer2 by DDK. The data suggest a complex interplay between the Mer2 terminal regions and the kinases. However, it has to be mentioned, that the phosphorylation assays were performed in absence of S-CDK, which can affect the result. Therefore, also the role of S-CDK has to be investigated to provide a bigger picture of the kinase activity on Mer2. Nonetheless, it is likely, that the phosphorylations of Mer2 change the conformation of the terminal regions, thus exposing a

previously hidden binding interface. This would explain, the suggested phospho-dependent interaction of Mer2 with Rec114 and Xrs2 (Arora et al., 2004; Henderson et al., 2006; Wan et al., 2008). However, further analysis of the role of Mer2 phosphorylation is necessary.

Collectively, I revealed that Mer2 serves as an interaction platform for the proteins involved in the regulation of DSB. Its tetrameric core interacts with the C-terminal α-helices of Spp1, while the terminal regions recognize the DNA entry/exit site of the nucleosome. The two conserved patches of Mer2, one within each terminal region are responsible for binding Mre11 (N-terminal patch), likely enhanced by SUMO, and Hop1 (C-terminal patch), preferably in unbuckled or exposed conformation. My data provide an insight into the molecular mechanism of the DSB regulation and can serve as a foundation for future studies of meiotic DSB-formation.

5 Methods

5.1 Protein preparation

5.1.1 Cloning

Polymerase chain reaction (PCR)

All used expression vectors were prepared using Gibson cloning (Gibson et al., 2009). First, the genes were amplified by PCR (polymerase chain reaction) using Flash High-Fidelity PCR Master Mix (Thermo Scientific). Sequences of *S. cerevisiae* SPP1, HOP1, RED1, and MRE11 were derived from SK1 strain genomic DNA. Due to the presence of an intron in MER2, this was amplified as two separate fragments and Gibson assembled. Used primers are listed in

Supplementary table 6. The reaction was set up in 25 µl as follows:

Template	60 ng
2x Buffer	12.5 µl
Forward primer (10 µM)	1.25 µl
Reverse primer (10 µM)	1.25 µl
H_2O	to 25 µl

The reaction was performed under the following conditions:

Initial denaturation	98 °C	10 s	
Denaturation	98 °C	1 s	x 30
Annealing	60 °C	5 s	
Elongation	72 °C	15 s/kb	
Final elongation	72°C	120 s	

The amplified product was analysed by gel electrophoresis (0.8% agarose) at 120 V for 40 min and visualized by GelGreen (Biotium). The desired fragment was isolated using Wizard SV Gel and PCR Clean-Up System (Promega) according to the manufacturer's protocol.

Gibson assembly

The purified gene of interest of inserted into the linearized vector by Gibson assembly cloning using the biGBac system (Weissmann et al., 2016). The library modified in our lab includes backbones with various N- and/or C-terminal tags for expression in *E. coli* (pColi) or insect cells (pLib, pBIG) (Altmannova et al., 2021). All vectors were linearized by endonucleases BamHI and HindIII (high fidelity, NEB). The cloning primers include universal overhangs complementary to the ends of the linearized vectors, which allow a fast and universal cloning strategy using only a few PCR products.

Table 3: Gibson overhangs

Target assembly junction	**Sequence (5´-3´)**
5´ extension for pColi	TTTGTTTAACTTTAAGAAGGAGACT GGATC
5´ extension for pLib	CCACCATCGGGCGCGGATCC
5´ extension for pColi or pLib with N-terminal tag	CTGTTCCAGGGGCCCGGATCC
3´ extension for pColi or pLib	TCCTCTAGTACTTCTCGACAAGCTT TTA
3´ extension for pColi or pLib with C-terminal tag	TCCAGATCCAGATCCGCTTCCACT

For the Gibson assembly, 15 µl of Gibson mix was combined with 5 µl of the amplified PCR product and linearized backbone with a three-fold molar excess of the insert. In the case of mutagenesis, where the assembly consists of two PCR products, the longer fragment was treated as the backbone. The mixture was incubated for 15 min at 50 °C. The reactions were designed as described in Supplementary table 4 and Supplementary table 5.

Gibson mix

Tris-HCl pH 7.5	100 mM
$MgCl_2$	10 mM
dNTP Mix	0.2 mM
DTT	10 mM
PEG 8000	50 mg/ml
NAD	1 mM
T5 Exonuclease (NEB)	4.8 U/ml
Phusion polymerase (NEB)	600 U/ml
Taq ligase (NEB)	4800 U/ml

Transformation

For transformation, 50 µl of chemically competent *E. coli* cells XL1 Blue (Agilent), C41 (Overexpress C41 (DE3), Sigma-Aldrich) or BL21 (BL21 Star (DE3) pLysS, Invitrogen) were incubated on ice with up to 130 ng of plasmid DNA (maximum 5 µl) for 30 min. The mixture was subsequently heat-shocked at 42 °C for 45 s followed by a 2 min incubation on ice. The cooled cells were diluted with 250 µl of LB and incubated at 37 °C and 200 rpm for another 1 h before spreading on LB plates. The plates were incubated overnight at 37 °C.

LB medium and plates

Peptone/tryptone	10 g/l
Yeast extract	5 g/l
NaCl	5 g/l
Adjust to pH 7	
Additionally for LB-plates:	
Agar	15 g/l
LB_{Amp}	0.1 g/l ampicillin

To validate the success of the cloning, a single colony of transformed XL1 Blue cells was incubated with 4 ml of LB_{Amp} at 37 °C and 200 rpm overnight. The plasmid was isolated using QIAprep Spin Miniprep Kit (Qiagen) according to the manufacturer's protocol. The sequence of the open reading frame was verified by in-house Sanger sequencing using T7 sequencing primers (aligning outside of the open reading frame) and aligned to the respective sequence from *S. cerevisiae* SK1 in Benchling.

5.1.2 Recombinant protein expression in *E. coli*

Small-scale expression

The preferable expression conditions were tested in 20 ml cultures. *E. coli* C41 or BL21 cells were transformed with an expression vector and several colonies were harvested into 20 ml of TB_{Amp} in a 100 ml Erlenmeyer flask. The cells were incubated at 37 °C and 200 rpm until they reached OD_{600} ~0.5-0.8 when they were moved to a pre-cooled shaker at 25 °C and 18 °C, respectively. After a few minutes, the expression was induced by 250 µM isopropyl β-D-1-thiogalactopyranoside (IPTG). The cells induced at 25 °C were incubated for three hours, the ones at 18 °C overnight (for ~20 hours). After the incubation, the cells

were harvested at 5000 ×g and 4 °C for 15 min. The cell pellet was washed with PBS and stored at -20 °C.

TB medium

Tryptone	12 g/l
Yeast extract	24 g/l
Glycerol	0.4% (v/v)
KH_2PO4	17 mM
K_2HPO_4	72 mM

Big-scale expression

For a big scale expression, 200 µl of competent *E. coli* C41 or BL21 cells were transformed with ~400 ng of plasmid and all colonies were harvested in total into 2 l of TB_{Amp}, split in 10x 2 l Erlenmeyer flasks (400 ml of media in each). The cells were incubated at 37 °C and 200 rpm until they reached OD_{600} ~0.4-0.6. As previously, the cells were moved to a pre-cooled shaker (25 °C or 18 °C) and after ~30 minutes induced with IPTG (0.25 mM). The cells were from 25 °C and 18 °C were harvested after 3 hours and overnight (~20 hours) respectively by centrifugation at 6000 ×g and 4 °C for 30 min. The cell pellet was washed with PBS, flash-frozen in liquid nitrogen and stored at -80 °C.

5.1.3 Recombinant protein expression in insect cells

The insect cells Sf9 (Vaughn et al., 1977), originating from *Spodoptera frugiperda* or Hi5 (BTI-Tn-5B1-4) (Wickham et al., 1992) from *Trichoplusia ni*, were grown in Sf-900 III serum-free medium (Gibco) at 27 °C and 100 rpm in Erlenmeyer flasks

(Pyrex borosilicate glass, SciLabware) filling one-tenth to one-fifth of the flask volume. Cells were passaged under sterile conditions every two to three days into a clean flask to achieve a cell density of 0.8-1.0 × 10^6 cells/ml in the case of Sf9 cells and 0.3-0.5 × 10^6 cells/ml in the case of Hi5. The latter tend to clamp, therefore, the Hi5 culture was left standing without rotation for as short time as possible.

Cells used for transfection or infections were split a day in advance to 1.0 × 10^6 cells/ml and then split to 1.0 × 10^6 cells/ml immediately before use (in case of transfection also with an exchange of media).

Bacmid generation

To generate bacmid required for expression in insect cells, *E. coli* competent cells EmBacY were transformed with pLib vector. The transformed cells were plated on an LB_{Bacmid} plate (section 7.1.2) and incubated at 37 °C for 48-72 hours to allow blue-white screening to occur (Bieniossek et al., 2008; Trowitzsch et al., 2010). One white colony was incubated with 3 ml of $LB_{Kan/Gent}$ at 37 °C and 200 rpm overnight and the bacmid was subsequently purified using the first three steps in the QIAprep Spin Miniprep Kit (Qiagen). The supernatant was transferred into a clean 1.5 ml tube and the DNA was precipitated by an addition of an equal volume of isopropanol -20 °C at least for one hour. The precipitated DNA was harvested at 4 °C and 17,000 ×g for 15 min and washed with ~700 µl of cold 70% (v/v) ethanol followed by another centrifugation for 5 min. The wash was repeated and the

ethanol was removed under sterile conditions. The dried pellet was resuspended in 30 µl of sterile H_2O.

To generate baculoviruses used for the expression of recombinant proteins in insect cells, 15 µl of bacmid were mixed with 250 µl of medium and 5 µl of FuGENE 6 transfection reagent (Promega) and incubated for 20 min at room temperature. 2.0×10^6 Sf9 cells for each transfection split the day before were spun down (60 ×g for 5 min) and resuspended in 2 ml of fresh media and pipetted into a 6-well plate together with the transfection mix. The cells were incubated at 27 °C for 72 hours.

Baculovirus amplification

2 ml of transfected cells from the previous step was combined with 10 ml of freshly resuspended Sf9 cells (at a density of 1.0×10^6 cells/ml) in a 10 cm dish and incubated at 27 °C for 72 hours. Afterwards, all the cells (including cells attached to the dish) were harvested (60 ×g for 5 min) and the supernatant containing the virus was sterile filtered with a 0.2 µM filter, resulting in V_0 stored at 4 °C. The cell pellet was frozen in liquid nitrogen and used for a pulldown to check the presence of the protein of interest (described in section 5.3.1).

The virus was further amplified by infecting 25 ml of Sf9 cells (1.0×10^6 cells/ml) with a 1:100 (v/v) ratio of V_0 (250 µl), followed by incubation at 27 °C and 100 rpm for 72 hours. To isolate the V_1, the cells were harvested and the supernatant was filtered in the same manner as for V_0. In another round of amplification, V_2 was generated V_1 and can be further used for protein expression.

Protein expression

To test the optimal expression conditions, 50 ml of Sf9 or Hi5 cells (1.0×10^6 cells/ml) were infected with freshly generated V_2 in a 1:100 or 1:1000 (v/v) ratio. 25 ml of either of those cultures were harvested 48 hours after infection, the remaining 25 ml after additional 24 hours (72 hours in total). The cells were harvested by centrifugation at 60 ×g and 4 °C for 5 min, washed with PBS and stored at -80 °C after flash freezing.

Big scale expression was performed in 1.8 l Fernbach flasks (Duran glass, DWK Life Sciences) filled with 400 ml of cells. The type of cells, virus amount and time of infection can vary depending on the results of the small-scale test described above. The infected cells were harvested at 60 ×g and 4 °C for 30 min and washed twice with PBS. Washed pellets were frozen in liquid nitrogen and stored at -80 °C.

5.1.4 Protein purification

Unless specified differently, all steps were performed on ice or at 4 °C with cold buffers. Buffers loaded on Äkta Pure (GE Healthcare) were sterile filtered (0.2 µM) before use.

Mer2 purification

Mer2 constructs were expressed as a 3C HRV cleavable N-terminal MBP fusion in chemically competent C41 *E. coli* cells. Protein expression was induced by the addition of 250 µM IPTG and the expression continued at 18 °C overnight. Cells washed with 1× PBS were either flash-frozen in liquid nitrogen and stored at -80 °C or directly used for purification.

The harvested cells were resuspended in 1:5 (mg/ml) lysis buffer and homogenized via Ultra-Turrax T18 (IKA) with 19 G Disperser (IKA) at 3000 rpm for 2 min. The cells were lysed by passing twice through the EmulsiFlex C3 (Avestin) at 1000 bar and cleared at 20,000 ×g and 4 °C for 30 min. Cleared lysate was applied on a 5 ml pre-equilibrated MBP-trap column (GE Healthcare) on Äkta Start (GE Healthcare) with a flow rate of 5 ml/min and washed with 10 ml of 1 mM ATP followed by extensive washing with lysis buffer (10 CV). Mer2 constructs were eluted with a gradient to 25 % lysis buffer containing 1 mM maltose over 20 CV and the samples of the eluate were analyzed by SDS-PAGE (according to Laemmli).

Elution fractions containing the protein of interest were pooled and diluted with No salt buffer to a final salt concentration of 75 mM. The diluted eluate was subsequently passed through a 6 ml anion exchange column (IEX) ResourceQ (GE Healthcare) with a flow rate of 5 ml/min equilibrated in a 1:10 mixture of High salt buffer:No salt buffer, resulting in a buffer with 100 mM NaCl. The unbound proteins were first washed with 3 CV of 100 mM NaCl buffer and then eluted by an increasing salt gradient to 600 mM NaCl (60 % High salt buffer), followed by step elution by 1 M NaCl (100 % High salt buffer).

Elution fractions were again checked on SDS-PAGE and the protein-containing elution fractions were concentrated on a Pierce concentrator (100 kDa MWCO for Mer2 constructs containing the core domain, 30 kDa MWCO for Mer2 constructs without the core, Thermo Scientific) and loaded on a size exclusion column (SEC) Superose 6 16/600 (GE Healthcare) pre-

equilibrated in SEC buffer with a flow rate 0.8 ml/min. Samples from the eluted fractions were analyzed on SDS-PAGE and the fractions containing clean Mer2 were concentrated using Pierce concentrators (same MWCO as mentioned above).

The concentrated proteins were analyzed on NanoPhotometer NP80 (Implen) to measure the absorbance of the proteins. Based on the absorption coefficient of the constructs and their size, the final concentration of the proteins could be determined. The proteins were flash-frozen in liquid nitrogen in 10-20 µl aliquots and stored at -80 °C.

Untagged Mer2_FL was prepared likewise until the concentration of protein eluted from ResourceQ. The concentrated eluent was diluted ~1:5 with SEC buffer for untagged Mer2 and concentrated once again to exchange the buffer composition. The concentrated protein was mixed with 3C HRV protease in a molar ratio of 50:1 and incubated at 4 °C for 6 hr. Afterwards, the cleaved protein was loaded on a Superose 6 16/600 pre- equilibrated in SEC buffer for untagged Mer2.

Lysis buffer

HEPES pH 7.5	50 mM
NaCl	300 mM
Glycerol	5% (v/v)
Triton X-100	0.1% (v/v)
$MgCl_2$	1 mM
β-mercaptoethanol	5 mM
DNAse	10 µg/ml
AEBSF (AppliChem)	25 µg/ml

No salt buffer

HEPES pH 7.5	50 mM
Glycerol	5% (v/v)
β-mercaptoethanol	5 mM

High salt buffer

HEPES pH 7.5	50 mM
NaCl	1 M
Glycerol	5% (v/v)
β-mercaptoethanol	5 mM

Size exclusion chromatography buffer

HEPES pH 7.5	10 mM
NaCl	300 M
Glycerol	10% (v/v)
TCEP (Carl Roth)	1 mM

Size exclusion chromatography buffer for untagged Mer2

HEPES pH 7.5	10 mM
NaCl	500 M
Glycerol	10% (v/v)
TCEP (Carl Roth)	1 mM
EDTA	1 mM
AEBSF	25 µg/ml

Spp1 purification

Spp1 constructs were produced as a 3C HRV cleavable N-terminal MBP or GST fusion in a similar manner as MBP-Mer2 using buffers described above. To purify GST-Spp1, cleared lysate was applied on a 5 ml GST-Trap 4B (GE Healthcare) pre-equilibrated with lysis buffer at a flow rate of 2 ml/min. The column was washed with 10 ml of 1 mM ATP followed by extensive washing with lysis buffer (10 CV). The protein was eluted with a gradient to 50 % of lysis buffer with 40 mM reduced glutathione.

Elution fractions containing either MBP- or GST-tagged Spp1 were passed through a pre-equilibrated ResourceQ. Both GST and MBP could be cleaved by adding 3C HRV protease to concentrated protein (using an Amicon concentrator with 30 kDa cutoff) in a 1:50 molar ratio. After a ~6 hr. incubation at 4 °C, the cleaved protein was loaded on a SEC column Superdex 200 16/600 pre-equilibrated in SEC buffer at a flow rate of 1 ml/min. The concentration of the eluted proteins was determined as described above and the proteins were stored at 10-20 µl -80 °C after flash freezing.

Hop1 purification

Hop1 constructs were produced as 3C HRV cleavable N-terminal Twin-StrepII tag in BL21 Star *E. coli* cells. The purification protocol is as well very similar to the one of Mer2 with buffers described above. The expression was induced by the addition of 250 μM IPTG, followed by incubation at 18 °C and 200 rpm overnight. Cells were lysed as described above. Cleared lysate was applied on a pre-equilibrated 6 ml Strep-Tactin XT Superflow Cartridge (IBA) at a flow rate of 2 ml/min before extensive washing in lysis buffer. The bound protein was eluted with an isocratic elution with 100 % lysis buffer containing 2.5 mM desthiobiotin. The fractions containing Hop1 were loaded on a 6 ml HiTrap Heparin HP column (GE Healthcare) pre-equilibrated with a 1:10 mixture of High salt buffer and No salt buffer (as for ResourceQ). Subsequently, the proteins were eluted with an increasing salt gradient to 600 mM NaCl (60 % High salt buffer) followed by a step to 1 M NaCl (100 % High salt buffer). Eluted Strep-Hop1 constructs were concentrated on an Amicon concentrator (30 kDa cutoff) and loaded on a Superdex 200 16/600 pre-equilibrated in SEC buffer.

Red1 purification

Red1 was produced by Saskia Funk and Veronika Altmannová in insect cells as described (Rousová et al., 2021) as a C-terminal MBP-fusion either alone or co-expressed with Strep-Hop1 from insect cells. In both cases, amplified baculovirus was used to infect Sf9 cells in 1:100 dilution before 72 hr cultivation and harvest. Cells were extensively washed and resuspended in Red1

lysis buffer. Resuspended cells were lysed by sonication in the presence of Benzonase (Sigma Aldrich) and a protease inhibitor cocktail (Serva) before clearance at 40,000 g and 4 °C for 1 hr. Cleared lysate was loaded on Strep-Tactin Superflow Cartridge (IBA, in case of Red1-Hop1 complex) or MBP- trap column (in case of Red1 alone) pre-equilibrated with Red1 lysis buffer. Proteins were eluted using a lysis buffer containing 2.5 mM desthiobiotin and 1 mM maltose, respectively (as described for Hop1 and Mer2). Protein containing elution fractions were further passed through HiTrap Heparin HP column and eluted with an increasing salt gradient from 100 mM to 1 M NaCl. Purified proteins were subsequently concentrated using Pierce concentrator with 30 kDa cutoff in SEC buffer. Because of the small yield of the proteins, the SEC purification step was neglected and the purity of the proteins was checked using the Refeyn One mass photometer (described in section 5.3.10).

Red1 lysis buffer

HEPES pH 7.5	50 mM
NaCl	300 mM
Glycerol	10% (v/v)
Triton X-100	0.1% (v/v)
$MgCl_2$	1 mM
β-mercaptoethanol	5 mM
Benzonase 28.78 U/µl (Sigma Aldrich)	1:100,000
Protease inhibitor cocktail (Serva)	1:500

Mre11 purification

Mre11 was produced by Veronika Altmannová as a C-terminal Twin-StrepII tag in insect cells as described (Rousová et

al., 2021) using the same expression conditions as for Red1 protein. The cell pellet was resuspended in Mre11 lysis buffer. Resuspended cells were lysed by sonication before clearance at 40,000 g and 4 °C for 1 hr. Cleared lysate was loaded on a 5 mL Strep-Tactin XT Superflow Cartridge (IBA) followed by a first wash using 25 mL of Mre11 wash buffer and a second wash step using 25 mL of Mre11 low salt buffer. The protein was eluted with 50 mL of Mre11 low salt buffer containing 50 mM biotin. Partially purified protein was further loaded onto a 5 mL Heparin column (GE Healthcare) pre- equilibrated in a low salt buffer and eluted with increasing salt gradient to 1 M NaCl (100% of Mre11 high salt buffer). The fractions containing Mre11 protein were concentrated on a 50 kDa MWCO Amicon concentrator and applied onto a Superdex 200 10/300 column (GE Healthcare) pre-equilibrated in Mre11 SEC buffer.

Mre11 lysis buffer

HEPES pH 7.5	50 mM
NaCl	300 mM
Glycerol	10% (v/v)
NP40	0.01% (v/v)
$MgCl_2$	1 mM
β-mercaptoethanol	5 mM
AEBSF (AppliChem)	25 µg/ml

Mre11 wash buffer

HEPES pH 7.5	20 mM
NaCl	500 mM
Glycerol	5% (v/v)
NP40	0.01% (v/v)
β-mercaptoethanol	5 mM

Mre11 low salt buffer

HEPES pH 7.5	20 mM
NaCl	150 mM
Glycerol	5% (v/v)
NP40	0.01% (v/v)
β-mercaptoethanol	5 mM

Mre11 high salt buffer

HEPES pH 7.5	20 mM
NaCl	1 M
Glycerol	5% (v/v)
NP40	0.01% (v/v)
β-mercaptoethanol	5 mM

Mre11 SEC buffer

HEPES pH 7.5	20 mM
NaCl	300 mM
Glycerol	5% (v/v)
TCEP	1 mM
β-mercaptoethanol	1 mM

5.2 Recombinant nucleosome production

Recombinant *Xenopus laevis* histones were purchased from 'The Histone Source' (Colorado State) except for

H3_K4C_C110A and H3_K4C-K36C_C110A cloned into pET3, which was kindly gifted by Francesca Matirolli. Plasmids for the production of 601–147 (pUC19) and 601–167 (pUC18) DNA were kindly gifted by Francesca Matirolli (Hubrecht Institute, Utrecht) and Andrea Musacchio (MPI Dortmund), respectively. DNA preparation and *X. laevis* histone expression, purification, octamer refolding, and mononucleosome reconstitution were performed as described (Luger et al., 1999). Both trimethylated H3 variants in C110A background were prepared as previously described (Simon et al., 2007). Reconstituted mononucleosomes were shifted to 20 mM Tris pH 7.5, 150 mM NaCl, 1 mM EDTA, 1 mM TCEP with the addition of 20% glycerol before freezing at -80 °C.

Nucleosome storage buffer

HEPES pH 7.5	20 mM
NaCl	150 mM
TCEP	1 mM
EDTA	1 mM

5.3 Biochemical and biophysical methods

5.3.1 Expression test pulldowns

Pulldowns from small scale expressions were performed to determine the optimal expression conditions. Pellets from 25 ml of *E. coli* were resuspended in 1 ml of cold lysis buffer (described in Mer2 purification protocol) and lysed by sonication (Sanoplus HD 2070, Bandelin) with a single 10 s pulse at 40 % power at 4 ºC. The lysate was cleared at 17,000 ×g and 4 ºC for 10 min.

Pellets from insect cell test expression were resuspended in 4.5 ml of lysis buffer and lysed by sonication with 50 % pulsation s pulse at 30 % power and 4 ºC for 10 s. The lysate was cleared at 17,000 ×g and 4 ºC at least for 1 hour.

The appropriate affinity resin (section 7.1.1) was sedimented at 1000 ×g for 1 min, washed extensively with lysis buffer and resuspended in it. Each cleared lysate was mixed with 60 µl of equilibrated resin and incubated for 1-2 hours (2 hours for MBP and GST resin) at 4 ºC with gentle rotation. The resin was afterwards sedimented and the supernatant removed. The beads were washed three times with 0.5 ml of lysis buffer before the addition of 40 µl of elution buffer (specific for each resin). The elution was performed on ice for 5-10 min. After another sedimentation, a sample of elution was taken and the resin was washed twice with 0.5 ml of lysis buffer before taking a sample of the beads. The pulldowns were analyzed on SDS-PAGE by loading 2.5 µl (insect cells) and 0.5 µl (*E. coli*) of crude and cleared lysate, 20 µl of eluate and 5 µl of beads.

5.3.2 Interaction pulldowns.

Interaction pulldowns were performed to examine the interaction between purified proteins. At least one binding partner was containing a tag (= bait) and was immobilized on beads, the other partner or partners (=prey) were either containing a different tag or were untagged. In all cases, a test pulldown in the absence of the bait protein was carried out first, to determine the optimal pulldown conditions with the minimum unspecific binding of the prey to the beads.

Streptactin pulldown

Streptactin pulldown was performed using Pierce streptavidin magnetic beads (Thermo scientific) pre-blocked with 300-500 µl of 1 mg/ml BSA (NEB) in a pulldown buffer for 2 hours at 4 ºC with rotation. The beads were washed after pre-blocking twice with 500 µl of pulldown buffer.

1 µM bait (Strep-Hop1 or Mre11-Strep) was incubated with 3 µM of each prey protein (Mer2 or Spp1) in a 40 µl reaction for 2 hours on ice without beads to allow the complex to form. 3 µl were taken as input. Afterwards, 10 µl of pre-blocked washed beads were added to the protein mixture and incubated for another 30 min at 4 ºC with rotation. After incubation. The beads were washed twice with 200 µl of pulldown buffer followed by elution of the proteins with 10 µl of 1× Laemmli buffer. The elution was incubated for 10 min on ice before harvesting the eluate. Samples were analyzed on 10% SDS-PAGE gel and afterwards stained with InstantBlue.

Pulldown buffer

HEPES pH 7.5	20 mM
NaCl	300 mM
Glycerol	5 %
Tween20	0.02 %
TCEP	1 mM

Amylose pulldown

Amylose pulldowns were performed similarly to the Streptactin pulldowns. Amylose beads (NEB) were as well pre-blocked with 1 mg/ml BSA in a pulldown buffer for 2 hours with

rotation at 4 ºC. 1 μM bait (Red-MBP_I743R or Red-MBP_I743R/Strep-Hop1) was incubated with 3 μM prey (Mer2) in 40 μl reaction for 2 hours on ice (3 μl were taken as input) and for another 1 hour with rotation after the addition of 10 μl of pre-blocked washed beads. After incubation, the beads were washed twice with 200 μl of pulldown buffer before elution of the proteins with 10 μl of pulldown buffer with 1 mM maltose. Elution was incubated on ice for 10 min before collecting the eluate. Samples were loaded on 10% SDS-PAGE gel and stained with InstantBlue.

Biotinylated nucleosome pulldown

Biotinylated nucleosomes (0.5 μM) or nucleosome core particles (NCP, 0.4 μM) were incubated with prey proteins (1.5 μM) for 30 min on ice in MN pulldown buffer in a reaction volume of 40 μl. 10 μl of protein mix were taken as input before adding 10 μl of pre-blocked washed magnetic Dynabeads M 270 streptavidin beads (Thermo Fisher Scientific) to the reaction. The samples with beads were incubated on ice for 2 min before applying the magnet and removing the supernatant. The beads were washed twice with 200 μl of the buffer. To release the streptavidin from the beads, 10 μl of 1× Laemmli buffer were added to the beads and incubated on ice for 10 min. Samples were analyzed on precast 10–20% SDS-PAGE gel (Invitrogen WedgeWell Tris-Glycine Mini Gels, Thermo Scientific) and stained by InstantBlue.

MN pulldown buffer

HEPES pH 7.5	20 mM
NaCl	150 mM
Glycerol	5 %
EDTA	1 mM
Triton X-100	0.05 %
TCEP	1 mM

5.3.3 SDS-PAGE according to Laemmli

Sodium dodecylsulfate polyacrylamide gel electrophoresis (SDS-PAGE) separates proteins based on their size. Samples were prepared by adding 0.2× volume of 6× SDS sample buffer (section 7.1.3), boiled at 95 ºC for 5 min and loaded on a 1 mm thick 10% polyacrylamide gel (section 7.1.3) prepared as described (Laemmli, 1970). Precision 1 µl of Plus Protein Dual Color Standards (Bio-rad) was used as a molecular weight standard. Electrophoresis was performed at 250 V for 45 min until the blue sample buffer reached the bottom of the gel. Gels were stained by InstantBlue (Expedeon) and imaged with ChemiDoc XRS+ (Bio-rad)

5.3.4 Western blot analysis

Western blot analysis was performed to detect tagged protein. The samples on an SDS-PAGE were transferred to a nitrocellulose membrane (Amersham) by a wet transfer. The gel and membrane were placed in between three sheets of Whatman paper on each side. The transfer was performed in transfer buffer with the membrane facing the anode at 300 mA and 4 ºC for 2 hours.

The membrane with transferred proteins was blocked for 1 hour at room temperature with a blocking buffer containing PBS with 0.1 % (v/v) Tween20 (PBS-T) and 5 % (w/v) non-fat dry milk. Primary antibodies were diluted in blocking buffer in concentration indicated in section 7.1.4 and incubated with the membrane for 1 hour at room temperature or 4 ºC overnight with rotation. The membrane was afterwards washed three times for 5 minutes with PBS-T and incubated with secondary antibody in blocking buffer for 1 hour at room temperature with rotation. After an additional washing step with PBS-T, the signal was developed using Amersham ECL Prime Western Blotting Detection Reagent (GE Healthcare) for 5 minutes and immediately visualized in the chemiluminescence channel of the ChemiDoc Xrs+ (Bio-rad).

5.3.5 Multi-angle light scattering (SEC-MALS)

Size exclusion chromatography coupled with multi-angle light scattering (SEC-MALS) was performed to determine the size of the protein or protein complexes. 50 µl of samples at 5–10 µM concentration were loaded onto a Superose 6 5/150 analytical size exclusion column (GE Healthcare) equilibrated in SEC-MALS buffer attached to 1260 Infinity II LC System (Agilent). The usual flow rate was 0.3 ml/min. MALS was carried out using a Wyatt DAWN detector attached in line with the size exclusion column.

SEC-MALS buffer

HEPES pH 7.5	20 mM
NaCl	300 mM – for samples without nucleosomes 150 mM – for samples with nucleosomes
TCEP	1 mM
EDTA	1 mM

5.3.6 Analytical size-exclusion chromatography

Analytical SEC was performed to detect complex formation in solution using Superose 6 5/150 GL or Superdex 200 5/150 column (GE Healthcare) in a buffer for analytical SEC. To detect complex formation, proteins were mixed at 5 μM concentration in 50 μl and incubated on ice for 1 hour before SEC analysis. All samples were eluted under isocratic elution at a flow rate of 0.15 ml/min. Fractions were subsequently analyzed by 10 % SDS-PAGE and InstantBlue staining.

Analytical SEC buffer

HEPES pH 7.5	20 mM
NaCl	300 mM – for the sample without nucleosomes 150 mM – for samples with nucleosomes
Glycerol	5 %
TCEP	1 mM
EDTA	1 mM

5.3.7 Microscale thermophoresis (MST)

Microscale thermophoresis (MST) was carried out to determine the binding affinity of two proteins. Triplicates of MST analysis were performed in MST buffer at 20°C on Monolith NT.115 (Nanotemper) using premium capillaries (Nanotemper). The final reaction included 20 nM RED-NHS labelled untagged

Spp1 (labelled according to manufacturer's protocol, Nanotemper) and titration series of MBP-Mer2 constructs (concentrations calculated based on oligomerisation stage of Mer2) with 10 points. The highest concentration of Mer2 is described below. The final curves were automatically fitted in Nanotemper analysis software.

MST buffer

HEPES pH 7.5	50 mM
NaCl	300 mM
Tween20	0.005 %
TCEP	1 mM

The maximum concentration of Mer2 constructs

MBP-Mer2_FL	15 mM
MBP-Mer2_140-256	50 mM
MBP-Mer2_N-139	90 mM
MBP-Mer2_255-C	30 mM
MBP control	90 mM

5.3.8 Isothermal calorimetry (ITC)

The binding affinity of proteins (or DNA) can be tested also via isothermal calorimetry (ITC). Due to the high amount of protein required, ITC was performed only once using MicroCal PEAQ-ITC (Malvern Panalytical) by John Weir with untagged Spp1 in the syringe and Mer2_140-256 (=Mer2_core) in the cell. The analysis was performed using software provided by the manufacturer.

ITC buffer

HEPES pH 7.5	20 mM
NaCl	150 mM
Glycerol	10 %
EDTA	20 µM
TCEP	1 mM

5.3.9 Electrophoretic mobility shift assays (EMSA)

Electrophoretic mobility shift assays (EMSAs) were carried out to determine the apparent binding affinity of proteins to nucleosomes or DNA. Quadruplicate EMSAs were carried out in EMSA buffer at a constant nucleosome/NCP/DNA concentration of 5 nM and protein concentration titrated from 5 nM to 0.4 µM in 11 reactions in a final volume of 10 µl. The reactions were incubated for 2 hours on ice before loading on 0.75 % TBE agarose gel in 0.2 % TBE. Gels were run at 60 V and 6 ºC for 2 hours followed by a quick washing step with 0.2 % TBE and staining with SYBRGold (Invitrogen). Gels were imaged using a ChemiDoc MP (Bio-rad). Nucleosome depletion in each lane was quantitated by ImageJ, using measurements of triplicate of the nucleosome alone for each gel as a baseline. Binding curves were fitted using Prism software and the following algorithm (Y = Bmax*Xh/(KDh + Xh)) by John Weir. It was necessary in each Mer2 case to add a Hill coefficient to obtain the best fit.

EMSA buffer

HEPES pH 7.5	20 mM
NaCl	150 mM
Glycerol	1.25 %
BSA	1 mg/ml
EDTA	1 mM
Tween-20	0.02 %
TCEP	2 mM

5.3.10 Mass photometry (MP)

The size of molecules in solution at very low concentrations can be detected by mass photometry (MP). Mer2 and mononucleosomes (600 nM) were mixed in MP buffer and incubated for 1 hr on ice before analysis using the Refeyn One mass photometer (Refeyn). Immediately before analysis, the sample was diluted at 1:10 with the aforementioned buffer. Molecular mass was determined in Analysis software provided by the manufacturer using a NativeMark (Invitrogen) based standard curve created under the identical buffer composition.

MP buffer

HEPES pH 7.5	20 mM
NaCl	150 mM
Glycerol	5 %
EDTA	1 mM
TCEP	1 mM

5.3.11 *In vivo* analyses

Spore viability assay, western blot from meiotic yeast culture and southern blot were performed by Vaishnavi Nivsarkar and Vivek B. Raina from the Vader laboratory (MPI Dortmund and

Cancer Centre Amsterdam) as described previously (Rousová et al., 2021). Co-immunoprecipitation mass-spectrometry and yeast-two hybrid assay and Veronika Altmannová as described ibidem.

5.3.12 Phosphorylation assay

Phosphorylation assays were performed by Saskia Funk with radioactive ATP. 5 µM Mer2 variant were mixed with 1 µM recombinant DDK (purified from yeast by John Weir) and 2 µl of 1 mM ATP in 10 µl reaction volume. The reaction was incubated at 30 ºC for 30 min and quenched with the addition of 2× SDS loading buffer followed by incubation at 80 ºC for 2 min. Samples were run on a 10 % SDS-gel at 250 V for 40 min and subsequently exposed overnight using a Phosphor screen and imaged in Amersham Typhoon Biomolecular Imager (GE Healthcare).

Phosphorylation buffer

HEPES pH 7.5	50 mM
NaCl	150 mM
Glycerol	10 %
$MgCl_2$	10 mM
β-mercaptoethanol	0.5 mM

5.4 Structural methods

5.4.1 Cross-linking mass spectrometry (XL-MS)

Cross-linking coupled with mass spectrometry (XL-MS) can provide a hint into the structural organization of the proteins or their complexes and reveal the binding interfaces of complexes.

For XL- MS analysis proteins were dissolved in 200 µl of XL-MS buffer to a final concentration of 3 µM, mixed with 3 µl of DSBU (200 mM dissolved in DMSO, Thermo Scientific) and incubated for 1 hour at 25 °C. The reaction was quenched by the addition of 20 µl of Tris pH 8.0 (1 M) and incubated for another 30 min at 25°C. The crosslinked sample was precipitated by the addition of 4× volumes of 100 % cold acetone overnight at –20 °C and subsequently analyzed as previously described (Pan et al., 2018) by Franziska Müller and Petra Janning (Max Planck Institute of Molecular Physiology, Dortmund, Germany). The crosslinks were visualized using xVis (Grimm et al., 2015).

XL-MS buffer

HEPES pH 7.5	30 mM
NaCl	300 mM – for the sample without nucleosomes 150 mM – for samples with nucleosomes
TCEP	1 mM
EDTA	1 mM

5.4.2 Small-angle X-ray scattering (SAXS)

Size exclusion chromatography coupled with small-angle X-ray scattering (SEC-SAXS) was performed to determine the shape of the protein or protein complexes on the SWING beamline (Soleil, France). 50 µl of samples at 2-5 mg/ml concentration were loaded onto a Superose 6 5/150 analytical size exclusion column (GE Healthcare) equilibrated in SAXS buffer attached to EigerX4M detector (Deictris) at a flow rate was 0.3 ml/min. The data were analyzed on the beamline using Foxtrot (Soleil, France) followed by an evaluation using the ATSAS package (EMBL Hamburg) by John Weir.

5.4.3 Crystallization

The optimal concentration for crystallization of proteins or protein complexes was determined by a Pre-Crystallization Test (Hampton Research) performed as recommended by the manufacturer. Depending on the result of the test, the concentration of the sample was adjusted before the preparation of the crystallization screen. For each screen, three drops with a different sample:precipitant ratio were set up (1:2, 1:1 and 2:1), each 500 nl big using Mosquito crystallization robot (sptlabtech). The crystallization screens (Hampton Research, Jena Bioscience and Molecular Dimensions) were pipetted by Integra Viaflo 96 (Integra). The plates were incubated at room temperature or 4 ºC and imaged by Rock Imager 182 (Formulatrix).

5.4.4 Gradient fixation (GraFix)

Gradient fixation (GraFix) was performed to stabilize samples by mild cross-linking, especially beneficial for electron microscopy studies. The experiment was performed as previously described (Stark, 2010). The proteins were dissolved in a final volume of 200 µl of GraFix buffer with 10 % glycerol to a final concentration of each component ~2-3 µM. The mixture was incubated for 1 hour on ice and 4 ml of a gradient of GraFix buffer with 10-40 % glycerol and 0-4 % paraformaldehyde (Fisher Scientific) was prepared using Gradient master 108 (Biocomp). The sample was applied on top of the gradient and spun down at 35,000 ×g at 4 ºC for 16 hours (using SW55Ti rotor, Beckman Coulter). Afterwards, 100 µl fractions were removed from the top of the gradient and analyzed by SDS-PAGE. The excess glycerol

was removed by desalting column (PD MiniTrap G-25, GE Healthcare) and the sample was shifted into GraFix buffer without glycerol.

GraFix buffer

HEPES pH 7.5	10 mM
NaCl	150 mM
Glycerol	10 or 35 %
TCEP	1 mM
EDTA	1 mM
NP40	0.01 %

5.4.5 Negative staining electron microscopy

Samples for negative staining electron microscopy were prepared in their respective SEC buffer at 20-40 nM concentration. Copper grids (400 mesh, square, Cu) were glow discharged (Edwards) and covered with 4 µl of the sample. After 5 min incubation at room temperature, the excess liquid was removed by filter paper and the grids were washed three times with a 10 µl drop of sterile H_2O. Afterwards, the grids were stained using 1 % uranyl acetate three times with 10 µl drop, followed by staining with 20 µl drop incubated on the grids for 2 mins. Dried grids were imaged using a Tecnai G^2 Spirit microscope (FEI).

5.4.6 Cryo-electron microscopy (cryoEM)

Samples for cryo-electron microscopy were prepared in a buffer without glycerol or detergent at a concentration of 0.5-2 mg/ml. 4 µl of the sample were applied on glow discharged (PELCO easiGlow, TED Paella) copper grids (Quantifoil R

1.2/1.3 100 Holey Carbon, Cu 300 mesh, Quantifoil) and blotted using Vitrobot (FEI, Thermo Scientific). Unless specified differently, the waiting time before blotting was set for 5s, blotting 5s with -1 force and frozen in liquid ethane to create a thin layer of amorphous ice. The frozen grids were moved to liquid nitrogen, clipped into autogrids and loaded in the Talos Arctica G2 electron microscope (FEI). The analysis was performed in EPU software (Thermo Scientific) according to the manufacturer's instructions.

cryoEM buffer

HEPES pH 7.5	10 mM
NaCl	150 mM
TCEP	1 mM
EDTA	1 mM

6 Literature

Acosta, I., Ontoso, D., San-Segundo, P.A., 2011. The budding yeast polo-like kinase Cdc5 regulates the Ndt80 branch of the meiotic recombination checkpoint pathway. Mol. Biol. Cell 22, 3478–3490. https://doi.org/10.1091/mbc.e11-06-0482

Acquaviva, L., Székvölgyi, L., Dichtl, B., Dichtl, B.S., de La Roche Saint André, C., Nicolas, A., Géli, V., 2013. The COMPASS subunit Spp1 links histone methylation to initiation of meiotic recombination. Science 339, 215–218. https://doi.org/10.1126/science.1225739

Adam, C., Guérois, R., Citarella, A., Verardi, L., Adolphe, F., Béneut, C., Sommermeyer, V., Ramus, C., Govin, J., Couté, Y., Borde, V., 2018. The PHD finger protein Spp1 has distinct functions in the Set1 and the meiotic DSB formation complexes. PLoS Genet. 14, e1007223. https://doi.org/10.1371/journal.pgen.1007223

Ajimura, M., Leem, S.H., Ogawa, H., 1993. Identification of new genes required for meiotic recombination in Saccharomyces cerevisiae. Genetics 133, 51–66. https://doi.org/10.1093/genetics/133.1.51

Allers, T., Lichten, M., 2001. Differential timing and control of noncrossover and crossover recombination during meiosis. Cell 106, 47–57. https://doi.org/10.1016/s0092-8674(01)00416-0

Allfrey, V.G., Faulkner, R., Mirsky, A.E., 1964. Acetylation and methylation of histones and their possible role in the regulation of RNA sythesis. Proc. Natl. Acad. Sci. U. S. A. 51, 786–794.

Altmannova, V., Blaha, A., Astrinidis, S., Reichle, H., Weir, J.R., 2021. InteBac: An integrated bacterial and baculovirus expression vector suite. Protein Sci. 30, 108–114. https://doi.org/10.1002/pro.3957

Aravind, L., Koonin, E.V., 1998. The HORMA domain: a common structural denominator in mitotic checkpoints, chromosome synapsis and DNA repair. Trends Biochem. Sci. 23, 284–286. https://doi.org/10.1016/s0968-0004(98)01257-2

Arora, C., Kee, K., Maleki, S., Keeney, S., 2004. Antiviral protein Ski8 is a direct partner of Spo11 in meiotic DNA break formation, independent of its cytoplasmic role in RNA metabolism. Mol. Cell 13, 549–559. https://doi.org/10.1016/s1097-2765(04)00063-2

Baudat, F., Buard, J., Grey, C., Fledel-Alon, A., Ober, C., Przeworski, M., Coop, G., Massy, B. de, 2010. PRDM9 Is a Major Determinant of Meiotic Recombination Hotspots in Humans and Mice. Science. https://doi.org/10.1126/science.1183439

Baudat, F., Nicolas, A., 1997. Clustering of meiotic double-strand breaks on yeast chromosome III. Proc. Natl. Acad. Sci. 94, 5213–5218. https://doi.org/10.1073/pnas.94.10.5213

Benjamin, K.R., Zhang, C., Shokat, K.M., Herskowitz, I., 2003. Control of landmark events in meiosis by the CDK Cdc28 and the meiosis-specific kinase Ime2. Genes Dev. 17, 1524–1539. https://doi.org/10.1101/gad.1101503

Bergerat, A., de Massy, B., Gadelle, D., Varoutas, P.C., Nicolas, A., Forterre, P., 1997. An atypical topoisomerase II from Archaea with implications for meiotic recombination. Nature 386, 414–417. https://doi.org/10.1038/386414a0

Bhagwat, N.R., Owens, S.N., Ito, M., Boinapalli, J.V., Poa, P., Ditzel, A., Kopparapu, S., Mahalawat, M., Davies, O.R., Collins, S.R., Johnson, J.R., Krogan, N.J., Hunter, N., 2021. SUMO is a pervasive regulator of meiosis. eLife 10, e57720. https://doi.org/10.7554/eLife.57720

Bieniossek, C., Richmond, T.J., Berger, I., 2008. MultiBac: multigene baculovirus-based eukaryotic protein complex production. Curr. Protoc. Protein Sci. Chapter 5, Unit 5.20. https://doi.org/10.1002/0471140864.ps0520s51

Bishop, D.K., Zickler, D., 2004. Early decision; meiotic crossover interference prior to stable strand exchange and synapsis. Cell 117, 9–15. https://doi.org/10.1016/s0092-8674(04)00297-1

Blat, Y., Protacio, R.U., Hunter, N., Kleckner, N., 2002. Physical and Functional Interactions among Basic Chromosome Organizational Features

Govern Early Steps of Meiotic Chiasma Formation. Cell 111, 791–802. https://doi.org/10.1016/S0092-8674(02)01167-4

Blitzblau, H.G., Bell, G.W., Rodriguez, J., Bell, S.P., Hochwagen, A., 2007. Mapping of Meiotic Single-Stranded DNA Reveals Double-Strand-Break Hotspots near Centromeres and Telomeres. Curr. Biol. 17, 2003–2012. https://doi.org/10.1016/j.cub.2007.10.066

Blitzblau, H.G., Hochwagen, A., 2013. ATR/Mec1 prevents lethal meiotic recombination initiation on partially replicated chromosomes in budding yeast. eLife 2, e00844. https://doi.org/10.7554/eLife.00844

Boekhout, M., Karasu, M.E., Wang, J., Acquaviva, L., Pratto, F., Brick, K., Eng, D.Y., Xu, J., Camerini-Otero, R.D., Patel, D.J., Keeney, S., 2019. REC114 Partner ANKRD31 Controls Number, Timing, and Location of Meiotic DNA Breaks. Mol. Cell 74, 1053-1068.e8. https://doi.org/10.1016/j.molcel.2019.03.023

Borde, V., Goldman, A.S.H., Lichten, M., 2000. Direct Coupling Between Meiotic DNA Replication and Recombination Initiation. Science 290, 806–809. https://doi.org/10.1126/science.290.5492.806

Borde, V., Robine, N., Lin, W., Bonfils, S., Géli, V., Nicolas, A., 2009. Histone H3 lysine 4 trimethylation marks meiotic recombination initiation sites. EMBO J. 28, 99–111. https://doi.org/10.1038/emboj.2008.257

Borde, V., Wu, T.-C., Lichten, M., 1999. Use of a Recombination Reporter Insert To Define Meiotic Recombination Domains on Chromosome III ofSaccharomyces cerevisiae. Mol. Cell. Biol. 19, 4832–4842. https://doi.org/10.1128/MCB.19.7.4832

Börner, G.V., Barot, A., Kleckner, N., 2008. Yeast Pch2 promotes domainal axis organization, timely recombination progression, and arrest of defective recombinosomes during meiosis. Proc. Natl. Acad. Sci. 105, 3327–3332. https://doi.org/10.1073/pnas.0711864105

Börner, G.V., Kleckner, N., Hunter, N., 2004. Crossover/noncrossover differentiation, synaptonemal complex formation, and regulatory surveillance

at the leptotene/zygotene transition of meiosis. Cell 117, 29–45. https://doi.org/10.1016/s0092-8674(04)00292-2

Brar, G.A., Hochwagen, A., Ee, L.S., Amon, A., 2009. The Multiple Roles of Cohesin in Meiotic Chromosome Morphogenesis and Pairing. Mol. Biol. Cell 20, 1030–1047. https://doi.org/10.1091/mbc.E08-06-0637

Briggs, S.D., Bryk, M., Strahl, B.D., Cheung, W.L., Davie, J.K., Dent, S.Y., Winston, F., Allis, C.D., 2001. Histone H3 lysine 4 methylation is mediated by Set1 and required for cell growth and rDNA silencing in Saccharomyces cerevisiae. Genes Dev. 15, 3286–3295. https://doi.org/10.1101/gad.940201

Brown, D.A., Di Cerbo, V., Feldmann, A., Ahn, J., Ito, S., Blackledge, N.P., Nakayama, M., McClellan, M., Dimitrova, E., Turberfield, A.H., Long, H.K., King, H.W., Kriaucionis, S., Schermelleh, L., Kutateladze, T.G., Koseki, H., Klose, R.J., 2017. The SET1 Complex Selects Actively Transcribed Target Genes via Multivalent Interaction with CpG Island Chromatin. Cell Rep. 20, 2313–2327. https://doi.org/10.1016/j.celrep.2017.08.030

Brown, M.S., Bishop, D.K., 2015. DNA Strand Exchange and RecA Homologs in Meiosis. Cold Spring Harb. Perspect. Biol. 7, a016659. https://doi.org/10.1101/cshperspect.a016659

Buhler, C., Borde, V., Lichten, M., 2007. Mapping Meiotic Single-Strand DNA Reveals a New Landscape of DNA Double-Strand Breaks in Saccharomyces cerevisiae. PLOS Biol. 5, e324. https://doi.org/10.1371/journal.pbio.0050324

Carballo, J.A., Panizza, S., Serrentino, M.E., Johnson, A.L., Geymonat, M., Borde, V., Klein, F., Cha, R.S., 2013. Budding yeast ATM/ATR control meiotic double-strand break (DSB) levels by down-regulating Rec114, an essential component of the DSB-machinery. PLoS Genet. 9, e1003545. https://doi.org/10.1371/journal.pgen.1003545

Chen, C., Jomaa, A., Ortega, J., Alani, E.E., 2014. Pch2 is a hexameric ring ATPase that remodels the chromosome axis protein Hop1. Proc. Natl. Acad. Sci. U. S. A. 111, E44–E53. https://doi.org/10.1073/pnas.1310755111

Claeys Bouuaert, C., Pu, S., Wang, J., Oger, C., Daccache, D., Xie, W., Patel, D.J., Keeney, S., 2021. DNA-driven condensation assembles the meiotic DNA break machinery. Nature 592, 144–149. https://doi.org/10.1038/s41586-021-03374-w

Cool, M., Malone, R.E., 1992. Molecular and genetic analysis of the yeast early meiotic recombination genes REC102 and REC107/MER2. Mol. Cell. Biol. 12, 1248–1256.

Davey, C.A., Sargent, D.F., Luger, K., Maeder, A.W., Richmond, T.J., 2002. Solvent Mediated Interactions in the Structure of the Nucleosome Core Particle at 1.9Å Resolution. J. Mol. Biol. 319, 1097–1113. https://doi.org/10.1016/S0022-2836(02)00386-8

Dehé, P.-M., Dichtl, B., Schaft, D., Roguev, A., Pamblanco, M., Lebrun, R., Rodríguez-Gil, A., Mkandawire, M., Landsberg, K., Shevchenko, Anna, Shevchenko, Andrej, Rosaleny, L.E., Tordera, V., Chávez, S., Stewart, A.F., Géli, V., 2006. Protein Interactions within the Set1 Complex and Their Roles in the Regulation of Histone 3 Lysine 4 Methylation *. J. Biol. Chem. 281, 35404–35412. https://doi.org/10.1074/jbc.M603099200

Dehé, P.-M.D., Géli, V.G., 2006. The multiple faces of Set1This paper is one of a selection of papers published in this Special Issue, entitled 27th International West Coast Chromatin and Chromosome Conference, and has undergone the Journal's usual peer review process. Biochem. Cell Biol. https://doi.org/10.1139/o06-081

De Muyt, A., Jessop, L., Kolar, E., Sourirajan, A., Chen, J., Dayani, Y., Lichten, M., 2012. BLM Helicase Ortholog Sgs1 Is a Central Regulator of Meiotic Recombination Intermediate Metabolism. Mol. Cell 46, 43–53. https://doi.org/10.1016/j.molcel.2012.02.020

Deshong, A.J., Ye, A.L., Lamelza, P., Bhalla, N., 2014. A Quality Control Mechanism Coordinates Meiotic Prophase Events to Promote Crossover Assurance. PLOS Genet. 10, e1004291. https://doi.org/10.1371/journal.pgen.1004291

Dou, Y., Milne, T.A., Ruthenburg, A.J., Lee, S., Lee, J.W., Verdine, G.L., Allis, C.D., Roeder, R.G., 2006. Regulation of MLL1 H3K4 methyltransferase activity by its core components. Nat. Struct. Mol. Biol. 13, 713–719. https://doi.org/10.1038/nsmb1128

Engebrecht, J., Hirsch, J., Roeder, G.S., 1990. Meiotic gene conversion and crossing over: their relationship to each other and to chromosome synapsis and segregation. Cell 62, 927–937.

Engebrecht, J.A., Voelkel-Meiman, K., Roeder, G.S., 1991. Meiosis-specific RNA splicing in yeast. Cell 66, 1257–1268. https://doi.org/10.1016/0092-8674(91)90047-3

Evans, R., O'Neill, M., Pritzel, A., Antropova, N., Senior, A., Green, T., Žídek, A., Bates, R., Blackwell, S., Yim, J., Ronneberger, O., Bodenstein, S., Zielinski, M., Bridgland, A., Potapenko, A., Cowie, A., Tunyasuvunakool, K., Jain, R., Clancy, E., Kohli, P., Jumper, J., Hassabis, D., 2021. Protein complex prediction with AlphaFold-Multimer. https://doi.org/10.1101/2021.10.04.463034

Felsenfeld, G., Groudine, M., 2003. Controlling the double helix. Nature 421, 448–453. https://doi.org/10.1038/nature01411

Fowler, K.R., Hyppa, R.W., Cromie, G.A., Smith, G.R., 2018. Physical basis for long-distance communication along meiotic chromosomes. Proc. Natl. Acad. Sci. U. S. A. 115, E9333–E9342. https://doi.org/10.1073/pnas.1801920115

Fried, M.G., Bromberg, J.L., 1997. Factors that affect the stability of protein-DNA complexes during gel electrophoresis. Electrophoresis 18, 6–11. https://doi.org/10.1002/elps.1150180103

Furuse, M., Nagase, Y., Tsubouchi, H., Murakami-Murofushi, K., Shibata, T., Ohta, K., 1998. Distinct roles of two separable in vitro activities of yeast Mre11 in mitotic and meiotic recombination. EMBO J. 17, 6412–6425. https://doi.org/10.1093/emboj/17.21.6412

Galbraith, A.M., Malone, R.E., 1992. Characterization of REC104, a gene required for early meiotic recombination in the yeast Saccharomyces cerevisiae. Dev. Genet. 13, 392–402. https://doi.org/10.1002/dvg.1020130603

Game, J.C., Zamb, T.J., Braun, R.J., Resnick, M., Roth, R.M., 1980. The Role of Radiation (rad) Genes in Meiotic Recombination in Yeast. Genetics 94, 51–68.

Garcia, V., Gray, S., Allison, R.M., Cooper, T.J., Neale, M.J., 2015. Tel1ATM-mediated interference suppresses clustered meiotic double-strand-break formation. Nature 520, 114–8. https://doi.org/10.1038/nature13993

Garcia, V., Phelps, S.E.L., Gray, S., Neale, M.J., 2011. Bidirectional resection of DNA double-strand breaks by Mre11 and Exo1. Nature 479, 241–244. https://doi.org/10.1038/nature10515

Garcia-Muse, T., Boulton, S.J., 2007. Meiotic recombination in Caenorhabditis elegans. Chromosome Res. Int. J. Mol. Supramol. Evol. Asp. Chromosome Biol. 15, 607–621. https://doi.org/10.1007/s10577-007-1146-x

Gardiner, J.M., Bullard, S.A., Chrome, C., Malone, R.E., 1997. Molecular and genetic analysis of REC103, an early meiotic recombination gene in yeast. Genetics 146, 1265–1274. https://doi.org/10.1093/genetics/146.4.1265

Gerton, J.L., DeRisi, J., Shroff, R., Lichten, M., Brown, P.O., Petes, T.D., 2000. Global mapping of meiotic recombination hotspots and coldspots in the yeast Saccharomyces cerevisiae. Proc. Natl. Acad. Sci. U. S. A. 97, 11383–11390. https://doi.org/10.1073/pnas.97.21.11383

Gibson, D.G., Young, L., Chuang, R.-Y., Venter, J.C., Hutchison, C.A., Smith, H.O., 2009. Enzymatic assembly of DNA molecules up to several hundred kilobases. Nat. Methods 6, 343–345. https://doi.org/10.1038/nmeth.1318

Gray, S., Allison, R.M., Garcia, V., Goldman, A.S.H., Neale, M.J., 2013. Positive regulation of meiotic DNA double-strand break formation by activation of the DNA damage checkpoint kinase Mec1(ATR). Open Biol. 3, 130019. https://doi.org/10.1098/rsob.130019

Gray, S., Cohen, P.E., 2016. Control of Meiotic Crossovers: From Double-Strand Break Formation to Designation. Annu. Rev. Genet. 50, 175–210. https://doi.org/10.1146/annurev-genet-120215-035111

Grimm, M., Zimniak, T., Kahraman, A., Herzog, F., 2015. xVis: a web server for the schematic visualization and interpretation of crosslink-derived spatial restraints. Nucleic Acids Res. 43, W362–W369. https://doi.org/10.1093/nar/gkv463

He, C., Liu, N., Xie, D., Liu, Y., Xiao, Y., Li, F., 2019. Structural basis for histone H3K4me3 recognition by the N-terminal domain of the PHD finger protein Spp1. Biochem. J. 476, 1957–1973. https://doi.org/10.1042/BCJ20190091

Henderson, K.A., Kee, K., Maleki, S., Santini, P.A., Keeney, S., 2006. Cyclin-Dependent Kinase Directly Regulates Initiation of Meiotic Recombination. Cell 125, 1321–1332. https://doi.org/10.1016/j.cell.2006.04.039

Herruzo, E., Lago-Maciel, A., Baztán, S., Santos, B., Carballo, J.A., San-Segundo, P.A., 2021. Pch2 orchestrates the meiotic recombination checkpoint from the cytoplasm. PLoS Genet. 17, e1009560. https://doi.org/10.1371/journal.pgen.1009560

Hollingsworth, N.M., Goetsch, L., Byers, B., 1990. The HOP1 gene encodes a meiosis-specific component of yeast chromosomes. Cell 61, 73–84. https://doi.org/10.1016/0092-8674(90)90216-2

Hong, E.L., Shinohara, A., Bishop, D.K., 2001. Saccharomyces cerevisiae Dmc1 Protein Promotes Renaturation of Single-strand DNA (ssDNA) and Assimilation of ssDNA into Homologous Super-coiled Duplex DNA *. J. Biol. Chem. 276, 41906–41912. https://doi.org/10.1074/jbc.M105563200

Hunter, N., 2015. Meiotic Recombination: The Essence of Heredity. Cold Spring Harb. Perspect. Biol. 7. https://doi.org/10.1101/cshperspect.a016618

Hunter, N., Kleckner, N., 2001. The single-end invasion: an asymmetric intermediate at the double-strand break to double-holliday junction transition of meiotic recombination. Cell 106, 59–70. https://doi.org/10.1016/s0092-8674(01)00430-5

Ivanov, E.L., Korolev, V.G., Fabre, F., 1992. XRS2, a DNA repair gene of Saccharomyces cerevisiae, is needed for meiotic recombination. Genetics 132, 651–664. https://doi.org/10.1093/genetics/132.3.651

Johzuka, K., Ogawa, H., 1995. Interaction of Mre11 and Rad50: two proteins required for DNA repair and meiosis-specific double-strand break formation in Saccharomyces cerevisiae. Genetics 139, 1521–1532. https://doi.org/10.1093/genetics/139.4.1521

Joyce, E.F., McKim, K.S., 2010. Chromosome Axis Defects Induce a Checkpoint-Mediated Delay and Interchromosomal Effect on Crossing Over during Drosophila Meiosis. PLOS Genet. 6, e1001059. https://doi.org/10.1371/journal.pgen.1001059

Jumper, J., Evans, R., Pritzel, A., Green, T., Figurnov, M., Ronneberger, O., Tunyasuvunakool, K., Bates, R., Žídek, A., Potapenko, A., Bridgland, A., Meyer, C., Kohl, S.A.A., Ballard, A.J., Cowie, A., Romera-Paredes, B., Nikolov, S., Jain, R., Adler, J., Back, T., Petersen, S., Reiman, D., Clancy, E., Zielinski, M., Steinegger, M., Pacholska, M., Berghammer, T., Bodenstein, S., Silver, D., Vinyals, O., Senior, A.W., Kavukcuoglu, K., Kohli, P., Hassabis, D., 2021. Highly accurate protein structure prediction with AlphaFold. Nature 596, 583–589. https://doi.org/10.1038/s41586-021-03819-2

Kalashnikova, A.A., Porter-Goff, M.E., Muthurajan, U.M., Luger, K., Hansen, J.C., 2013. The role of the nucleosome acidic patch in modulating higher order chromatin structure. J. R. Soc. Interface 10, 20121022. https://doi.org/10.1098/rsif.2012.1022

Karányi, Z., Halász, L., Acquaviva, L., Jónás, D., Hetey, S., Boros-Oláh, B., Peng, F., Chen, D., Klein, F., Géli, V., Székvölgyi, L., 2018. Nuclear dynamics of the Set1C subunit Spp1 prepares meiotic recombination sites for break formation. J. Cell Biol. 217, 3398–3415. https://doi.org/10.1083/jcb.201712122

Kariyazono, R., Oda, A., Yamada, T., Ohta, K., 2019. Conserved HORMA domain-containing protein Hop1 stabilizes interaction between proteins of meiotic DNA break hotspots and chromosome axis. Nucleic Acids Res. 47, 10166–10180. https://doi.org/10.1093/nar/gkz754

Kauppi, L., Barchi, M., Lange, J., Baudat, F., Jasin, M., Keeney, S., 2013. Numerical constraints and feedback control of double-strand breaks in mouse meiosis. Genes Dev. 27, 873–886. https://doi.org/10.1101/gad.213652.113

Kee, K., Protacio, R.U., Arora, C., Keeney, S., 2004. Spatial organization and dynamics of the association of Rec102 and Rec104 with meiotic chromosomes. EMBO J. 23, 1815–1824. https://doi.org/10.1038/sj.emboj.7600184

Keeney, S., 2008. Spo11 and the Formation of DNA Double-Strand Breaks in Meiosis, in: Egel, R., Lankenau, D.-H. (Eds.), Recombination and Meiosis: Crossing-Over and Disjunction, Genome Dynamics and Stability. Springer Berlin Heidelberg, Berlin, Heidelberg, pp. 81–123. https://doi.org/10.1007/7050_2007_026

Keeney, S., Giroux, C.N., Kleckner, N., 1997. Meiosis-specific DNA double-strand breaks are catalyzed by Spo11, a member of a widely conserved protein family. Cell 88, 375–384.

Keeney, S., Lange, J., Mohibullah, N., 2014. Self-organization of meiotic recombination initiation: general principles and molecular pathways. Annu. Rev. Genet. 48, 187–214. https://doi.org/10.1146/annurev-genet-120213-092304

Kim, D.-H., Tang, Z., Shimada, M., Fierz, B., Houck-Loomis, B., Bar-Dagen, M., Lee, S., Lee, S.-K., Muir, T.W., Roeder, R.G., Lee, J.W., 2013. Histone H3K27 Trimethylation Inhibits H3 Binding and Function of SET1-Like H3K4 Methyltransferase Complexes. Mol. Cell. Biol. 33, 4936–4946. https://doi.org/10.1128/MCB.00601-13

Kim, K.P., Weiner, B.M., Zhang, L., Jordan, A., Dekker, J., Kleckner, N., 2010. Sister cohesion and structural axis components mediate homolog bias of meiotic recombination. Cell 143, 924–937. https://doi.org/10.1016/j.cell.2010.11.015

Kim, Y., Rosenberg, S.C., Kugel, C.L., Kostow, N., Rog, O., Davydov, V., Su, T.Y., Dernburg, A.F., Corbett, K.D., 2014. The Chromosome Axis Controls

Meiotic Events through a Hierarchical Assembly of HORMA Domain Proteins. Dev. Cell 31, 487–502. https://doi.org/10.1016/j.devcel.2014.09.013

Kirmizis, A., Santos-Rosa, H., Penkett, C.J., Singer, M.A., Vermeulen, M., Mann, M., Bähler, J., Green, R.D., Kouzarides, T., 2007. Arginine methylation at histone H3R2 controls deposition of H3K4 trimethylation. Nature 449, 928–932. https://doi.org/10.1038/nature06160

Klapholz, S., Waddell, C.S., Esposito, R.E., 1985. The role of the SPO11 gene in meiotic recombination in yeast. Genetics 110, 187–216. https://doi.org/10.1093/genetics/110.2.187

Kleckner, N., 2006. Chiasma formation: chromatin/axis interplay and the role(s) of the synaptonemal complex. Chromosoma 115, 175–194. https://doi.org/10.1007/s00412-006-0055-7

Klein, F., Mahr, P., Galova, M., Buonomo, S.B., Michaelis, C., Nairz, K., Nasmyth, K., 1999. A central role for cohesins in sister chromatid cohesion, formation of axial elements, and recombination during yeast meiosis. Cell 98, 91–103. https://doi.org/10.1016/S0092-8674(00)80609-1

Konopka, L., 2019. Biochemical Analysis of the Meiotic Double-Strand Break Regulatory Proteins Rec114 and Mei4. Eberhardt Karls Univeristät Tübingen.

Kugou, K., Fukuda, T., Yamada, S., Ito, M., Sasanuma, H., Mori, S., Katou, Y., Itoh, T., Matsumoto, K., Shibata, T., Shirahige, K., Ohta, K., 2009. Rec8 Guides Canonical Spo11 Distribution along Yeast Meiotic Chromosomes. Mol. Biol. Cell 20, 3064–3076. https://doi.org/10.1091/mbc.E08-12-1223

Laemmli, U.K., 1970. Cleavage of Structural Proteins during the Assembly of the Head of Bacteriophage T4. Nature 227, 680–685. https://doi.org/10.1038/227680a0

Lam, I., Keeney, S., 2014. Mechanism and regulation of meiotic recombination initiation. Cold Spring Harb. Perspect. Biol. 7, a016634. https://doi.org/10.1101/cshperspect.a016634

Lange, J., Pan, J., Cole, F., Thelen, M.P., Jasin, M., Keeney, S., 2011. ATM controls meiotic double-strand-break formation. Nature 479, 237–240. https://doi.org/10.1038/nature10508

Lange, J., Yamada, S., Tischfield, S.E., Pan, J., Kim, S., Zhu, X., Socci, N.D., Jasin, M., Keeney, S., 2016. The Landscape of Mouse Meiotic Double-Strand Break Formation, Processing, and Repair. Cell 167, 695-708.e16. https://doi.org/10.1016/j.cell.2016.09.035

Lee, J.-H., Skalnik, D.G., 2005. CpG-binding protein (CXXC finger protein 1) is a component of the mammalian Set1 histone H3-Lys4 methyltransferase complex, the analogue of the yeast Set1/COMPASS complex. J. Biol. Chem. 280, 41725–41731. https://doi.org/10.1074/jbc.M508312200

Li, J., Hooker, G.W., Roeder, G.S., 2006. Saccharomyces cerevisiae Mer2, Mei4 and Rec114 form a complex required for meiotic double-strand break formation. Genetics 173, 1969–1981. https://doi.org/10.1534/genetics.106.058768

Liedtke, D., 2020. Crystallization of Spp1 and Mer2. Eberhardt Karls Universität Tübingen.

Lowary, P.T., Widom, J., 1998. New DNA sequence rules for high affinity binding to histone octamer and sequence-directed nucleosome positioning. J. Mol. Biol. 276, 19–42. https://doi.org/10.1006/jmbi.1997.1494

Luger, K., 2003. Structure and dynamic behavior of nucleosomes. Curr. Opin. Genet. Dev. 13, 127–135. https://doi.org/10.1016/S0959-437X(03)00026-1

Luger, K., Rechsteiner, T.J., Richmond, T.J., 1999. Preparation of nucleosome core particle from recombinant histones. Methods Enzymol. 304, 3–19. https://doi.org/10.1016/s0076-6879(99)04003-3

Luo, X., Fang, G., Coldiron, M., Lin, Y., Yu, H., Kirschner, M.W., Wagner, G., 2000. Structure of the Mad2 spindle assembly checkpoint protein and its interaction with Cdc20. Nat. Struct. Biol. 7, 224–229. https://doi.org/10.1038/73338

Lynn, A., Soucek, R., Börner, G.V., 2007. ZMM proteins during meiosis: crossover artists at work. Chromosome Res. Int. J. Mol. Supramol. Evol. Asp. Chromosome Biol. 15, 591–605. https://doi.org/10.1007/s10577-007-1150-1

Mahadevan, J., Skalnik, D.G., 2016. Efficient differentiation of murine embryonic stem cells requires the binding of CXXC finger protein 1 to DNA

or methylated histone H3-Lys4. Gene 594, 1–9. https://doi.org/10.1016/j.gene.2016.08.048

Maleki, S., Neale, M.J., Arora, C., Henderson, K.A., Keeney, S., 2007. Interactions between Mei4, Rec114, and other proteins required for meiotic DNA double-strand break formation in Saccharomyces cerevisiae. Chromosoma 116, 471–486. https://doi.org/10.1007/s00412-007-0111-y

Malone, R.E., Bullard, S., Hermiston, M., Rieger, R., Cool, M., Galbraith, A., 1991. Isolation of mutants defective in early steps of meiotic recombination in the yeast Saccharomyces cerevisiae. Genetics 128, 79–88.

Malone, R.E., Esposito, R.E., 1981. Recombinationless meiosis in Saccharomyces cerevisiae. Mol. Cell. Biol. 1, 891–901. https://doi.org/10.1128/mcb.1.10.891-901.1981

Martini, E., Borde, V., Legendre, M., Audic, S., Regnault, B., Soubigou, G., Dujon, B., Llorente, B., 2011. Genome-wide analysis of heteroduplex DNA in mismatch repair-deficient yeast cells reveals novel properties of meiotic recombination pathways. PLoS Genet. 7, e1002305. https://doi.org/10.1371/journal.pgen.1002305

Masai, H., Arai, K.-I., 2002. Cdc7 kinase complex: a key regulator in the initiation of DNA replication. J. Cell. Physiol. 190, 287–296. https://doi.org/10.1002/jcp.10070

Matos, J., Lipp, J.J., Bogdanova, A., Guillot, S., Okaz, E., Junqueira, M., Shevchenko, A., Zachariae, W., 2008. Dbf4-dependent CDC7 kinase links DNA replication to the segregation of homologous chromosomes in meiosis I. Cell 135, 662–678. https://doi.org/10.1016/j.cell.2008.10.026

Matsumoto, S., Ogino, K., Noguchi, E., Russell, P., Masai, H., 2005. Hsk1-Dfp1/Him1, the Cdc7-Dbf4 Kinase in Schizosaccharomyces pombe, Associates with Swi1, a Component of the Replication Fork Protection Complex *. J. Biol. Chem. 280, 42536–42542. https://doi.org/10.1074/jbc.M510575200

Menees, T.M., Roeder, G.S., 1989. MEI4, a yeast gene required for meiotic recombination. Genetics 123, 675–682.

Miller, T., Krogan, N.J., Dover, J., Erdjument-Bromage, H., Tempst, P., Johnston, M., Greenblatt, J.F., Shilatifard, A., 2001. COMPASS: a complex of proteins associated with a trithorax-related SET domain protein. Proc. Natl. Acad. Sci. U. S. A. 98, 12902–12907. https://doi.org/10.1073/pnas.231473398

Mimitou, E.P., Yamada, S., Keeney, S., 2017. A global view of meiotic double-strand break end resection. Science 355, 40–45. https://doi.org/10.1126/science.aak9704

Miyoshi, T., Ito, M., Kugou, K., Yamada, S., Furuichi, M., Oda, A., Yamada, T., Hirota, K., Masai, H., Ohta, K., 2012. A Central Coupler for Recombination Initiation Linking Chromosome Architecture to S Phase Checkpoint. Mol. Cell 47, 722–733. https://doi.org/10.1016/j.molcel.2012.06.023

Møens, P.B., Pearlman, R.E., 1988. Chromatin organization at meiosis. BioEssays 9, 151–153. https://doi.org/10.1002/bies.950090503

Mohibullah, N., Keeney, S., 2017. Numerical and spatial patterning of yeast meiotic DNA breaks by Tel1. Genome Res. 27, 278–288. https://doi.org/10.1101/gr.213587.116

Morillon, A., Karabetsou, N., Nair, A., Mellor, J., 2005. Dynamic Lysine Methylation on Histone H3 Defines the Regulatory Phase of Gene Transcription. Mol. Cell 18, 723–734. https://doi.org/10.1016/j.molcel.2005.05.009

Mu, X., Murakami, H., Mohibullah, N., Keeney, S., 2020. Chromosome-autonomous feedback down-regulates meiotic DNA break competence upon synaptonemal complex formation. Genes Dev. https://doi.org/10.1101/gad.342873.120

Murakami, H., Keeney, S., 2014. Temporospatial coordination of meiotic DNA replication and recombination via DDK recruitment to replisomes. Cell 158, 861–873. https://doi.org/10.1016/j.cell.2014.06.028

Murakami, H., Lam, I., Huang, P.-C., Song, J., van Overbeek, M., Keeney, S., 2020. Multilayered mechanisms ensure that short chromosomes recombine in meiosis. Nature 582, 124–128. https://doi.org/10.1038/s41586-020-2248-2

Murakami, H., Nicolas, A., 2009. Locally, meiotic double-strand breaks targeted by Gal4BD-Spo11 occur at discrete sites with a sequence preference. Mol. Cell. Biol. 29, 3500–3516. https://doi.org/10.1128/MCB.00088-09

Musselman, C.A., Kutateladze, T.G., 2011. Handpicking epigenetic marks with PHD fingers. Nucleic Acids Res. 39, 9061–9071. https://doi.org/10.1093/nar/gkr613

Myers, S., Bowden, R., Tumian, A., Bontrop, R.E., Freeman, C., MacFie, T.S., McVean, G., Donnelly, P., 2010. Drive against hotspot motifs in primates implicates the PRDM9 gene in meiotic recombination. Science 327, 876–879. https://doi.org/10.1126/science.1182363

Nandabalan, K., Roeder, G.S., 1995. Binding of a cell-type-specific RNA splicing factor to its target regulatory sequence. Mol. Cell. Biol. 15, 1953–1960. https://doi.org/10.1128/MCB.15.4.1953

Neale, M.J., Pan, J., Keeney, S., 2005. Endonucleolytic processing of covalent protein-linked DNA double-strand breaks. Nature 436, 1053–1057. https://doi.org/10.1038/nature03872

Niu, H., Wan, L., Baumgartner, B., Schaefer, D., Loidl, J., Hollingsworth, N.M., 2005. Partner Choice during Meiosis Is Regulated by Hop1-promoted Dimerization of Mek1. Mol. Biol. Cell 16, 5804–5818. https://doi.org/10.1091/mbc.E05-05-0465

Ogino, K., Masai, H., 2006. Rad3-Cds1 mediates coupling of initiation of meiotic recombination with DNA replication. Mei4-dependent transcription as a potential target of meiotic checkpoint. J. Biol. Chem. 281, 1338–1344. https://doi.org/10.1074/jbc.M505767200

Page, S.L., Hawley, R.S., 2003. Chromosome choreography: the meiotic ballet. Science 301, 785–789. https://doi.org/10.1126/science.1086605

Palmer, S., Schildkraut, E., Lazarin, R., Nguyen, J., Nickoloff, J.A., 2003. Gene conversion tracts in Saccharomyces cerevisiae can be extremely short and highly directional. Nucleic Acids Res. 31, 1164–1173. https://doi.org/10.1093/nar/gkg219

Pan, D., Brockmeyer, A., Mueller, F., Musacchio, A., Bange, T., 2018. Simplified Protocol for Cross-linking Mass Spectrometry Using the MS-Cleavable Cross-linker DSBU with Efficient Cross-link Identification. Anal. Chem. 90, 10990–10999. https://doi.org/10.1021/acs.analchem.8b02593

Pan, J., Sasaki, M., Kniewel, R., Murakami, H., Blitzblau, H.G., Tischfield, S.E., Zhu, X., Neale, M.J., Jasin, M., Socci, N.D., Hochwagen, A., Keeney, S., 2011. A hierarchical combination of factors shapes the genome-wide topography of yeast meiotic recombination initiation. Cell 144, 719–731. https://doi.org/10.1016/j.cell.2011.02.009

Panizza, S., Mendoza, M.A., Berlinger, M., Huang, L., Nicolas, A., Shirahige, K., Klein, F., 2011. Spo11-accessory proteins link double-strand break sites to the chromosome axis in early meiotic recombination. Cell 146, 372–383. https://doi.org/10.1016/j.cell.2011.07.003

Parvanov, E.D., Petkov, P.M., Paigen, K., 2010. Prdm9 Controls Activation of Mammalian Recombination Hotspots. Science 327, 835. https://doi.org/10.1126/science.1181495

Pennings, S., Meersseman, G., Bradbury, E.M., 1991. Mobility of positioned nucleosomes on 5 S rDNA. J. Mol. Biol. 220, 101–110. https://doi.org/10.1016/0022-2836(91)90384-I

Petes, T.D., 2001. Meiotic recombination hot spots and cold spots. Nat. Rev. Genet. 2, 360–369. https://doi.org/10.1038/35072078

Petronczki, M., Siomos, M.F., Nasmyth, K., 2003. Un ménage à quatre: the molecular biology of chromosome segregation in meiosis. Cell 112, 423–440. https://doi.org/10.1016/s0092-8674(03)00083-7

Pittman, D.L., Cobb, J., Schimenti, K.J., Wilson, L.A., Cooper, D.M., Brignull, E., Handel, M.A., Schimenti, J.C., 1998. Meiotic Prophase Arrest with Failure of Chromosome Synapsis in Mice Deficient for Dmc1, a Germline-Specific RecA Homolog. Mol. Cell 1, 697–705. https://doi.org/10.1016/S1097-2765(00)80069-6

Pratto, F., Brick, K., Cheng, G., Lam, K.-W.G., Cloutier, J.M., Dahiya, D., Wellard, S.R., Jordan, P.W., Camerini-Otero, R.D., 2021. Meiotic

recombination mirrors patterns of germline replication in mice and humans. Cell 184, 4251-4267.e20. https://doi.org/10.1016/j.cell.2021.06.025

Prieler, S., Penkner, A., Borde, V., Klein, F., 2005. The control of Spo11's interaction with meiotic recombination hotspots. Genes Dev. 19, 255–269. https://doi.org/10.1101/gad.321105

Prugar, E., Burnett, C., Chen, X., Hollingsworth, N.M., 2017. Coordination of Double Strand Break Repair and Meiotic Progression in Yeast by a Mek1-Ndt80 Negative Feedback Loop. Genetics 206, 497–512. https://doi.org/10.1534/genetics.117.199703

Pyatnitskaya, A., Borde, V., De Muyt, A., 2019. Crossing and zipping: molecular duties of the ZMM proteins in meiosis. Chromosoma 128, 181–198. https://doi.org/10.1007/s00412-019-00714-8

Qu, Q., Takahashi, Y., Yang, Y., Hu, H., Zhang, Y., Brunzelle, J.S., Couture, J.-F., Shilatifard, A., Skiniotis, G., 2018. Structure and Conformational Dynamics of a COMPASS Histone H3K4 Methyltransferase Complex. Cell 174, 1117-1126.e12. https://doi.org/10.1016/j.cell.2018.07.020

Raina, V.B., Vader, G., 2020. Homeostatic Control of Meiotic Prophase Checkpoint Function by Pch2 and Hop1. Curr. Biol. 30, 4413-4424.e5. https://doi.org/10.1016/j.cub.2020.08.064

Rockmill, B., Engebrecht, J.A., Scherthan, H., Loidl, J., Roeder, G.S., 1995. The yeast MER2 gene is required for chromosome synapsis and the initiation of meiotic recombination. Genetics 141, 49–59.

Roeder, G., Rockmill, B., Engebrecht, J., Thompson, E.A., Menees, T., 1989. Isolation and characterization of yeast mutants defective in meiotic chromosome segregation. Prog. Clin. Biol. Res.

Roguev, A., Schaft, D., Shevchenko, A., Pijnappel, W.W.M.P., Wilm, M., Aasland, R., Stewart, A.F., 2001. The Saccharomyces cerevisiae Set1 complex includes an Ash2 homologue and methylates histone 3 lysine 4. EMBO J. 20, 7137–7148. https://doi.org/10.1093/emboj/20.24.7137

Rousová, D., Nivsarkar, V., Altmannova, V., Raina, V.B., Funk, S.K., Liedtke, D., Janning, P., Müller, F., Reichle, H., Vader, G., Weir, J.R., 2021. Novel

mechanistic insights into the role of Mer2 as the keystone of meiotic DNA break formation. eLife 10, e72330. https://doi.org/10.7554/eLife.72330

Ruthenburg, A.J., Allis, C.D., Wysocka, J., 2007. Methylation of lysine 4 on histone H3: intricacy of writing and reading a single epigenetic mark. Mol. Cell 25, 15–30. https://doi.org/10.1016/j.molcel.2006.12.014

San Filippo, J., Sung, P., Klein, H., 2008. Mechanism of eukaryotic homologous recombination. Annu. Rev. Biochem. 77, 229–257. https://doi.org/10.1146/annurev.biochem.77.061306.125255

Sanchez, R., Zhou, M.-M., 2011. The PHD Finger: A Versatile Epigenome Reader. Trends Biochem. Sci. 36, 364–372. https://doi.org/10.1016/j.tibs.2011.03.005

Sasanuma, H., Hirota, K., Fukuda, T., Kakusho, N., Kugou, K., Kawasaki, Y., Shibata, T., Masai, H., Ohta, K., 2008. Cdc7-dependent phosphorylation of Mer2 facilitates initiation of yeast meiotic recombination. Genes Dev. 22, 398–410. https://doi.org/10.1101/gad.1626608

Sasanuma, H., Murakami, H., Fukuda, T., Shibata, T., Nicolas, A., Ohta, K., 2007. Meiotic association between Spo11 regulated by Rec102, Rec104 and Rec114. Nucleic Acids Res. 35, 1119–1133. https://doi.org/10.1093/nar/gkl1162

Schiller, C.B., Seifert, F.U., Linke-Winnebeck, C., Hopfner, K.-P., 2014. Structural Studies of DNA End Detection and Resection in Homologous Recombination. Cold Spring Harb. Perspect. Biol. 6, a017962. https://doi.org/10.1101/cshperspect.a017962

Schneider, J., Wood, A., Lee, J.-S., Schuster, R., Dueker, J., Maguire, C., Swanson, S.K., Florens, L., Washburn, M.P., Shilatifard, A., 2005. Molecular regulation of histone H3 trimethylation by COMPASS and the regulation of gene expression. Mol. Cell 19, 849–856. https://doi.org/10.1016/j.molcel.2005.07.024

Schwacha, A., Kleckner, N., 1995. Identification of double Holliday junctions as intermediates in meiotic recombination. Cell 83, 783–791. https://doi.org/10.1016/0092-8674(95)90191-4

Shima, H., Suzuki, M., Shinohara, M., 2005. Isolation and Characterization of Novel xrs2 Mutations in Saccharomyces cerevisiae. Genetics 170, 71–85. https://doi.org/10.1534/genetics.104.037580

Shonn, M.A., McCarroll, R., Murray, A.W., 2002. Spo13 protects meiotic cohesin at centromeres in meiosis I. Genes Dev. 16, 1659–1671. https://doi.org/10.1101/gad.975802

Simon, M.D., Chu, F., Racki, L.R., de la Cruz, C.C., Burlingame, A.L., Panning, B., Narlikar, G.J., Shokat, K.M., 2007. The site-specific installation of methyl-lysine analogs into recombinant histones. Cell 128, 1003–1012. https://doi.org/10.1016/j.cell.2006.12.041

Smith, A.V., Roeder, G.S., 1997. The yeast Red1 protein localizes to the cores of meiotic chromosomes. J. Cell Biol. 136, 957–967. https://doi.org/10.1083/jcb.136.5.957

Smith, E., Shilatifard, A., 2010. The Chromatin Signaling Pathway: Diverse Mechanisms of Recruitment of Histone-Modifying Enzymes and Varied Biological Outcomes. Mol. Cell 40, 689–701. https://doi.org/10.1016/j.molcel.2010.11.031

Sollier, J., Lin, W., Soustelle, C., Suhre, K., Nicolas, A., Géli, V., de La Roche Saint-André, C., 2004. Set1 is required for meiotic S-phase onset, double-strand break formation and middle gene expression. EMBO J. 23, 1957–1967. https://doi.org/10.1038/sj.emboj.7600204

Sommermeyer, V., Béneut, C., Chaplais, E., Serrentino, M.E., Borde, V., 2013. Spp1, a member of the Set1 Complex, promotes meiotic DSB formation in promoters by tethering histone H3K4 methylation sites to chromosome axes. Mol. Cell 49, 43–54. https://doi.org/10.1016/j.molcel.2012.11.008

Stanzione, M., Baumann, M., Papanikos, F., Dereli, I., Lange, J., Ramlal, A., Tränkner, D., Shibuya, H., de Massy, B., Watanabe, Y., Jasin, M., Keeney, S., Tóth, A., 2016. Meiotic DNA break formation requires the unsynapsed chromosome axis-binding protein IHO1 (CCDC36) in mice. Nat. Cell Biol. 18, 1208–1220. https://doi.org/10.1038/ncb3417

Stark, H., 2010. GraFix: stabilization of fragile macromolecular complexes for single particle cryo-EM. Methods Enzymol. 481, 109–126. https://doi.org/10.1016/S0076-6879(10)81005-5

Sturm, K., 2020. Biochemical reconstitution and analysis of the Rec114-Mei4 complex. Eberhard Karls Universität Tübingen.

Subramanian, V.V., Hochwagen, A., 2014. The Meiotic Checkpoint Network: Step-by-Step through Meiotic Prophase. Cold Spring Harb. Perspect. Biol. 6, a016675. https://doi.org/10.1101/cshperspect.a016675

Subramanian, V.V., MacQueen, A.J., Vader, G., Shinohara, M., Sanchez, A., Borde, V., Shinohara, A., Hochwagen, A., 2016. Chromosome Synapsis Alleviates Mek1-Dependent Suppression of Meiotic DNA Repair. PLoS Biol. 14, e1002369. https://doi.org/10.1371/journal.pbio.1002369

Sun, H., Treco, D., Schultes, N.P., Szostak, J.W., 1989. Double-strand breaks at an initiation site for meiotic gene conversion. Nature 338, 87–90. https://doi.org/10.1038/338087a0

Sun, H., Treco, D., Szostak, J.W., 1991. Extensive 3′-overhanging, single-stranded DNA associated with the meiosis-specific double-strand breaks at the ARG4 recombination initiation site. Cell 64, 1155–1161. https://doi.org/10.1016/0092-8674(91)90270-9

Sun, X., Huang, L., Markowitz, T.E., Blitzblau, H.G., Chen, D., Klein, F., Hochwagen, A., 2015. Transcription dynamically patterns the meiotic chromosome-axis interface. eLife 4, e07424. https://doi.org/10.7554/eLife.07424

Symington, L.S., 2016. Mechanism and Regulation of DNA End Resection in Eukaryotes. Crit. Rev. Biochem. Mol. Biol. 51, 195–212. https://doi.org/10.3109/10409238.2016.1172552

Takahashi, Y., Westfield, G.H., Oleskie, A.N., Trievel, R.C., Shilatifard, A., Skiniotis, G., 2011. Structural analysis of the core COMPASS family of histone H3K4 methylases from yeast to human. Proc. Natl. Acad. Sci. 108, 20526–20531. https://doi.org/10.1073/pnas.1109360108

Takahashi, Y.H., Lee, J.S., Swanson, S.K., Saraf, A., Florens, L., Washburn, M.P., Trievel, R.C., Shilatifard, A., 2009. Regulation of H3K4 Trimethylation via Cps40 (Spp1) of COMPASS Is Monoubiquitination Independent: Implication for a Phe/Tyr Switch by the Catalytic Domain of Set1. Mol. Cell. Biol. 29, 3478–3486. https://doi.org/10.1128/MCB.00013-09

Tessé, S., Bourbon, H.-M., Debuchy, R., Budin, K., Dubois, E., Liangran, Z., Antoine, R., Piolot, T., Kleckner, N., Zickler, D., Espagne, E., 2017. Asy2/Mer2: an evolutionarily conserved mediator of meiotic recombination, pairing, and global chromosome compaction. Genes Dev. 31, 1880–1893. https://doi.org/10.1101/gad.304543.117

Tischfield, S.E., Keeney, S., 2012. Scale matters: the spatial correlation of yeast meiotic DNA breaks with histone H3 trimethylation is driven largely by independent colocalization at promoters. Cell Cycle Georget. Tex 11, 1496–1503. https://doi.org/10.4161/cc.19733

Trowitzsch, S., Bieniossek, C., Nie, Y., Garzoni, F., Berger, I., 2010. New baculovirus expression tools for recombinant protein complex production. J. Struct. Biol. 172, 45–54. https://doi.org/10.1016/j.jsb.2010.02.010

Ur, S.N., Corbett, K.D., 2021. Architecture and Dynamics of Meiotic Chromosomes. Annu. Rev. Genet. 55, 497–526. https://doi.org/10.1146/annurev-genet-071719-020235

Vader, G., 2015. Pch2(TRIP13): controlling cell division through regulation of HORMA domains. Chromosoma 124, 333–339. https://doi.org/10.1007/s00412-015-0516-y

Varadi, M., Anyango, S., Deshpande, M., Nair, S., Natassia, C., Yordanova, G., Yuan, D., Stroe, O., Wood, G., Laydon, A., Žídek, A., Green, T., Tunyasuvunakool, K., Petersen, S., Jumper, J., Clancy, E., Green, R., Vora, A., Lutfi, M., Figurnov, M., Cowie, A., Hobbs, N., Kohli, P., Kleywegt, G., Birney, E., Hassabis, D., Velankar, S., 2022. AlphaFold Protein Structure Database: massively expanding the structural coverage of protein-sequence space with high-accuracy models. Nucleic Acids Res. 50, D439–D444. https://doi.org/10.1093/nar/gkab1061

Vaughn, J.L., Goodwin, R.H., Tompkins, G.J., McCawley, P., 1977. The establishment of two cell lines from the insectspodoptera frugiperda (lepidoptera; noctuidae). In Vitro 13, 213–217. https://doi.org/10.1007/BF02615077

Wan, L., Niu, H., Futcher, B., Zhang, C., Shokat, K.M., Boulton, S.J., Hollingsworth, N.M., 2008. Cdc28-Clb5 (CDK-S) and Cdc7-Dbf4 (DDK) collaborate to initiate meiotic recombination in yeast. Genes Dev. 22, 386–397. https://doi.org/10.1101/gad.1626408

Weissmann, F., Petzold, G., VanderLinden, R., Huis In 't Veld, P.J., Brown, N.G., Lampert, F., Westermann, S., Stark, H., Schulman, B.A., Peters, J.-M., 2016. biGBac enables rapid gene assembly for the expression of large multisubunit protein complexes. Proc. Natl. Acad. Sci. U. S. A. 113, E2564-2569. https://doi.org/10.1073/pnas.1604935113

West, A.M., Rosenberg, S.C., Ur, S.N., Lehmer, M.K., Ye, Q., Hagemann, G., Caballero, I., Usón, I., MacQueen, A.J., Herzog, F., Corbett, K.D., 2019. A conserved filamentous assembly underlies the structure of the meiotic chromosome axis. eLife 8, e40372. https://doi.org/10.7554/eLife.40372

West, A.M.V., Komives, E.A., Corbett, K.D., 2018. Conformational dynamics of the Hop1 HORMA domain reveal a common mechanism with the spindle checkpoint protein Mad2. Nucleic Acids Res. 46, 279–292. https://doi.org/10.1093/nar/gkx1196

Wickham, T.J., Davis, T., Granados, R.R., Shuler, M.L., Wood, H.A., 1992. Screening of Insect Cell Lines for the Production of Recombinant Proteins and Infectious Virus in the Baculovirus Expression System. Biotechnol. Prog. 8, 391–396. https://doi.org/10.1021/bp00017a003

Wilkins, A.S., Holliday, R., 2009. The Evolution of Meiosis From Mitosis. Genetics 181, 3–12. https://doi.org/10.1534/genetics.108.099762

Woltering, D., Baumgartner, B., Bagchi, S., Larkin, B., Loidl, J., de los Santos, T., Hollingsworth, N.M., 2000. Meiotic Segregation, Synapsis, and Recombination Checkpoint Functions Require Physical Interaction between the Chromosomal Proteins Red1p and Hop1p. Mol. Cell. Biol. 20, 6646–6658.

Wu, P.-Y.J., Nurse, P., 2014. Replication Origin Selection Regulates the Distribution of Meiotic Recombination. Mol. Cell 53, 655–662. https://doi.org/10.1016/j.molcel.2014.01.022

Wu, T.C., Lichten, M., 1994. Meiosis-induced double-strand break sites determined by yeast chromatin structure. Science 263, 515–518. https://doi.org/10.1126/science.8290959

Xu, L., Ajimura, M., Padmore, R., Klein, C., Kleckner, N., 1995. NDT80, a meiosis-specific gene required for exit from pachytene in Saccharomyces cerevisiae. Mol. Cell. Biol. 15, 6572–6581.

Yamada, S., Kim, S., Tischfield, S.E., Jasin, M., Lange, J., Keeney, S., 2017. Genomic and chromatin features shaping meiotic double-strand break formation and repair in mice. Cell Cycle Georget. Tex 16, 1870–1884. https://doi.org/10.1080/15384101.2017.1361065

Yang, C., Hu, B., Portheine, S.M., Chuenban, P., Schnittger, A., 2020. State changes of the HORMA protein ASY1 are mediated by an interplay between its closure motif and PCH2. Nucleic Acids Res. 48, 11521–11535. https://doi.org/10.1093/nar/gkaa527

Young, G., Hundt, N., Cole, D., Fineberg, A., Andrecka, J., Tyler, A., Olerinyova, A., Ansari, A., Marklund, E.G., Collier, M.P., Chandler, S.A., Tkachenko, O., Allen, J., Crispin, M., Billington, N., Takagi, Y., Sellers, J.R., Eichmann, C., Selenko, P., Frey, L., Riek, R., Galpin, M.R., Struwe, W.B., Benesch, J.L.P., Kukura, P., 2018. Quantitative mass imaging of single biological macromolecules. Science 360, 423–427. https://doi.org/10.1126/science.aar5839

Zakharyevich, K., Ma, Y., Tang, S., Hwang, P.Y.-H., Boiteux, S., Hunter, N., 2010. Temporally and biochemically distinct activities of Exo1 during meiosis: double-strand break resection and resolution of double Holliday junctions. Mol. Cell 40, 1001–1015. https://doi.org/10.1016/j.molcel.2010.11.032

Zakharyevich, K., Tang, S., Ma, Y., Hunter, N., 2012. Delineation of joint molecule resolution pathways in meiosis identifies a crossover-specific resolvase. Cell 149, 334–347. https://doi.org/10.1016/j.cell.2012.03.023

Zhang, L., Kim, K.P., Kleckner, N.E., Storlazzi, A., 2011. Meiotic double-strand breaks occur once per pair of (sister) chromatids and, via Mec1/ATR and Tel1/ATM, once per quartet of chromatids. Proc. Natl. Acad. Sci. 108, 20036–20041. https://doi.org/10.1073/pnas.1117937108

Zhao, Q., Xie, Y., Zheng, Y., Jiang, S., Liu, W., Mu, W., Liu, Z., Zhao, Y., Xue, Y., Ren, J., 2014. GPS-SUMO: a tool for the prediction of sumoylation sites and SUMO-interaction motifs. Nucleic Acids Res. 42, W325–W330. https://doi.org/10.1093/nar/gku383

Zickler, D., Kleckner, N., 1999. Meiotic chromosomes: integrating structure and function. Annu. Rev. Genet. 33, 603–754. https://doi.org/10.1146/annurev.genet.33.1.603

Zimmermann, L., Stephens, A., Nam, S.-Z., Rau, D., Kübler, J., Lozajic, M., Gabler, F., Söding, J., Lupas, A.N., Alva, V., 2017. A Completely Reimplemented MPI Bioinformatics Toolkit with a New HHpred Server at its Core. J. Mol. Biol. https://doi.org/10.1016/j.jmb.2017.12.007

7 Supplementary material

7.1 Materials

7.1.1 Columns and resins

Affinity columns and resins

Affinity resin	**Targeted tag**	**Elution**
Amylose Resin (NEB)	MBP	1 mM D-maltose
Pierce Glutathione Agarose (Thermo Scientific)	GST	40 mM reduced glutathione
StrepTactin Superflow Plus (Quiagen)	2x StrepII	2.5 mM desthiobiotin
Pierce Streptavidin Magnetic beads (Thermo scientific)	Biotin 2x StrepII	Laemmli buffer
Dynabeads M 270 streptavidin beads (Thermo Scientific)	Biotin 2x StrepII	Laemmli buffer
Affinity columns	**Targeted tag**	**Elution**
MBP-Trap HP (GE Healthcare) 5 ml	MBP	0.25 mM D-maltose (gradient)
GSTrap 4B (GE Healthcare)	GST	40 mM reduced glutathione (gradient)
StrepTactin XT Superflow Cartridge (IBA) 5 ml	2x StrepII	2.5 mM desthiobiotin (isocratic)

Ion exchange and size exclusion chromatography columns

Column	**Provider**	**Volume**
ResourceQ	GE Healthcare	6 ml
ResourceS	GE Healthcare	6 ml
Heparin HP	GE Healthcare	6 ml

Superdex 200 5/150	GE Healthcare	3 ml
Superdex 200 10/300 Increase	GE Healthcare	23.6 ml
Superdex 200 HiPrep 16/600	GE Healthcare	120.6 ml
Superose 6 5/150	GE Healthcare	3 ml
Superose 6 10/300 Increase	GE Healthcare	23.6 ml
Superose 6 16/600	GE Healthcare	128 ml

7.1.2 Medium

LB (lysogeny broth) medium and plates

Peptone/tryptone	10 g/l
Yeast extract	5 g/l
NaCl	5 g/l
Adjust to pH 7	
Additionally for LB-plates:	
Agar	15 g/l
LB_{Amp}	0.1 g/l ampicillin
$LB_{Kan/Gent}$	25 mg/l kanamycin 10 mg/l gentamicin
LB_{Bacmid}	10 mg/l tetracycline 50 mg/l kanamycin 10 mg/l gentamicin 0.2 mM IPTG 0.1 g/l X-Gal

TB (terrific broth) medium used for *E. coli* expression

Tryptone	12 g/l
Yeast extract	24 g/l
Glycerol	0.4% (v/v)
KH_2PO4	17 mM
K_2HPO_4	72 mM

7.1.3 General buffers

Electrophoresis running buffer (TAE)

Tris-HCl, pH 8.0	40 mM
Acetic acid	18 mM
EDTA	1 mM

5× TBE buffer

Tris-borate pH 8.3	445 mM
Boric acid	445 mM
EDTA	10 mM

10× PBS (phosphate-buffered saline)

NaCl	1.37 M
KCl	27 mM
Na_2HPO_4	100 mM
KH_2PO_4	18 mM

Adjust to pH 7.4

10× Transfer buffer

Tris base	250 mM
Glycine	192 mM
20% SDS	1% (v/v)

For 1x buffer, add MeOH to final 10%

1× Laemmli buffer

SDS	3.5 mM
Glycine	192 mM
Tris base	25 mM

6× SDS-PAGE sample buffer

Tris-HCl	375 mM
SDS	9% (v/v)
Glycerol	50% (v/v)

Beta-mercaptoethanol	9% (v/v)
Bromphenolblue	0.03% (v/v)

SDS-gels

	10% resolving gel	**Stacking gel**
H_2O	39.6 ml	20.4 ml
30% acrylamide mix	33.4 ml	4.98 ml
1.5 M Tris pH 8.8	25 ml	-
1M Tris pH 6.8	-	3.78 ml
10%SDS	1 ml	0.3 ml
10% APS	1 ml	0.3 ml
TEMED	40 µl	30 µl

7.1.4 Antibodies for western blotting

Antibody	**Specification**	**Dilution**	**Secondary antibody**
αMBP	Maltose binding protein polyclonal rabbit IgG, Invitrogen, Lot: SH254903	1:1000	αRabbit
αStrep	8-aas Strep-Tag II monoclonal mouse IgG, Novagen, Lot: 2795151	1:1000	αMouse
αMer2	prepared in house within this study	1:1000	αRabbit
αMouse	Polyclonal goat anti-mouse IgG, H&L chain-specific HRP conjugate, Calbiochem, Lot: 2894290	1:10,000	-
αRabbit	Polyclonal anti-rabbit IgG, H&L chain-specific HRP conjugate, Calbiochem, Lot: 2869818	1:10,000	-

7.1.5 Equipment and software

Device	**Company**	
Äkta Go	GE Healthcare	
Äkta Pure	GE Healthcare	
Äkta Start	GE Healthcare	
Biometra Trio48-PCR Thermocycler	Analytic Jena	
ChemiDoc MP Imaging System	Bio-Rad	
Dragonfly	sptlabtech	
EmulsiFlex-3C	Avestin	
Tecnai G^2 Spirit electron microscope	FEI, Thermo Scientific	
Glow discharger	Edwards	
Gradient master 108	Biocomp	
Hettich Mikro 200R	Hettich	
Hettich Rotina 380R	Hettich	Swing out rotor 4-times (1754)
LED Blue Light Transluminator	Herolab	UVT-22 BE-LED
Micro Star 17R	VWR	
MiniDawn Treos	Wyatt technology	
Mosquito	sptlabtech	
NanoPhotometer NP80	Implen	
Optilab T-rEX	Wyatt technology	
Optima L-100 XP Ultracentrifuge	Beckman Coulter	45 Ti Rotor SW55 Ti Rotor
PowerPac Basic	Bio-rad	
Quantifoil R1.2/1.3 100 Holey Carbon Films, Cu 300 mesh	Quantifoil	For cryo-electron microscopy

400 mesh Cu square grids		For negative staining microscopy
Refeyn One Mass Photometer	Refeyn	
Rock Imager 182	Formulatrix	
S1000 Thermal Cycler	Bio-Rad	
MicroCal PEAQ-ITC	Malvern Panalytical	
Monolith NT.115	Nanotemper	Premium capillaries
Sonicator Sunoplus HD 2070.2	Bandelin electronic	Standard horn SH70 G with a pointed tip
Sorvall RC 6+ Centrifuge	Thermo Scientific	Fiberlite F10-4x1000 LEX Rotor
T18 digital Ultra-Turrax	IKA	
Talos Arctica G2 cryo-electron microscope	FEI, Thermo Scientific	
Thermo Heraeus pico 17 centrifuge	Thermo Scientific	
Thermomixer comfort	Eppendorf	
Trans-Blot Turbo Transfer System	Bio-Rad	
VIAFLO384	Integra Biosciences	
Vitrobot	Thermo Scientific	
PELCO easiGlow	TED Paella	

Software	**Provider**	**Used for**
Astra	Wyatt technology	SEC-MALS control system
ATSAS	EMBL Hamburg	SAXS data analysis
benchling.com	Benchling	Sequence analysis, biophysical protein property prediction

EPU	Thermo Scientific	control of the electron microscope, data analysis
Excel 2016 MSO	Microsoft	FPLC chromatogram plotting
Foxtrot	Soleil, France	SAXS data analysis
Illustrator CS6	Adobe	Image editing
Image Lab 5.2.1	Bio-Rad	Blot and gel imaging
Photoshop CS6	Adobe	Image editing
RefeynAquire MP	Refeyn	Collection of mass-photometry data
RefeynDiscover MP	Refeyn	Analysis of mass-photometry data
Snapgene 4.1.8	GST Biotech	Primer design, *in silico* cloning
Unicorn 7.1	GE Healthcare	Äkta Pure control system

7.2 Expression constructs

Supplementary table 4: Cloning of expression vectors. Tem – template used for PCR; Fw – forward primer; Rv – reverse primer; Bc – used backbone; Nr – the number in the lab registry

Name	**Tem**	**Fw**	**Rv**	**Bc**	**Nr**
pColi_GST-Spp1	p014	o226	o029	p103	p341
pColi_MBP-Spp1_N-170	p014	o226	o1415	p104	p1224
pColi_MBP-Spp1_169-C	p014	o858	p029	p104	p735
pColi_MBP-Mer2_FL	p011	o342	o022	p104	p146
pColi_MBP-Mer2_140-256	p011	0422	o424	p104	p186
pColi_MBP-Mer2_140-C	p011	o422	o022	p104	p1330
pColi_MBP-Mer2_257-C	p011	o1083	o022	p104	p940
pColi_MBP-Mer2_4A	g043	o342	o022	p104	p1368
pColi_MBP-Mer2_N-139	p011	o342	o1082	p104	p939
pColi_MBP-Mer2_N-256	p011	0342	o424	p104	p868
pColi_MBP-Mer2_N-295	p146	o342	o1936	p104	p1779
pColi_MBP-Mer2-N-256_S29/30A	p670	o342	o424	p104	p837

pColi_MBP-Mer2-N-256_S29/30D	p671	o342	o424	p104	p838
pColi_MBP-Mer2-N-256_S29/30E	p695	o342	o424	p104	p840
pColi_MBP-Mer2-N-256_S29A	p664	o342	o424	p104	p836
pColi_MBP-Mer2-N-256_S29D	p665	o342	o424	p104	p858
pColi_MBP-Mer2-N-256_S29E	p666	o342	o424	p104	p840
pColi_MBP-Mer2-N-256_S30A	p667	o342	o424	p104	p836
pColi_MBP-Mer2-N-256_S30D	p668	o342	o424	p104	p849
pColi_MBP-Mer2-N-256_S30E	p669	o342	o424	p104	p841
pColi_Strep-Hop1	p438	o225	o038	p176	p658
pColi_Strep-Hop1_256-C	p438	o1226	o038	p176	p1104
pLib_Strep-Hop1	p438	o225	o038	p258	p661
pLib_Red1-MBP_I743R		o039	o650	p1134	p1417

Supplementary table 5: Mutagenesis of expression vectors. Performed via Gibson mutagenesis, with two PCR products Gibson assembled using forward and reverse primer o480 and o481 respectively. Tem – template; Fw1 – forward primer; Rv2 – reverse primer; Nr – the number in the lab registry.

Name	**Tem**	**Fw1**	**Rv2**	**Nr**
pColi_MBP-Mer2_S29A	p146	o806	o807	p664
pColi_MBP-Mer2_S29D	p146	o808	o809	p665
pColi_MBP-Mer2_S29E	p146	o810	o811	p666
pColi_MBP-Mer2_S30A	p146	o812	o813	p667
pColi_MBP-Mer2_S30D	p146	o814	o815	p668
pColi_MBP-Mer2_S30E	p146	o816	o817	p669
pColi_MBP-Mer2_S29/30A	p146	o818	o819	p670
pColi_MBP-Mer2_S29/30D	p146	o820	o821	p671

pColi_MBP-Mer2_S29/30E	p146	o822	o823	p695
pColi_MBP-Mer2_3A	p146	o1546	o1546	o1319
pColi_Strep-Hop1_K593A	p438	o1236	o1237	p1139
pET_H3_K4C_C110A	p642	o903	o904	p654
pET_H3_K4C_K36C_C110A	p654	o1323	o1324	p1552

Supplementary table 6: Cloning primers. Nr – the number in the lab registry

Name	**Nr**	**Sequence 5´-3´**
Mer2_Rv	o022	TCCTCTAGTACTTCTCGACAAGCTT TTATCACAGCTCAGATTCCAGAGTG TCG
Spp1_Rv	o029	TCCTCTAGTACTTCTCGACAAGCTT TTACAAACCTCTTCTTAAAATTTCC
Hop1_Rv	o038	TCCTCTAGTACTTCTCGACAAGCTT CTACCAGTTACTTTTCAAAGTCTTT TTAGAGACGC
Mer2_139_Rv	o1082	TCCTCTAGTACTTCTCGACAAGCTT TTATGTCTTCTTCTCGTCGCCTTTCG
Mer2_257_Fw	o1083	CTGTTCCAGGGGCCCGGATCCAGA ATGATGGTCACAAGGTCCATGAAA CGC
Spp1_170_Rv	o1415	TCCTCTAGTACTTCTCGACAAGCTT TTAGTCATCTGTTTTTACAACTATA TTGTTATCAATGAAATCCAGTTGTC CAAATTTCTTG
Mer2_295_Rv	o1936	TCCTCTAGTACTTCTCGACAAGCTT TTACGCACGCTTCAGCCGATGGC
Hop1_Fw	o225	CTGTTCCAGGGGCCCGGATCCATGT CTAATAAACAACTAGTAAAGCCAA AAACAGAGAC
Spp1_Fw	o226	CTGTTCCAGGGGCCCGGATCCATGT CATTACCACAATGGTGTCC

Mer2_Fw	o342	CTGTTCCAGGGGCCCGGATCCATG GTCGCTAGAGGTAGAACAGACGAG ATATCTAC
Mer2_140_Fw	o422	CTGTTCCAGGGGCCCGGATCCAAG TCGGATTCCAGCTACAGGCAGGTA TTAGTCG
Mer2-256_Rv	o424	TCCTCTAGTACTTCTCGACAAGCTT TTATGGTGGCGGCACGGACTTCTTA CGCTG
Amp_Rv	o480	CGCTCGTCGTTTGGTATGGCTTCAT TCAG
Amp_Fw	o481	CTGAATGAAGCCATACCAAACGAC GAGCG
Mer2_S29A_Fw	o806	CGTTGATGATTACAGAAACAGCTTC ACCGTTCAGATCTATATTCTCCC
Mer2_S29A_Rv	o807	GGGAGAATATAGATCTGAACGGTG AAGCTGTTTCTGTAATCATCAACG
Mer2_S29D_Fw	o808	CGTTGATGATTACAGAAACAGATT CACCGTTCAGATCTATATTCTCCC
Mer2_S29D_Rv	o809	GGGAGAATATAGATCTGAACGGTG AATCTGTTTCTGTAATCATCAACG
Mer2_S29E_Fw	o810	CGTTGATGATTACAGAAACAGAGT CACCGTTCAGATCTATATTCTCCC
Mer2_S29E_Rv	o811	GGGAGAATATAGATCTGAACGGTG ACTCTGTTTCTGTAATCATCAACG
Mer2_S30A_Fw	o812	CGTTGATGATTACAGAAACATCAG CTCCGTTCAGATCTATATTCTCCC
Mer2_S30A_Rv	o813	GGGAGAATATAGATCTGAACGGAG CTGATGTTTCTGTAATCATCAACG
Mer2_S30D_Fw	o814	CGTTGATGATTACAGAAACATCAG ATCCGTTCAGATCTATATTCTCCC
Mer2_S30D_Rv	o815	GGGAGAATATAGATCTGAACGGAT CTGATGTTTCTGTAATCATCAACG

Mer2_S30E_Fw	o816	CGTTGATGATTACAGAAACATCAG AGCCGTTCAGATCTATATTCTCCC
Mer2_S30E_Fw	o817	GGGAGAATATAGATCTGAACGGCT CTGATGTTTCTGTAATCATCAACG
Mer2_S29/30A_Fw	o818	CGTTGATGATTACAGAAACAGCTG CTCCGTTCAGATCTATATTCTCCC
Mer2_S29/30A_Rv	o819	GGGAGAATATAGATCTGAACGGAG CAGCTGTTTCTGTAATCATCAACG
Mer2_S29/30D_Fw	o820	CGTTGATGATTACAGAAACAGATG ATCCGTTCAGATCTATATTCTCCC
Mer2_S29/30D_Rv	o821	GGGAGAATATAGATCTGAACGGAT CATCTGTTTCTGTAATCATCAACG
Mer2_S29/30E_Fw	o822	CGTTGATGATTACAGAAACAGAGG AGCCGTTCAGATCTATATTCTCCC
Mer2_S29/30E_Rv	o823	GGGAGAATATAGATCTGAACGGCT CCTCTGTTTCTGTAATCATCAACG
Spp1_169_Fw	o858	CTGTTCCAGGGGCCCGGATCCGAT GACGAAAAGGAAATATTCGATCAA ATTGTTGTACGAGACATGAC
H3_K4C_Fw	o903	ATGGCCCGTACCTGTCAGACCGCCC GTAAATCCACCGGAGG
H3_K4C_Rv	o904	CCTCCGGTGGATTTACGGGCGGTCT GACAGGTACGGGCCAT

Vector maps:

p104:

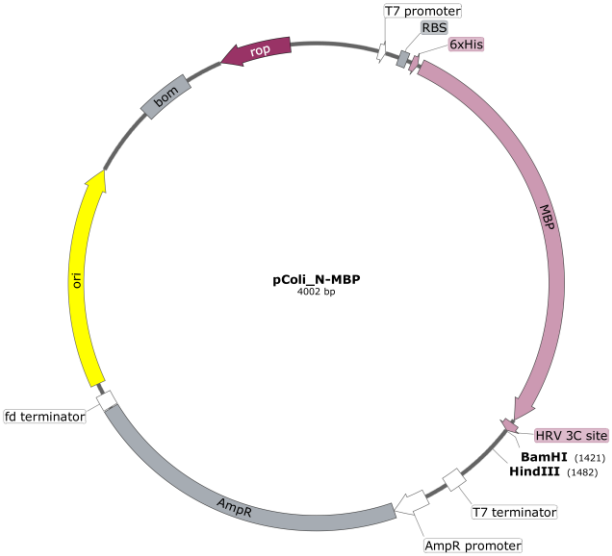

p103:

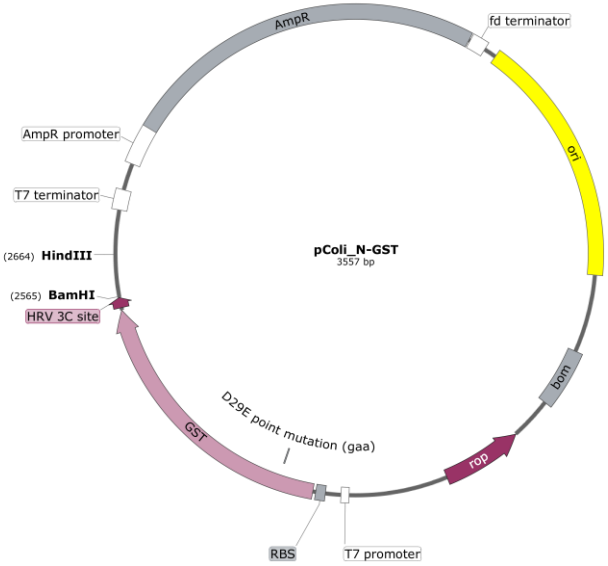

p176:

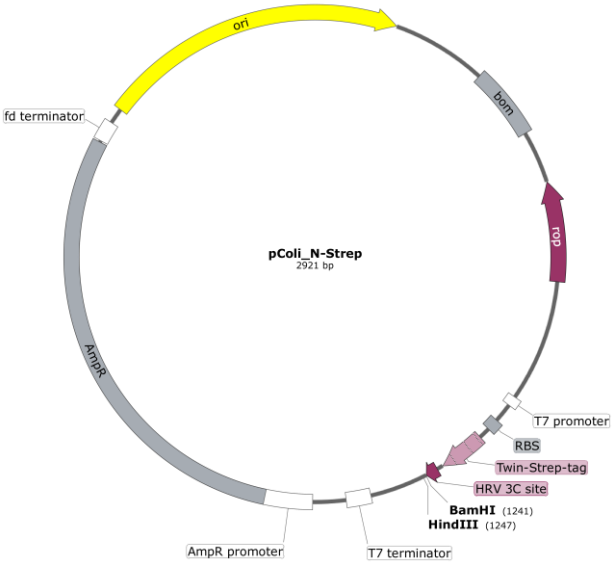
ori
bom
rop
T7 promoter
RBS
Twin-Strep-tag
HRV 3C site
BamHI (1241)
HindIII (1247)
T7 terminator
AmpR promoter
AmpR
fd terminator
pColi_N-Strep
2921 bp

p1667:

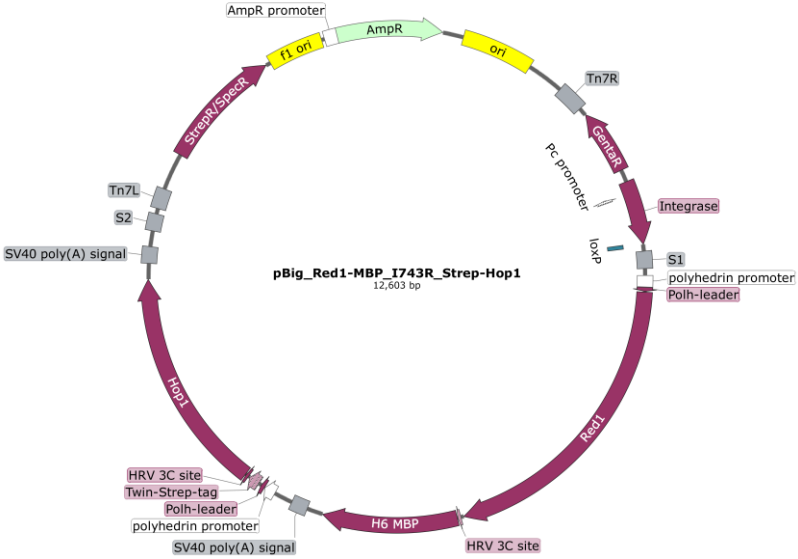
AmpR promoter
AmpR
f1 ori
ori
Tn7R
StrepR/SpecR
GentaR
Pc promoter
Integrase
Tn7L
S2
loxP
S1
SV40 poly(A) signal
polyhedrin promoter
Polh-leader
pBig_Red1-MBP_I743R_Strep-Hop1
12,603 bp
Hop1
Red1
HRV 3C site
Twin-Strep-tag
Polh-leader
polyhedrin promoter
SV40 poly(A) signal
H6 MBP
HRV 3C site

p1157:

g043:

ATGGTCGCTAGAGGTAGAACAGACGAGATATCTACAGATGTTTCA
GAGGCTAATTCTGAGCACTCGTTGATGATTACAGAAACATCATCA
CCGTTCAGATCTATATTCTCCCACAGTGGGAAAGTAACGAATGCA
GGCGCTTTAGAGGAATCGGCTAAGCAGATACTGGAATGGGCAGGT
AAACTGGAATTGGAGAGTATGGCACTGGCTGCAAACTCTGACAAG
CTAATTAAAGTTTTAAATGAAAATTCTAAGACATTATGTAAATCG
CTAAACAAGTTTAACCAGCTACTGGAACAAGATGCTGCTACGAAC
GGAAACGTGAAAACCTTAATAAAGGATTTGGCTTCCCAGATTGAA
AACCAACTGGACAAAGTGTCAACAGCAATGTTATCGAAAGGCGA
CGAGAAGAAGACAAAGTCGGATTCCAGCTACAGGCAGGTATTAG
TCGAAGAAATAAGCAGGTATAATTCCAAGATAACGCGACACGTA
ACTAACAAGCAGCATGAGACGGAAAAGTCGATGAGGTGCACCCA
GGAGATGCTCTTCAACGTCGGCAGCCAACTGGAGGACGTGCATAA
AGTGCTCCTGTCTCTATCCAAAGACATGCACAGTCTACAAACCCG
CCAGACTGCTCTAGAGATGGCGTTTCGAGAAAAGGCAGATCACGC
CTACGATCGCCCGGATGTGTCTCTGAATGGCACCACACTCCTGCA
CGATATGGACGAAGCCCACGATAAGCAGCGTAAGAAGTCCGTGC

CGCCACCAAGAATGATGGTCACAAGGTCCATGAAACGCAGAAGA
TCCAGCTCCCCAACCCTATCCACCAGCCAAAACCACAATAGCGAA
GACAATGATGACGCTAGCCATCGGCTGAAGCGTGCGGCCAGGACC
ATTATTCCCTGGGAGGAACTAAGACCCGACACTCTGGAATCTGAG
CTGTGA

7.3 Protein sequences

N-terminal MBP-tag with overhang:

MAHHHHHHSSGMKIEEGKLVIWINGDKGYNGLAEVGKKFEKDTGIK
VTVEHPDKLEEKFPQVAATGDGPDIIFWAHDRFGGYAQSGLLAEITP
DKAFQDKLYPFTWDAVRYNGKLIAYPIAVEALSLIYNKDLLPNPPKT
WEEIPALDKELKAKGKSALMFNLQEPYFTWPLIAADGGYAFKYENG
KYDIKDVGVDNAGAKAGLTFLVDLIKNKHMNADTDYSIAEAAFNKG
ETAMTINGPWAWSNIDTSKVNYGVTVLPTFKGQPSKPFVGVLSAGIN
AASPNKELAKEFLENYLLTDEGLEAVNKDKPLGAVALKSYEEELAK
DPRIAATMENAQKGEIMPNIPQMSAFWYAVRTAVINAASGRQTVDE
ALKDAQTSSGLEVLFQGPGS

C-terminal MBP-tag with overhang:

SGSGSGSGMKIEEGKLVIWINGDKGYNGLAEVGKKFEKDTGIKVTVE
HPDKLEEKFPQVAATGDGPDIIFWAHDRFGGYAQSGLLAEITPDKAF
QDKLYPFTWDAVRYNGKLIAYPIAVEALSLIYNKDLLPNPPKTWEEIP
ALDKELKAKGKSALMFNLQEPYFTWPLIAADGGYAFKYENGKYDIK
DVGVDNAGAKAGLTFLVDLIKNKHMNADTDYSIAEAAFNKGETAM
TINGPWAWSNIDTSKVNYGVTVLPTFKGQPSKPFVGVLSAGINAASP
NKELAKEFLENYLLTDEGLEAVNKDKPLGAVALKSYEEELAKDPRIA
ATMENAQKGEIMPNIPQMSAFWYAVRTAVINAASGRQTVDEALKDA
QT

N-terminal GST-tag with overhang:

MSPILGDWKIKGLVQPTRLLLEYLEEKYDEHLYERDEGDKWRNKKF
ELGLEFPNLPYYIDGDVKLTQSMAIIRYIADKHNMLGGCPKERAEISM
LEGAVLDIRYGVSRIAYSKDFETLKVDFLSKLPEMLKMFEDRLCHKT

YLNGDHVTHPDFMLYDALDVVLYMDPMCLDAFPKLVCFKKRIEAIP
QIDKYLKSSKYIAWPLQGWQATFGGGDHPPKSDLEVLFQGPGS

N-terminal Strep-tag with overhang:

MGSSASAWSHPQFEKGGGSGGGSGGSAWSHPQFEKSSGSLEVLFQG
PGS

Spp1:

MSLPQWCPPHSTLKRNPTTGEDVYCICKRPDYGELMVGCDGCDDWF
HFTCLHIPEQFKDLVFSFYCPYCQAGITGKNKDAIINGEGSLPKTLWK
RKCRISDCYKPCLQDSKYCSEEHGREFVNDIWSRLKTDEDRAVVKK
MVEQTGHIDKFKKFGQLDFIDNNIVVKTDDEKEIFDQIVVRDMTLKT
LEDDLQEVQEISLPLFKKKLELLEVYLGWLDNVYTEMRKLDDDAAS
HVECGKEDSKGTKRKKKKNSSRSRARKNICGYCSTYERIPCSVEEFV
RDFGSNEEATKIHEVCTKWKCNRHLDWVSTNQEQYLQQIDSLESMQ
ERLQHLIQARKKQLNIQYYEEILRRGL

Spp1$^{N\text{-}170}$:

MSLPQWCPPHSTLKRNPTTGEDVYCICKRPDYGELMVGCDGCDDWF
HFTCLHIPEQFKDLVFSFYCPYCQAGITGKNKDAIINGEGSLPKTLWK
RKCRISDCYKPCLQDSKYCSEEHGREFVNDIWSRLKTDEDRAVVKK
MVEQTGHIDKFKKFGQLDFIDNNIVVKTDD

Spp1$^{169\text{-}C}$:

DDEKEIFDQIVVRDMTLKTLEDDLQEVQEISLPLFKKKLELLEVYLG
WLDNVYTEMRKLDDDAASHVECGKEDSKGTKRKKKKNSSRSRARK
NICGYCSTYERIPCSVEEFVRDFGSNEEATKIHEVCTKWKCNRHLDW
VSTNQEQYLQQIDSLESMQERLQHLIQARKKQLNIQYYEEILRRGL

Mer2^{FL}:

MVARGRTDEISTDVSEANSEHSLMITETSSPFRSIFSHSGKVTNAGALE
ESDKQILEWAGKLELESMELRENSDKLIKVLNENSKTLCKSLNKFNQ
LLEQDAATNGNVKTLIKDLASQIENQLDKVSTAMLSKGDEKKTKSDS
SYRQVLVEEISRYNSKITRHVTNKQHETEKSMRCTQEMLFNVGSQLE
DVHKVLLSLSKDMHSLQTRQTALEMAFREKADHAYDRPDVSLNGTT

LLHDMDEAHDKQRKKSVPPPRMMVTRSMKRRRSSSPTLSTSQNHNS
EDNDDASHRLKRAARTIIPWEELRPDTLESEL

Mer2$^{140\text{-}256}$ = Mer2^{core}:

KSDSSYRQVLVEEISRYNSKITRHVTNKQHETEKSMRCTQEMLFNVG
SQLEDVHKVLLSLSKDMHSLQTRQTALEMAFREKADHAYDRPDVSL
NGTTLLHDMDEAHDKQRKKSVPPP

Mer2$^{140\text{-}C}$ = Mer2$^{\Delta N}$

KSDSSYRQVLVEEISRYNSKITRHVTNKQHETEKSMRCTQEMLFNVG
SQLEDVHKVLLSLSKDMHSLQTRQTALEMAFREKADHAYDRPDVSL
NGTTLLHDMDEAHDKQRKKSVPPPRMMVTRSMKRRRSSSPTLSTSQ
NHNSEDNDDASHRLKRAARTIIPWEELRPDTLESEL

Mer2$^{257\text{-}C}$:

RMMVTRSMKRRRSSSPTLSTSQNHNSEDNDDASHRLKRAARTIIPWE
ELRPDTLESEL

Mer2$^{N\text{-}139}$:

MVARGRTDEISTDVSEANSEHSLMITETSSPFRSIFSHSGKVTNAGALE
ESDKQILEWAGKLELESMELRENSDKLIKVLNENSKTLCKSLNKFNQ
LLEQDAATNGNVKTLIKDLASQIENQLDKVSTAMLSKGDEKKT

Mer2$^{N\text{-}256}$ = Mer2$^{\Delta C}$:

MVARGRTDEISTDVSEANSEHSLMITETSSPFRSIFSHSGKVTNAGALE
ESDKQILEWAGKLELESMELRENSDKLIKVLNENSKTLCKSLNKFNQ
LLEQDAATNGNVKTLIKDLASQIENQLDKVSTAMLSKGDEKKTKSDS
SYRQVLVEEISRYNSKITRHVTNKQHETEKSMRCTQEMLFNVGSQLE
DVHKVLLSLSKDMHSLQTRQTALEMAFREKADHAYDRPDVSLNGTT
LLHDMDEAHDKQRKKSVPPP

Mer2_N-295:

MVARGRTDEISTDVSEANSEHSLMITETSSPFRSIFSHSGKVTNAGALE
ESDKQILEWAGKLELESMELRENSDKLIKVLNENSKTLCKSLNKFNQ
LLEQDAATNGNVKTLIKDLASQIENQLDKVSTAMLSKGDEKKTKSDS
SYRQVLVEEISRYNSKITRHVTNKQHETEKSMRCTQEMLFNVGSQLE
DVHKVLLSLSKDMHSLQTRQTALEMAFREKADHAYDRPDVSLNGTT

LLHDMDEAHDKQRKKSVPPPRMMVTRSMKRRRSSSPTLSTSQNHNS
EDNDDASHRLKRA

Mer2^{3A}:

MVARGRTDEISTDVSEANSEHSLMITETSSPFRSIFSHSGKVTNAGALE
ESDKQILEAAGALEAESMELRENSDKLIKVLNENSKTLCKSLNKFNQ
LLEQDAATNGNVKTLIKDLASQIENQLDKVSTAMLSKGDEKKTKSDS
SYRQVLVEEISRYNSKITRHVTNKQHETEKSMRCTQEMLFNVGSQLE
DVHKVLLSLSKDMHSLQTRQTALEMAFREKADHAYDRPDVSLNGTT
LLHDMDEAHDKQRKKSVPPPRMMVTRSMKRRRSSSPTLSTSQNHNS
EDNDDASHRLKRAARTIIPWEELRPDTLESEL

Mer2^{4A}:

MVARGRTDEISTDVSEANSEHSLMITETSSPFRSIFSHSGKVTNAGALE
ESAKQILEWAGKLELESMALAANSDKLIKVLNENSKTLCKSLNKFNQ
LLEQDAATNGNVKTLIKDLASQIENQLDKVSTAMLSKGDEKKTKSDS
SYRQVLVEEISRYNSKITRHVTNKQHETEKSMRCTQEMLFNVGSQLE
DVHKVLLSLSKDMHSLQTRQTALEMAFREKADHAYDRPDVSLNGTT
LLHDMDEAHDKQRKKSVPPPRMMVTRSMKRRRSSSPTLSTSQNHNS
EDNDDASHRLKRAARTIIPWEELRPDTLESEL

Mer2$^{\Delta C_S29A}$:

MVARGRTDEISTDVSEANSEHSLMITETASPFRSIFSHSGKVTNAGAL
EESDKQILEWAGKLELESMELRENSDKLIKVLNENSKTLCKSLNKFN
QLLEQDAATNGNVKTLIKDLASQIENQLDKVSTAMLSKGDEKKTKS
DSSYRQVLVEEISRYNSKITRHVTNKQHETEKSMRCTQEMLFNVGSQ
LEDVHKVLLSLSKDMHSLQTRQTALEMAFREKADHAYDRPDVSLNG
TTLLHDMDEAHDKQRKKSVPPP

Mer2$^{\Delta C_S29D}$:

MVARGRTDEISTDVSEANSEHSLMITETDSPFRSIFSHSGKVTNAGAL
EESDKQILEWAGKLELESMELRENSDKLIKVLNENSKTLCKSLNKFN
QLLEQDAATNGNVKTLIKDLASQIENQLDKVSTAMLSKGDEKKTKS
DSSYRQVLVEEISRYNSKITRHVTNKQHETEKSMRCTQEMLFNVGSQ
LEDVHKVLLSLSKDMHSLQTRQTALEMAFREKADHAYDRPDVSLNG
TTLLHDMDEAHDKQRKKSVPPP

Mer2$^{\Delta C_S29E}$:

MVARGRTDEISTDVSEANSEHSLMITETESPFRSIFSHSGKVTNAGALE
ESDKQILEWAGKLELESMELRENSDKLIKVLNENSKTLCKSLNKFNQ
LLEQDAATNGNVKTLIKDLASQIENQLDKVSTAMLSKGDEKKTKSDS
SYRQVLVEEISRYNSKITRHVTNKQHETEKSMRCTQEMLFNVGSQLE
DVHKVLLSLSKDMHSLQTRQTALEMAFREKADHAYDRPDVSLNGTT
LLHDMDEAHDKQRKKSVPPP

Mer2$^{\Delta C_S30A}$:

MVARGRTDEISTDVSEANSEHSLMITETSAPFRSIFSHSGKVTNAGAL
EESDKQILEWAGKLELESMELRENSDKLIKVLNENSKTLCKSLNKFN
QLLEQDAATNGNVKTLIKDLASQIENQLDKVSTAMLSKGDEKKTKS
DSSYRQVLVEEISRYNSKITRHVTNKQHETEKSMRCTQEMLFNVGSQ
LEDVHKVLLSLSKDMHSLQTRQTALEMAFREKADHAYDRPDVSLNG
TTLLHDMDEAHDKQRKKSVPPP

Mer2$^{\Delta C_S30D}$:

MVARGRTDEISTDVSEANSEHSLMITETSDPFRSIFSHSGKVTNAGAL
EESDKQILEWAGKLELESMELRENSDKLIKVLNENSKTLCKSLNKFN
QLLEQDAATNGNVKTLIKDLASQIENQLDKVSTAMLSKGDEKKTKS
DSSYRQVLVEEISRYNSKITRHVTNKQHETEKSMRCTQEMLFNVGSQ
LEDVHKVLLSLSKDMHSLQTRQTALEMAFREKADHAYDRPDVSLNG
TTLLHDMDEAHDKQRKKSVPPP

Mer2$^{\Delta C_S30E}$:

MVARGRTDEISTDVSEANSEHSLMITETSEPFRSIFSHSGKVTNAGALE
ESDKQILEWAGKLELESMELRENSDKLIKVLNENSKTLCKSLNKFNQ
LLEQDAATNGNVKTLIKDLASQIENQLDKVSTAMLSKGDEKKTKSDS
SYRQVLVEEISRYNSKITRHVTNKQHETEKSMRCTQEMLFNVGSQLE
DVHKVLLSLSKDMHSLQTRQTALEMAFREKADHAYDRPDVSLNGTT
LLHDMDEAHDKQRKKSVPPP

Mer2$^{\Delta C_S29/30A}$:

MVARGRTDEISTDVSEANSEHSLMITETAAPFRSIFSHSGKVTNAGAL
EESDKQILEWAGKLELESMELRENSDKLIKVLNENSKTLCKSLNKFN
QLLEQDAATNGNVKTLIKDLASQIENQLDKVSTAMLSKGDEKKTKS

DSSYRQVLVEEISRYNSKITRHVTNKQHETEKSMRCTQEMLFNVGSQ
LEDVHKVLLSLSKDMHSLQTRQTALEMAFREKADHAYDRPDVSLNG
TTLLHDMDEAHDKQRKKSVPPP

Mer2$^{\Delta C_S29/30D}$:

MVARGRTDEISTDVSEANSEHSLMITETDDPFRSIFSHSGKVTNAGAL
EESDKQILEWAGKLELESMELRENSDKLIKVLNENSKTLCKSLNKFN
QLLEQDAATNGNVKTLIKDLASQIENQLDKVSTAMLSKGDEKKTKS
DSSYRQVLVEEISRYNSKITRHVTNKQHETEKSMRCTQEMLFNVGSQ
LEDVHKVLLSLSKDMHSLQTRQTALEMAFREKADHAYDRPDVSLNG
TTLLHDMDEAHDKQRKKSVPPP

Mer2$^{\Delta C_S29/30E}$:

MVARGRTDEISTDVSEANSEHSLMITETEEPFRSIFSHSGKVTNAGAL
EESDKQILEWAGKLELESMELRENSDKLIKVLNENSKTLCKSLNKFN
QLLEQDAATNGNVKTLIKDLASQIENQLDKVSTAMLSKGDEKKTKS
DSSYRQVLVEEISRYNSKITRHVTNKQHETEKSMRCTQEMLFNVGSQ
LEDVHKVLLSLSKDMHSLQTRQTALEMAFREKADHAYDRPDVSLNG
TTLLHDMDEAHDKQRKKSVPPP

Mer2$^{S29/30A}$:

MVARGRTDEISTDVSEANSEHSLMITETAAPFRSIFSHSGKVTNAGAL
EESDKQILEWAGKLELESMELRENSDKLIKVLNENSKTLCKSLNKFN
QLLEQDAATNGNVKTLIKDLASQIENQLDKVSTAMLSKGDEKKTKS
DSSYRQVLVEEISRYNSKITRHVTNKQHETEKSMRCTQEMLFNVGSQ
LEDVHKVLLSLSKDMHSLQTRQTALEMAFREKADHAYDRPDVSLNG
TTLLHDMDEAHDKQRKKSVPPPRMMVTRSMKRRRSSSPTLSTSQNH
NSEDNDDASHRLKRAARTIIPWEELRPDTLESEL

Mer2$^{S29/30D}$:

MVARGRTDEISTDVSEANSEHSLMITETDDPFRSIFSHSGKVTNAGAL
EESDKQILEWAGKLELESMELRENSDKLIKVLNENSKTLCKSLNKFN
QLLEQDAATNGNVKTLIKDLASQIENQLDKVSTAMLSKGDEKKTKS
DSSYRQVLVEEISRYNSKITRHVTNKQHETEKSMRCTQEMLFNVGSQ
LEDVHKVLLSLSKDMHSLQTRQTALEMAFREKADHAYDRPDVSLNG

TTLLHDMDEAHDKQRKKSVPPPRMMVTRSMKRRRSSSPTLSTSQNH
NSEDNDDASHRLKRAARTIIPWEELRPDTLESEL

Mer2$^{S29/30E}$:

MVARGRTDEISTDVSEANSEHSLMITETEEPFRSIFSHSGKVTNAGAL
EESDKQILEWAGKLELESMELRENSDKLIKVLNENSKTLCKSLNKFN
QLLEQDAATNGNVKTLIKDLASQIENQLDKVSTAMLSKGDEKKTKS
DSSYRQVLVEEISRYNSKITRHVTNKQHETEKSMRCTQEMLFNVGSQ
LEDVHKVLLSLSKDMHSLQTRQTALEMAFREKADHAYDRPDVSLNG
TTLLHDMDEAHDKQRKKSVPPPRMMVTRSMKRRRSSSPTLSTSQNH
NSEDNDDASHRLKRAARTIIPWEELRPDTLESEL

Hop1:

MSNKQLVKPKTETKTEITTEQSQKLLQTMLTMSFGCLAFLRGLFPDDI
FVDQRFVPEKVEKNYNKQNTSQNNSIKIKTLIRGKSTQADLLLDWLE
KGVFKSIRLKCLKALSLGIFLEDPTDLLENYIFSFDYDEENNVNINVNL
SGNKKGNKNADPENETISLLDSRRMVQQLMRRFIIITQSLEPLPQKKF
LTMRLMFNDNVDEDYQPELFKDATFDKRATLKVPTNLDNDAFDVGT
LNTKHHKVALSVLSAATSSMEKAGNTNFIRVDPFDLILQQQEENKLE
ESAPTKPQNFVTSQTTNVLGNLLNSSQASIQPTQFVSNNPVTGICSCEC
GLEVPKAATVLKTCKSCRKTLHGICYGNFLHSSIEKCFTCIFGPSLDTK
WSKFQDLMMIRKVFRFLVRKKKGFPASITELIDSFINVEDQNNEVKER
VAFALFVFFLDETLCLDNGGKPSQTIRYVTSSVLVDVKGIIIPNTRKQL
NVNHEYKWHFTTSSPKSESFYQEVLPNSRKQVESWLQDITNLRKVYS
EALSPSSTLQELDLNSSLPTQDPIISGQKRRRYDLDEYLEEDKSSVVND
TIKAKDFDESVPAKIRKISVSKKTLKSNW

Hop1$^{256\text{-}C}$ = Hop1$^{\Delta HORMA}$

SSMEKAGNTNFIRVDPFDLILQQQEENKLEESAPTKPQNFVTSQTTNV
LGNLLNSSQASIQPTQFVSNNPVTGICSCECGLEVPKAATVLKTCKSC
RKTLHGICYGNFLHSSIEKCFTCIFGPSLDTKWSKFQDLMMIRKVFRF
LVRKKKGFPASITELIDSFINVEDQNNEVKERVAFALFVFFLDETLCLD
NGGKPSQTIRYVTSSVLVDVKGIIIPNTRKQLNVNHEYKWHFTTSSPK
SESFYQEVLPNSRKQVESWLQDITNLRKVYSEALSPSSTLQELDLNSS

LPTQDPIISGQKRRRYDLDEYLEEDKSSVVNDTIKAKDFDESVPAKIR
KISVSKKTLKSNW

Hop1^{K593A}:

MSNKQLVKPKTETKTEITTEQSQKLLQTMLTMSFGCLAFLRGLFPDDI
FVDQRFVPEKVEKNYNKQNTSQNNSIKIKTLIRGKSTQADLLLDWLE
KGVFKSIRLKCLKALSLGIFLEDPTDLLENYIFSFDYDEENNVNINVNL
SGNKKGNKNADPENETISLLDSRRMVQQLMRRFIIITQSLEPLPQKKF
LTMRLMFNDNVDEDYQPELFKDATFDKRATLKVPTNLDNDAFDVGT
LNTKHHKVALSVLSAATSSMEKAGNTNFIRVDPFDLILQQQEENKLE
ESAPTKPQNFVTSQTTNVLGNLLNSSQASIQPTQFVSNNPVTGICSCEC
GLEVPKAATVLKTCKSCRKTLHGICYGNFLHSSIEKCFTCIFGPSLDTK
WSKFQDLMMIRKVFRFLVRKKKGFPASITELIDSFINVEDQNNEVKER
VAFALFVFFLDETLCLDNGGKPSQTIRYVTSSVLVDVKGIIIPNTRKQL
NVNHEYKWHFTTSSPKSESFYQEVLPNSRKQVESWLQDITNLRKVYS
EALSPSSTLQELDLNSSLPTQDPIISGQKRRRYDLDEYLEEDKSSVVND
TIKAKDFDESVPAKIRAISVSKKTLKSNW

Red1^{I743R}:

MEGLKKKIFGVCLKNDLAQTRNETKGIHYGLMTLETSKQLEEFLHLL
VIKREVIQNFELLFHIINVAVKITDSNLPSDDIWHFILKLRFSSEINIDED
SKVLNYLLETGIAMENPVSWKCLAVISSILSSVPQSKKIITNLIETEHA
KKIGQLFDNIQDLQQGNFLVEILSNCFKKSASNSKKVEKIPQLWQSRS
KNKFFFENEFYPFSSKNGSLQTCQFLCNNFMSTLSFTGILRQVSYSGSE
TLKNLRIFKKKDDENSYFIQCIYNKIYLWLDEKAPLEFERKKIRITKNL
KNKIQIKLRQPFHECVRTTADKTALLFNKTRGFQLEFEDEKLGETFFH
NVNNIPKISEVQNFLVLDYIEEEPENEGEEEEQTRRADEQKEDEEEESL
DELSTPMVYPIKSSISHNHNEKVQLVTPDRSVSIRSDEWDLKSNTEDE
EGNVLTDLKISSTKETRRQTDYVHIDSEDQSPVVSAQMRKMRRESTK
TLEILRQEFKDKDVQNKEDQSEQIQNPFVNTSSLVVGKSCLVNPKEKP
NIDQTVVGITELKSNSSIKKRDINILDTIFGQPPSKKQKQFHKKEKKKQ
QKKLTNFKPIIDVPSQDKRNLRSNAPTKPKSIKVSKLRTDKKVTGEKS
SPETTAEKVDDQTVRSNDEQAVSRATKEKRFPDVNEGKEITNDDAK
VSLESKKNNETFVDSSVVEKHTPPDKDCNNCNITDILESTTVIDLHSPH
GLSAPGQNTFTNKLQEQRYSSINHFSNELVRKISIINQELNKKILKELSE

KYQKLFAELQDNFQNDTNEMLKFMGEIKDMMNLPEDQLVHAIRTRK
FDNNKR

H3_K4C_C110A:

MARTCQTARKSTGGKAPRKQLATKAARKSAPATGGVKKPHRYRPG
TVALREIRRYQKSTELLIRKLPFQRLVREIAQDFKTDLRFQSSAVMAL
QEASEAYLVALFEDTNLAAIHAKRVTIMPKDIQLARRIRGERA*GSEF
ELRRQACGRTRAPPPPPL

H3_K4C_K36C_C110A:

MARTCQTARKSTGGKAPRKQLATKAARKSAPATGGVCKPHRYRPG
TVALREIRRYQKSTELLIRKLPFQRLVREIAQDFKTDLRFQSSAVMAL
QEASEAYLVALFEDTNLAAIHAKRVTIMPKDIQLARRIRGERA*GSEF
ELRRQACGRTRAPPPPPL